REACTOR MATERIALS

A Quarterly Technical Progress Review

Prepared for DIVISION OF TECHNICAL INFORMATION, USAEC, by
E. M. SIMONS, D.L. KELLER, and ASSOCIATES, BATTELLE MEMORIAL INSTITUTE

Summer 1967

● VOLUME 10

● NUMBER 2

TECHNICAL PROGRESS REVIEWS

The United States Atomic Energy Commission publishes the Technical Progress Reviews to meet the needs of industry and government for concise summaries of current nuclear developments. Issued quarterly, each journal digests and evaluates the latest findings in a specific area of nuclear technology and science

The journals are:

Isotopes and Radiation Technology
P. S. Baker, A. F. Rupp, and Associates
Oak Ridge National Laboratory

Nuclear Safety
Wm. B. Cottrell, W. H. Jordan, J. P. Blakely, and Associates
Nuclear Safety Information Center, Oak Ridge National Laboratory

Power Reactor Technology
Argonne National Laboratory

Reactor Materials
E. M. Simons and Associates
Battelle Memorial Institute

All are available from the U. S. Government Printing Office. See the back cover for ordering instructions.

The views expressed in this publication do not necessarily represent those of the United States Atomic Energy Commission, its divisions or offices, or of any Commission advisory committee or contractor.

Availability of Reports Cited in This Review

United States Atomic Energy Commission (USAEC) reports are available at USAEC depository libraries and are sold by the Clearinghouse for Federal Scientific and Technical Information (CFSTI), National Bureau of Standards, U. S. Department of Commerce, 5285 Port Royal Road, Springfield, Va. 22151. All reports sold by CFSTI are $3.00 for printed copy and $0.65 for microfiche. Each separately bound part of a report is priced as a separate report. Some reports may not be available because of their preliminary nature; however, the information contained in them will generally be found in later progress or topical reports on the subject.

Other U. S. Government agency reports identified in this journal generally are available from CFSTI.

Private-organization reports should be requested from the originator.

United Kingdom Atomic Energy Authority (UKAEA) and Atomic Energy of Canada Limited (AECL) reports are available at USAEC depository libraries. UKAEA reports are sold by Her Majesty's Stationery Office, London; AECL reports are sold by the Technical Information Officer, Atomic Energy of Canada Limited, Chalk River, Ontario, Canada. UKAEA and AECL reports issued after March 1, 1967, are sold by CFSTI to purchasers in the United States and its territories.

Contents

Reactor Materials

Vol. 10, No. 2

Fuel and Fertile Materials (Section I)

Uranium Metal and Alloys 69
Plutonium 71
Thorium 74
Metal–Ceramic Fuels 74
Coated-Particle Fuels 74
Uranium and Thorium Oxides 75
Uranium Carbides, Nitrides, Phosphides, and Sulfides 77
Fuel–Water Reactions 78
Basic Studies of Irradiation Effects in Fuel Materials 79
References 80

Moderator Materials (Section II)

Graphite 83
Beryllium and Beryllium Alloys 84
Beryllium Oxide 87
Solid Hydrides 88
References 89

Nuclear Poisons (Section III)

Gadolinium 91
Dispersion and Nonmetallic Poison Materials 91
References 92

Cladding and Structural Materials (Section IV)

Corrosion 93
Metal–Water Reactions 104
Radiation Effects in Nonfuel Materials 104
Selected Metallurgical Aspects of Cladding Materials 106
Selected Mechanical Properties of Cladding and Structural Materials . . . 112
Ceramic Technology 114
Nonfuel Refractories 115
References 117

Special Fabrication Techniques (Section V)

Melting and Casting 121
Hot and Cold Working of Cast Materials . . 122
Powder Metallurgy 124
Pressure Bonding 126
Plating 126
Explosive Metalworking 127
Joining 128
Nondestructive Testing 131
References 132

Reactor Materials

is one of a series of quarterly technical progress reviews broadly covering the field of nuclear science and technology. Under the auspices of the USAEC Division of Technical Information, *Reactor Materials* is prepared by Battelle personnel from worldwide literature. It covers properties, behavior, and fabrication processes of materials applicable to nuclear reactor components and associated equipment.

The reader will recognize that the scope of this Review is too broad to permit detailed coverage of every topic. Rather, the authors and editors attempt to combine the highlights of significant new developments into an information summary of current research for both management and the technical specialist. As a rule, enough of the results are presented to define the research and summarize the findings. For readers desiring more information on any particular topic, a complete set of references is provided at the end of each section.

Each quarter a number of bibliographies, monographs, and books appear on subjects within the scope of *Reactor Materials*. Although the main purpose of this Review is to call attention to findings that are new and significant, such publications are noted in the text because they often represent excellent compilations of available information on important materials topics.

E. M. SIMONS
S. W. POREMBKA, JR.
D. L. KELLER

Battelle Memorial Institute

Issued quarterly by the U. S. Atomic Energy Commission. Use of funds for printing this publication approved by the Director of the Bureau of the Budget on July 8, 1966.

Section I

Reactor Materials

Fuel and Fertile Materials

Uranium Metal and Alloys

Unalloyed Uranium

The kinetics of oxidation of uranium between 300 and 625°C was studied at Argonne National Laboratory,[1] using a metal-heat-sink reaction cell designed to minimize self-heating. Pure uranium from two sources, as well as uranium containing 1 at.% copper or 1 at.% aluminum, showed substantially identical self-accelerating reaction rates up to 400°C. Oxidation of the pure uranium and of the copper alloy underwent a transition to a slower reaction, in which the oxides were somewhat protective above 500°C. The copper-alloy oxide was considerably more protective than that of the pure metal. The self-accelerating reaction in the aluminum alloy continued to higher temperatures. The results of isothermal oxidation studies for the beta-quenched pure uranium were expressed in the form of empirical equations. From 300 to 450°C the oxidation rate was found to be proportional to $(\text{time})^{5/4}$, whereas above 450°C a decelerating rate proportional to $(\text{time})^{5/6}$ was measured. There is evidence that this change in the reaction kinetics at 450°C is linked to a changed character of the oxide.

Investigators at Atomics International[2] have reviewed and analyzed the steady-state creep data for alpha uranium to determine the boundaries of controlling processes and to establish the existence of unreported mechanisms. Four different processes were found to be controlling at 250 to 660°C. Irradiation-induced cavitation swelling correlates well with a creep process, probably involving nonconservative dislocation motion and boundary migration.

The feasibility of using heat-tinting methods to identify inclusions in uranium metal by color metallography has been demonstrated by Dow Chemical Co.[3] The particles that can be distinguished include UC, U_6Fe, U_3Si, and UAl_2. Electron-metallography studies on uranium have been carried out by Mallinckrodt Chemical Works.[4] Workers there have also reported[5] on uranium and dilute uranium-alloy texture-evaluation studies. Axial and circumferential textures were assessed and employed in studies of alloy content vs. mode of cooling from beta-phase heat-treatment. Oil quenching or isothermal transformation at about 500°C was found to yield the most random structures in extruded core blanks. Circumferential texture variance within centrifugally cast core blanks is associated with the appearance of grain clusters in the macrostructure and can be minimized by isothermal transformation at the upper nose of the TTT diagram for the alloy involved.

The British[6] have published their recent work on the irradiation growth of uranium. Anisotropic distortion of uranium during irradiation was found to be sensitive not only to irradiation temperature but also to the neutron dose and dose rate. The experimental behavior is explained in terms of aggregation, thermal stability, and radiation annealing of the planar vacancy clusters created in displacement cascades.

Alpha-Phase Uranium Alloys

Using electron-microprobe analysis, Mallinckrodt workers[7] performed phase studies in the U–Fe–Si system to determine the solubility of both iron and silicon in beta and gamma uranium and their effect on the transformation temperature of uranium. The results are presented in Figs. I-1 and I-2 and in Table I-1.

In similar studies[8,9] the ternary solubility of aluminum and iron in uranium was determined, with the results presented in Fig. I-3 and I-4.

In further studies[10] high-temperature hot-hardness tests were performed on various "adjusted" uranium alloys containing minor amounts of iron and silicon with parts per million additions of aluminum, chromium, or molybdenum. The hot-hardness tests were performed at 400°C under a 600-lb load applied for 22 hr using both spring-loaded and lever-loaded equipment. The data indicated that the diameter of indentation decreased as the alloy content of the uranium increased. The resistance to indentation, however, appeared to be a function of the degree of solid-solution hardening and not of the total alloy content. A sensitive response to thermal history, therefore, seemed likely. No correlation with resistance to in-reactor swelling was obtained.

The Swedish[11] have reported on the isothermal transformation of gamma-phase adjusted uranium in the beta range. Properties of adjusted uranium (uranium alloyed with 200 to 500 ppm iron and 500 to

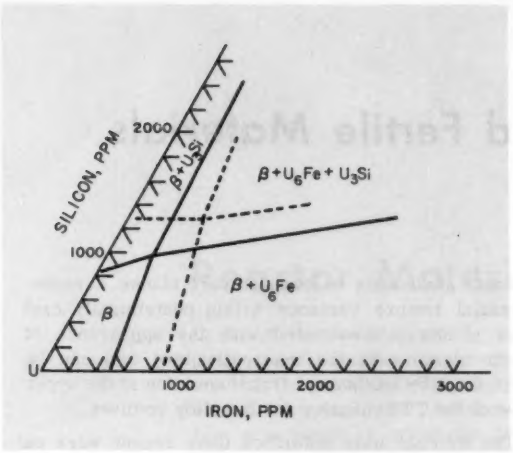

Fig. I-1 The 700 and 750°C isothermal sections of the U–Fe–Si ternary system as determined with the electron microprobe.[7] ——, 700°C; ---, 750°C.

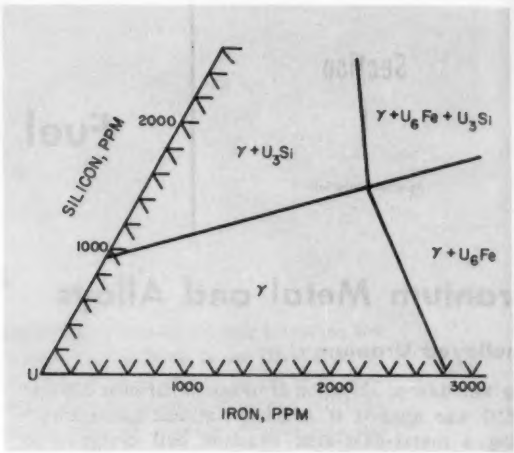

Fig. I-2 The 790°C isothermal sections of the U–Fe–Si ternary system as determined with the electron microprobe.[7]

Table I-1 ALLOTROPIC TRANSFORMATION TEMPERATURES* FOR THE U–Fe–Si TERNARY SYSTEM[7]

Alloying addition to "pure" uranium, wt.%		Transformation temperature, °C	
Silicon	Iron	$\alpha \rightleftharpoons \beta$	$\beta \rightleftharpoons \gamma$
0	0	668	771
0.3	0	665	785
1.63	0.81	666	782
0.53	0.27	663	780
0.67	1.10	665	780
0.26	2.0	665	771
0	0.26	667	763

*Precision = 2°C.

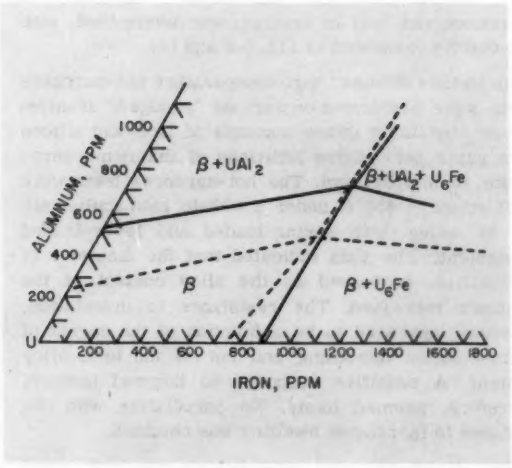

Fig. I-3 The 750°C isothermal section of the U–Fe–Al ternary system as determined with the electron microprobe.[8] ——, present work; ---, Russell.[9]

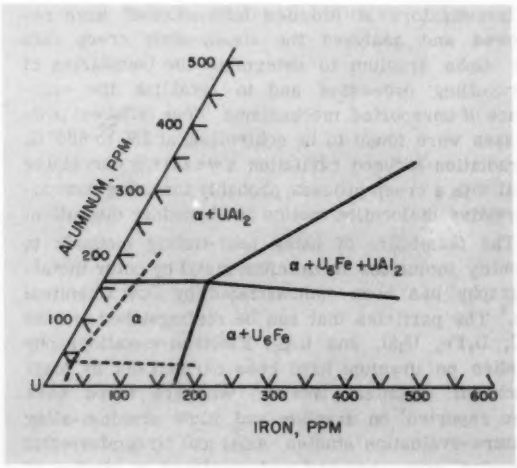

Fig. I-4 The 650°C isothermal section of the U–Fe–Al ternary system as determined with the electron microprobe.[8] ——, present work; ---, Russell.[9]

1200 ppm aluminum) depend largely on the dissolution and precipitation of second-phase particles. Some information was obtained on the precipitation of second-phase particles during isothermal transformation in the beta range directly following a solution treatment in the gamma range. Two adjusted-uranium-type alloys, one with 1200 ppm aluminum, 550 ppm iron, and 500 ppm carbon, the other with 900 ppm aluminum, 350 ppm iron, and 400 ppm carbon, as specimens 2 mm thick, were given a solution treatment in the gamma range by annealing at 800°C for 10 min in argon, directly followed by isothermal holding at 760, 750, 740, 720, 700, and 680°C for periods ranging from 2 sec to 90 min, interrupted by quenching in water. On the basis of observations in a light microscope and on thin foils in an electron microscope, a temperature-vs.-time diagram for the precipitation of second-phase particles was established. These particles were identified by electron diffraction as UAl_2; U_6Fe was not detected.

Argonne[12] has reported on the irradiation performance of the Experimental Boiling Water Reactor (EBWR) Core-IA fuel elements (Zircaloy-2-clad U–5 wt.% Zr–1.5 wt.% Nb plates). These elements received a maximum burnup of 0.6 at.%. Although the maximum rate of volume increase per atomic percent burnup was 7.6% at the point of maximum burnup, increases as high as 13.3% per atomic percent burnup were found in regions of lower burnup. Scale build-ups, in regions free of nucleate boiling, contributed to the higher centerline fuel temperatures by acting as thermal-insulation barriers between the cladding and the water coolant. The temperatures, which were calculated to be in excess of 500°C, resulted in an annealing out of the residual stresses that existed in the fuel elements. These results indicate that, for satisfactory performance at high power levels, the centerline fuel temperature of EBWR-type fuel elements should be maintained below 500°C, through the adequate control of scale accumulation.

A historical review[13] of the development of uranium and alpha-uranium alloys from 1959 to 1966 and a paper dealing with transformation characteristics[14] have been published by Mallinckrodt. Phase equilibria in U–Co–Fe alloys were studied in Portugal,[15] and the Germans[16] published the results of investigations on the system $U-UMn_2-UAl_2-UFe_2$.

Gamma-Phase Uranium Alloys

Oak Ridge National Laboratory[17] has examined the transformation characteristics of a U–7.5 wt.% Nb–2.5 wt.% Zr alloy. The TTT diagram is presented in Fig. I-5. Also investigated were the high-temperature tensile properties of a U–8.5 wt.% Nb alloy, with results shown in Fig. I-6.

(M. S. Farkas)

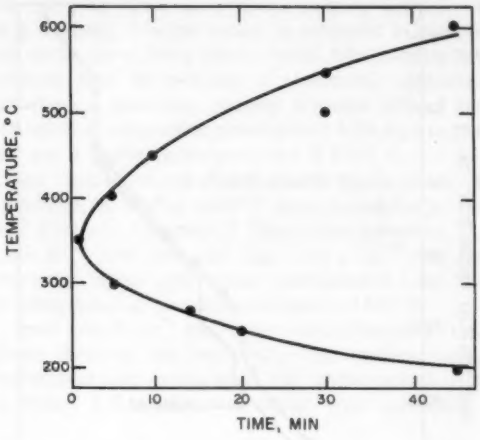

Fig. I-5 Time–temperature transformation diagram, showing the start of transformation for the U–7.5 wt.% Nb–2.5 wt.% Zr alloy.[17]

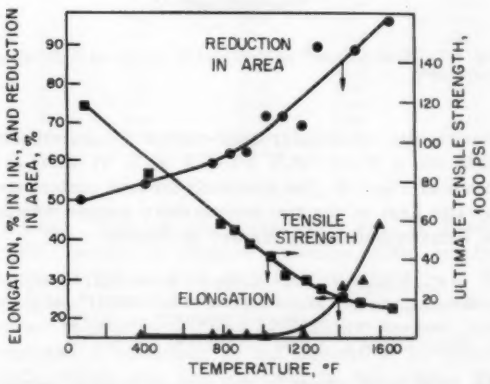

Fig. I-6 Tensile properties of U–8.5 wt.% Nb alloy[17] (heating rate, 4°F/sec; crosshead speed, 0.15 in./sec).

Plutonium

Argonne[18,19] has reported the results of investigations of the thermal properties of U–Pu base alloys. As shown in Fig. I-7, the heat content of a U–15 wt.% Pu–10 wt.% Zr alloy increases monotonically from about 10 cal/g at 300°C to about 55 cal/g at 1150°C. The solid-state heats of transformation of the alloy totaled 8 cal/g. Equations representing the heat content and specific heat for regions outside the transformations (T = °C) are:

$$\Delta H_{(25\text{ to }600^\circ\text{C})} = -0.9 + 0.0310\,T + 0.0000155\,T^2 \text{ cal/g}$$
$$\Delta H_{(650\text{ to }1150^\circ\text{C})} = 14.2 + 0.0185\,T + 0.0000152\,T^2 \text{ cal/g}$$
$$C_{p(25\text{ to }600^\circ\text{C})} = 0.0310 + 0.000310\,T \text{ cal/(g)(°C)}$$
$$C_{p(650\text{ to }1150^\circ\text{C})} = 0.0185 + 0.000304\,T \text{ cal/(g)(°C)}$$

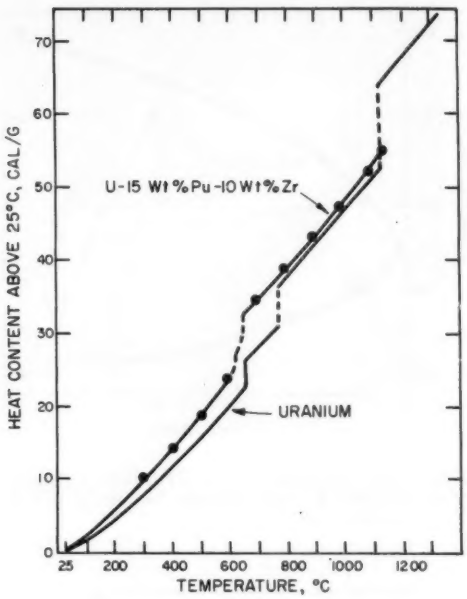

Fig. I-7 Heat content[18] of U–15 wt.% Pu–10 wt.% Zr alloy above 25°C.

The results of similar heat-content measurements made on a U–15 wt.% Pu–6.5 wt.% Ti alloy are shown in Fig. I-8. The equations for heat content and specific heat in the two temperature ranges outside the transformation regions are as follows:

$$\Delta H_{(25 \text{ to } 550°C)} = -0.7 + 0.0324T + 0.0000126T^2 \text{ cal/g}$$
$$\Delta H_{(850 \text{ to } 1150°C)} = 57.1 - 0.0531T + 0.0000521T^2 \text{ cal/g}$$
$$C_{p(25 \text{ to } 550°C)} = 0.0324 + 0.0000252T \text{ cal/(g)(°C)}$$
$$C_{p(850 \text{ to } 1150°C)} = 0.0531 + 0.000104T \text{ cal/(g)(°C)}$$

The total heat effect in the transformation region, 550 to 850°C, is 28.7 cal/g.

Los Alamos has recently reported the results of investigations on the stability of the delta phase in Pu–Ga alloys.[20] Conclusions reached in the study are given below.

1. The delta phase in cast alloys containing between 0.1 and 1.0 wt.% gallium is unstable during thermal cycling between –40 and +76°C.
2. Heat-treatment at 425°C for 70 hr increases the stability of the alloys, but their stability depends on the severity of the treatment to which they are subjected as well as on their gallium contents as follows:
   a. 0.6 wt.% gallium stabilizes the delta phase at –80°C but not at –194°C
   b. 0.45 wt.% gallium or more stabilizes delta during cycling between –40 and +76 or +90°C but not at –80°C or lower
   c. 0.3 wt.% gallium or more stabilizes delta at 4°C but not at –40°C or lower
   d. 0.1 or 0.2 wt.% gallium is not sufficient to stabilize delta at 4°C and perhaps not at room temperature
3. In the present work the maximum conversion of delta to alpha in alloys containing from 0.1 to 0.6 wt.% gallium was attained by thermal cycling between –194°C and room temperature.
4. The rate of cooling to –80°C appeared to have a slight effect on the stabilities of the alloys containing 0.5 wt.% or less gallium, in that a faster rate (100°C/min) resulted in slightly higher densities than did a slower rate (4°C/min).
5. The alloy containing 0.3 wt.% gallium was unstable when deformed by swaging at room temperature, but subsequent cycling between –40 and +76°C was then less effective toward converting the remaining delta phase to alpha than similar cycling had been toward converting the delta phase in undeformed specimens of the same alloy composition. Deformation had little, if any, effect on alloys containing more than 0.3 wt.% gallium. (V. W. Storhok)

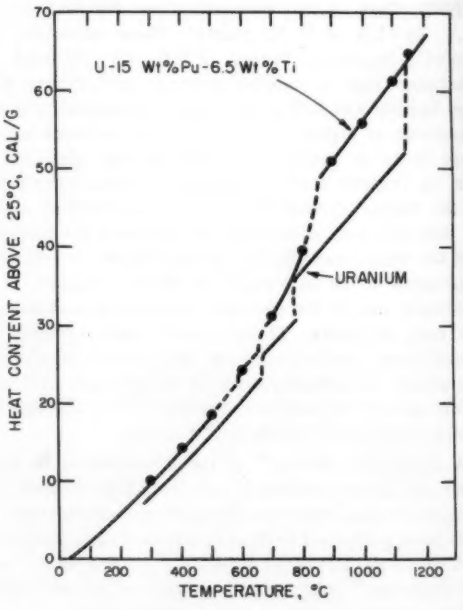

Fig. I-8 Heat content[18] of U–15 wt.% Pu–6.5 wt.% Ti alloy above 25°C.

Plutonium Compounds

At Harwell[21] the compatibility of plutonium carbides with silicon carbide is being studied in the temperature range 900 to 1400°C. Plutonium monocarbide (PuC) reacts with SiC to form Pu_2C_3 and Pu_3Si_5 at rates sufficiently rapid to make this com-

bination impractical in reactor systems at temperatures as low as 1100°C. The compound Pu_2C_3 was found to be inert in contact with SiC at 1300°C, so that SiC could be used as a coating material or dispersion matrix for Pu_2C_3 fuel. The solubility of silicon in PuC and Pu_2C_3 was determined to be less than 0.1 wt.%.

Argonne[22,23] is conducting a series of compatibility tests involving stoichiometric (4.83 wt.% equivalent carbon) and hyperstoichiometric (5.25 wt.% equivalent carbon) mixed uranium–plutonium monocarbides with several high-temperature cladding materials, with the following results:

Haynes 56

No reaction was observed after 42 days (1000 hr) at 900°C with either stoichiometric or hyperstoichiometric (U,Pu)C.

Alloy 16-25-6

A mottled surface, accompanied by disappearance of grain boundaries to a depth of 25 to 35 μ, was observed at 800°C after 42 days. No mottling occurred at 700°C after 42 days, although some grain-boundary disappearance was noted.

V–15 wt.% Cr–5 wt.% Ti

No reaction was observed after 42 days of exposure at 800°C.

Inconel 625

A reaction zone was observed in both stoichiometric and hyperstoichiometric (U,Pu)C at 700 and 800°C. The reaction zone consisted of three regions: (1) a layer in the direction of the fuel, (2) a mottled region in the direction of the cladding, and (3) a precipitate in the cladding beyond (2). Average reaction-zone thicknesses for 42-day tests are shown in Table I-2.

Table I-2 THICKNESSES OF REACTION LAYERS BETWEEN INCONEL 625 AND (U,Pu)C AFTER 42-DAY EXPOSURES[23]

	Average thickness of reaction zone, μ		
	In direction of fuel	In direction of cladding	Precipitates in cladding
Stoichiometric and hyperstoichiometric (U,Pu)C at 700°C	18	20	25
Stoichiometric (U,Pu)C at 800°C	25	23	105
Hyperstoichiometric (U,Pu)C at 800°C	36	26	120

Argonne[23] is preparing $(U_{0.85}Pu_{0.15})C$ by a fluidized process. Alloy metal rods are hydrided, and then the hydrided powder is fluidized in a mixture of CH_4 and H_2 at 550 to 800°C at 2 to 4 atm. The carbiding rate rapidly decreases after 4.0 to 4.2 wt.% carbon is reached, and it is advantageous to rehydride the residual metal before a stoichiometric (U,Pu)C product can be obtained [stoichiometric (U,Pu)C = 4.8 wt.% carbon]. Twelve hours is required to complete the cycle for a 300-g batch. Initial fabricability tests indicate that the powder is moderately sinterable, achieving a maximum density of about 91% of theoretical at a compaction pressure of 4.23 metric tons/cm² and a sintering temperature of 1650°C.

The self-diffusion coefficients of uranium and plutonium in UO_2 at 2400°C were measured by General Electric Company.[24] The values observed, $D_U = 2.6 \times 10^{-10}$ cm²/sec and $D_{Pu} = 3.4 \times 10^{-10}$ cm²/sec, generally agree with values extrapolated from other investigations at temperatures below 1700°C.

Lyon and Baily[25] have determined the solid–liquid phase diagram for the PuO_2–UO_2 system using a thermal-arrest technique. The observations listed in Table I-3 were made using solid solutions of

Table I-3 SOLIDUS–LIQUIDUS OF UO_2–PuO_2 SYSTEM[25]

Mole % PuO_2	Liquidus, °C		Solidus, °C	
	Observed	Calculated	Observed	Calculated
0	2840 ± 20	2840	2840 ± 20	2840
10	2825	2806	2805	2788
20	2790	2770	2760	2737
25	2760	2752	2710	2712
40	2690	2693	2635	2640
55	2630	2630	2580	2572
70	2555	2559	2490	2508
85	2460	2491	2420	2447
100	2390	2390	2390	2390

$(U,Pu)O_2$, with an oxygen-to-metal ratio of 2.000 ± 0.002, sealed in tungsten capsules under purified argon at 200 psig to suppress volatilization of the samples. Other investigators, observing melting under helium in a tungsten-filament furnace, have reported a maximum in the liquidus at 10 mole % PuO_2 which was not observed in this study. The effect of initial stoichiometry was determined on $(U_{0.8}Pu_{0.2})O_{2\pm x}$ samples. The melting point increased as the O/M ratio decreased from 2.06 to 1.97, the most rapid increase being observed between 1.985 and 1.97.

Sintering studies have been conducted on PuO_2 powders prepared from plutonium(III) oxalate and plutonium(IV) peroxide by Los Alamos Scientific Laboratory.[26] Pellets pressed from PuO_2 prepared by the peroxide method first showed reduction to alpha Pu_2O_3 following a 6-hr sinter in dry argon between 1250 and 1350°C. Sintering in dry CO_2 prevented the formation of alpha Pu_2O_3. It was calculated that an oxygen partial pressure of 3.6×10^{-9} atm is sufficient to prevent detectable decomposition of PuO_2 at a temperature of 1650°C for 6 hr. The PuO_2 prepared from the oxalate showed the formation of alpha Pu_2O_3 at a sintering temperature approximately 150°C higher than that for the peroxide-prepared material in an argon atmosphere.

A process has been developed by the French[27] for the sintering of $(U,Pu)O_2$ pellets that reportedly results in a more positive control of sintering shrinkage. Calcined PuO_2 and either UO_3 or U_3O_8 powders are blended, compacted, and sintered in a two-stage cycle: at 300 to 400°C to reduce the uranium oxide to UO_2, followed by a high-temperature sinter at 1600 to 1650°C in argon containing 10 vol.% hydrogen. This pre-sintered material, called "chamotte," is crushed and blended with virgin PuO_2-UO_3 (or U_3O_8) in a ratio of about 4:1. This blend is compacted into pellets and sintered as above. The virgin powder constitutes the bond between the chamotte grains. Sintering shrinkage is reduced by the addition of the chamotte grains, and pellets with 96 to 99% of theoretical density are obtainable. (W. M. Pardue and D. F. Askey)

Thorium

The partial phase diagram in the Th–C system between thorium and ThC was investigated by the Japanese.[28] The peritectic point of the reaction, liquid + ThC ⇌ alpha thorium, was found at 16 at.% carbon and about 1875°C, and the peritectic composition of ThC was 33 at.% carbon. The eutectic reaction occurred at 1650°C, and its compositions of alpha thorium and beta thorium was 6.5 and <0.5 at.% carbon, respectively.

Compatibility tests were conducted at Oak Ridge between thorium and various uranium compounds.[29] The compounds UB_2 and UB_4 were found to be compatible with thorium at temperatures up to 1000°C for 100 hr. Other compounds investigated but found to be reactive with thorium were US, UP, (U,Th)C, and $(U,Th)O_2$.

The thermal conductivity of thorium metal, measured over the temperature range from 75 to 800°C by workers at Union Carbide Corporation,[17] increased linearly from 0.355 watt/(cm)(°C) at 75°C to 0.430 watt/(cm)(°C) at 800°C. The purity of the material was not given. (R. L. Martin)

Metal–Ceramic Fuels

Dispersion Fuels (Less Than 50 Vol.% Ceramic Phase)

Workers at the National Reactor Testing Station[30] are studying in some detail the role of porosity in dispersion-fuel swelling. Uniform swelling was related to solid fission products and the initial core density. It was shown for the dispersion fuels considered (UAl_x, U_3O_8 and UO_2 in aluminum, and UO_2 in stainless steel) that controlled initial porosity promotes fuel stability for low-temperature, high-burnup conditions. In some cases swelling was $\frac{1}{8}$ to $\frac{1}{3}$ of the value calculated for dense fuel. (D. E. Lozier)

Cermets (Over 50 Vol.% Ceramic Phase)

The fabrication and irradiation testing of low-density (85% of theoretical) 60 vol.% UO_2–stainless-steel cermet pellets are in progress for the fast "settled-bed reactor" concept work at Brookhaven National Laboratory.[31] In irradiations conducted at 1200°F (648°C), fuel-pellet surface temperatures, pellets sustained thermal stresses and burnups as high as 37,000 psi and 3.8 at.%, respectively, without detectable matrix failure. The promising performance of these low-density pellets suggested that higher burnups could have been sustained. (R. A. Smith)

Coated-Particle Fuels

General Atomic[32] is developing and evaluating metal carbide barriers for pyrolytic carbon (PyC) coatings on nuclear fuel particles for improved retention of fission products. Carbides of the metals silicon, zirconium, and beryllium are of most interest, with emphasis on SiC. Initial evaluation indicates that the release of ^{140}Ba and ^{91}Sr is lower by a factor of 100 to 500, as compared to PyC without a SiC layer within the PyC coating. An objective of another study[33] at General Atomics is a more complete understanding of properties required for an inner buffer coating of porous PyC to enhance radiation stability of fuel particles. For this study, porous PyC coatings were applied to 150- to 250-μ-diameter fuel particles by pyrolysis of acetylene at temperatures of 900 to 1200°C and at reactant concentrations of 60 to 100% in a fluidized-bed coating unit. The lowest density PyC coatings (0.7 to 0.8 g/cm^3) were obtained at 950 to 1000°C. It was noted that the density of the coating decreases with an increase in acetylene concentration. Workers at Oak Ridge[29] report similar findings on the preparation of porous PyC. The lowest density coating (0.6 g/cm^3) was obtained with undiluted acetylene at a supply rate of 6.2 cm^3/min for each square centimeter of particle surface. With the undiluted acetylene the effect of coating temperature in the range of 950 to 1150°C was insignificant. Total accessible porosity was 65% or greater in coatings having a density of 0.6 g/cm^3.

Also at Oak Ridge, development of remotely operable production-scale PyC-coating equipment[34] is being continued. A 5-in.-diameter fluidized-bed unit for application for PyC at temperatures up to 2800°C is being assembled and tested. With speculation that an entrained-bed method might offer advantages over the more conventional fluidized-bed units, use of an entrained-bed unit is also being explored. A schematic layout of the entrained-bed unit is shown

in Fig. I-9. Particles are entrained and partially coated in the central column of the unit, disentrained in the upper section, and returned to the bottom of the unit for recycle. Batches of 2500 g of 200- to 400-μ-diameter ThO_2 sol–gel particles have been coated, but exhaust-filter blockage caused premature interruption of all runs thus far.

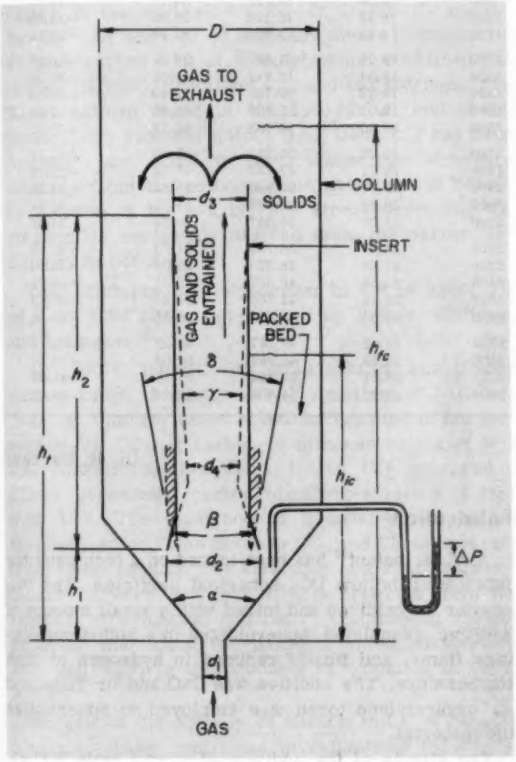

Fig. I-9 Entrained bed for pyrolytic carbon coating of nuclear fuel particles.[34] D = column inside diameter, d_1 = nozzle inside diameter, d_2 and d_4 = insert diameters for various geometries, α = bottom cone angle, β, γ, and δ = various insert tapers, h_1 = distance between nozzle and lower end of insert, h_2 = length of insert, h_t = minimum total conveying height, h_{ic} = initial height of charge, h_{fc} = final height of (coated) charge (this height can exceed the upper end of the insert without choking the system if conveying is consistently maintained), and ΔP = differential pressure measured in the packed bed near the lower end of the insert against atmosphere for a column open at the top.

A study of the effects of deposition conditions on the properties of PyC coatings derived from propane[35,36] has been completed by workers at Oak Ridge. Results obtained with propane are similar to those obtained with methane, with one major exception. The PyC coatings applied at 1200°C with a propane supply rate of 3.2 cm^3/min for each square centimeter of particle surface are randomly oriented, have a density of 2.0 g/cm^3, and are deposited at a rate of 9 μ/min. Achievement of comparable coatings from methane requires a deposition temperature of 2000°C at gas flow rates that limit the deposition rate to 1 μ/min.

Workers at Battelle Memorial Institute[37] are investigating the feasibility of coating fuel particles with graphite by precipitation from liquid-metal solutions. It is reasoned that the substitution of ordered graphite for the turbostratic material obtained in vapor deposition should lead to more stable coatings. Initial experiments have demonstrated that graphite coatings can be deposited on surfaces in contact with carbon-saturated nickel solutions. The coatings were formed on controlled cooling of the liquid-metal solution from 1600°C. (N. D. Veigel)

Uranium and Thorium Oxides

Properties and Behavior

A recent International Atomic Energy Agency publication[38]* presents an up-to-date summary on the thermal conductivity of both unirradiated and irradiated UO_2, in addition to the mechanisms of heat transfer in UO_2. Most of the data available into 1965 have been summarized, and this reference is a good source of practical information for use in UO_2 heat-transfer calculations.

Papers on fission-gas release from UO_2, presented at the Gatlinburg Fission-Gas Release Symposium of the American Nuclear Society in June 1965, are available in the April 1966 issue of *Nuclear Applications*.[39] The papers deal mainly with fission-gas release during irradiation, the trapping of migrating species in UO_2, and the engineering aspects of fission-gas release in UO_2 fuels.

Italian investigators[40] have measured knock-out for fission fragments recoiling from UO_2. For sintered UO_2 with a density of 10.74 g/cm^3, a knock-out coefficient of 260 (oxygen + uranium atoms) per recoil was measured. From the analysis of the data, it was concluded that the knocked-out atoms leaving the surface of the UO_2 have kinetic energies not far above the thermal range.

Thermodynamic data on UO_2 and ThO_2 have been compiled at Oak Ridge.[41] The data for UO_2 are listed in Table I-4. The heat-capacity data follow the equation $C_p = 13.51 + (1.91 \times 10^{-2})T - (1.16 \times 10^{-5})T^2 - (8.54 \times 10^2)/T$ over the temperature range from 298

*Available from the National Agency for International Publications, Inc., 319 East 34th Street, New York, N. Y. 10016.

to 876°K with an average error of 0.4%, whereas the enthalpy data fit the relation

$$H_T^\circ - H_{298}^\circ = 5.48923T + (2.29415 \times 10^{-2})T^2 - (1.64614 \times 10^{-5})T^3 + (5.31362 \times 10^{-9})T^4 - (5.72023 \times 10^{-13})T^5 - 3280.31 \text{ cal/mole}$$

over the temperature range from 483 to 2623°K. The data for ThO_2 are given in Table I-5. In the case of the ThO_2, the enthalpy data follow the expression

$$H_T^\circ - H_{298}^\circ = 16.5643T + 1.11607 \times 10^{-3}T^2 + 2.19547 \times 10^5/T - 5774.21 \text{ cal/mole}$$

with an average error of 0.58%.

Lattice and grain-boundary diffusion of uranium ions in polycrystalline UO_2 were measured by Japanese workers[42] in the temperature range 1900 to 2150°C using a sectioning technique with ^{237}U as a tracer. The lattice diffusion coefficient was found to be given by

$$D = 5.82 \times 10^{-5} \exp(-72{,}700/RT) \text{ cm}^2/\text{sec}$$

The grain-boundary diffusion data were correlated in terms of the expression

$$D' \times 2a = 5.19 \times 10^{-9} \exp(-47{,}200/RT) \text{ cm}^3/\text{sec}$$

where D' and $2a$ are the grain-boundary diffusion coefficient and grain-boundary width, respectively.

Table I-4 THERMODYNAMIC DATA[41] FOR UO_2

Temp., °K	C_p°, cal/(mole)(°K)	$H_T^\circ - H_{298}^\circ$, cal/mole	S_T°, cal/(mole)(°K)	$(F_T^\circ - H_{298}^\circ)/T$, cal/(mole)(°K)
298.15	15.32	0	18.63	−18.63
300	15.36	28	18.72	−18.63
400	17.23	1,663	23.41	−19.26
500	18.56	3,456	27.41	−20.50
600	19.46	5,361	30.88	−21.95
700	20.01	7,337	33.93	−23.44
800	20.30	9,354	36.62	−24.93
900	20.40	11,391	39.02	−26.36
1000	20.38	13,431	41.17	−27.74
1100	20.31	15,465	43.11	−29.05
1200	20.23	17,492	44.87	−30.29
1300	20.20	19,513	46.49	−31.48
1400	20.27	21,536	47.99	−32.60
1500	20.45	23,571	49.39	−33.68
1600	20.79	25,632	50.72	−34.70
1700	21.30	27,735	51.99	−35.68
1800	22.01	29,899	53.23	−36.62
1900	22.90	32,143	54.44	−37.53
2000	23.99	34,486	55.65	−38.40
2100	25.27	36,947	56.85	−39.25
2200	26.73	39,546	58.06	−40.08
2300	28.34	42,299	59.28	−40.89
2400	30.09	45,219	60.52	−41.68
2500	31.92	48,319	61.79	−42.46
2600	33.82	51,605	63.07	−43.23
2700	35.72	55,082	64.39	−43.99
2800	37.57	58,747	65.72	−44.74
2900	39.31	62,592	67.07	−45.48
3000	40.88	66,604	68.43	−46.23

Table I-5 THERMODYNAMIC DATA[41] FOR ThO_2

Temp., °K	C_p°, cal/(mole)(°K)	$H_T^\circ - H_{298}^\circ$, cal/mole	S_T°, cal/(mole)(°K)	$(F_T^\circ - H_{298}^\circ)/T$, cal/(mole)(°K)
298.15	14.76	0	15.59	−15.59
300	14.79	27	15.68	−15.59
400	16.08	1,579	20.14	−16.19
500	16.80	3,226	23.81	−17.36
600	17.29	4,932	26.92	−18.70
700	17.68	6,681	29.61	−20.07
800	18.01	8,466	32.00	−21.41
900	18.30	10,282	34.13	−22.71
1000	18.58	12,126	36.08	−23.95
1100	18.84	13,997	37.86	−25.14
1200	19.09	15,893	39.51	−26.27
1300	19.34	17,814	41.05	−27.34
1400	19.58	19,760	42.49	−28.38
1500	19.81	21,730	43.85	−29.36
1600	20.05	23,723	45.13	−30.31
1700	20.28	25,740	46.36	−31.22
1800	20.51	27,780	47.52	−32.09
1900	20.74	29,842	48.64	−32.93
2000	20.97	31,928	49.71	−33.74
2100	21.20	34,037	50.74	−34.53
2200	21.43	36,169	51.73	−35.29
2300	21.66	38,323	52.69	−36.02
2400	21.88	40,500	53.61	−36.74
2500	22.11	42,700	54.51	−37.43
2600	22.34	44,922	55.38	−38.10
2700	22.56	47,167	56.23	−38.76
2800	22.79	49,434	57.05	−39.40
2900	23.01	51,724	57.86	−40.02
3000	23.24	54,036	58.64	−40.63

(R. H. Barnes)

Fabrication

A U. S. patent[43] has been issued on a technique for fabricating hollow UO_2 spherical particles. The UO_2 powder is oxidized and mixed with a small amount of additive, granulated, spheroidized in a high-temperature flame, and finally reduced in hydrogen at high temperature. The additive was CaO and/or TiO_2, and an oxyacetylene torch was employed to spheroidize the material.

The effects of the addition of up to 5 mole % CaO, Cr_2O_3, and Y_2O_3 on the sintering of UO_2 have been investigated in Germany.[44] It was assumed that the additional oxide did not form a liquid phase during sintering. The oxides were produced by mixed precipitation and sintered at 1350 to 1700°C in argon and hydrogen. It was found that both CaO and Y_2O_3 cause grain refinement as a result of solid-solution formation. Additions of Cr_2O_3 resulted in grain growth that was attributed to a special oxidation–reduction mechanism.

Fargo[45] reports on an economical technique for producing UO_2 fuel plates. The UO_2 powder is first mixed with a cellulose compound and an organic solvent. The plastic mass is then rolled into a thin continuous strip from which fuel plates are cut or punched. Densities in the order of 94 to 97% of theoretical have been achieved on sintering. The O/U ratio of the final sintered shapes is reported as being 2.00. (T. R. Wright)

Uranium Carbides, Nitrides, Phosphides, and Sulfides

Properties and Behavior

The addition of 15 wt.% PuC to UC produced no observable change from ternary-phase relations at compositions containing slightly less than 50 at.% carbon in the systems U–Mo–C, U–Ti–C, and U–Zr–C.[46] An alloy of 43 at.% (uranium + plutonium) + 47 at.% carbon + 10 at.% molybdenum contained the phases (U,Pu)C, (U,Pu)MoC_{2-x}, and molybdenum. The X-ray pattern found at the low-carbon end of the homogeneity range of $UMoC_2$ (i.e., $UMoC_{2-x}$) has been indexed[47] and found to be a monoclinic structure obtained from the orthorhombic structure of $UMoC_2$ by rotation of the *c*-axis. The stress producing the rotation is apparently derived from the carbon deficiency in $UMoC_{2-x}$.

The solubility of molybdenum in UN is about 0.1 wt.% at 2600°C, as determined by Potter, Godfrey, and Leitnaker.[48]

At 1700°C the UC–UN solid solution has a very narrow range of homogeneity.[49] Additions of 3 mole % "UO" to this series of solutions resulted in the formation of UC_2 at carbon-to-nitrogen ratios of 3:1 and possibly as low as 1:1, but UO_2 appeared in alloys possessing carbon-to-nitrogen ratios of less than 1:3. The existence of a quasi-binary of low terminal solubilities between UO_2 and UN is apparent from these results. The existence of a similar quasi-binary between UO_2 and U_2N_3 is apparent from the results of Uchikoshi and Ishii[50] (confirming earlier reports) who found two-phase oriented mixtures of UO_2 and U_2N_3 in the products of oxidation of UN at 900°C.

Studies of the activity of carbon in UC at General Electric[51] have confirmed investigations by Storms reported in a previous review, which showed that most of the carbon-activity change in the entire U–C system occurs across the very narrow homogeneity range of UC. The activity of carbon in UC in equilibrium with uranium decreases rapidly from 2027 to 1500°C.

A method by which uranium carbide can be made compatible with stainless steel and other cladding materials has been patented by Webb and Koenig.[52] The method involves alloying the UC with elements that, like the constituents of stainless steel, react with the excess carbon or uranium in the UC but do not react (in most cases) with the UC itself. The application of this technique to (U,Pu)C is being studied at Argonne[53] and is at least partially effective.

In common with the effect of most soluble alloying additions on UC, it has been found that oxygen additions to UC to form U(C,O) make it more resistant to hydrolysis by water.[54]

Over a period of several hundred hours at 400 to 500°C, UC reacts with nitrogen to form U_2N_3 and free carbon.[55] A quasi-binary system between graphite and $U_2(N,C)_3$ is implied by these data. The PuC reacts with somewhat more difficulty with nitrogen to give PuN and free carbon.

At centerline temperatures[56] of 660 to 980°C and surface temperatures of 400 to 560°C, hypostoichiometric slugs of UC (4.6 wt.% carbon) survived burnups of 20,000 to 28,000 Mwd/metric ton of uranium with a gas release of 0.7% and density changes of 5.2 to 8.6%. The ½-in.-diameter slugs were sodium bonded to 0.010-in.-thick 304 stainless steel, which was not embrittled by the exposure. This report also contains an extensive review of irradiation results on both hypostoichiometric and hyperstoichiometric UC.

In Canadian studies,[57] ten ½-in.-diameter slugs of slightly hypostoichiometric UC were irradiated in SAP to various burnups with four of the slugs continued to a burnup of 11,000 Mwd/metric ton of uranium. Measured central temperatures decreased from 1620°C at the beginning to 1020°C at the end of the irradiations. The irradiations were terminated when the element with the highest burnup split its cladding. The slugs showed maximum diametral expansions of up to 1.5% and maximum decreases in density of up to 6%. Maximum fission-gas release was 1.25%. Fission-gas-bubble formation was particularly noticeable in the uranium film at grain boundaries and became more pronounced toward the central axis of the slugs.

Samples of UN–20 wt.% PuN, irradiated by Battelle–Northwest to a rather low burnup (2.4×10^{20} fissions/cm^3) at an extremely high heat rating (2130 watts/cm), have shown radial stratification of impurities and fission products.[58,59] The samples were hypostoichiometric, only 70% dense, and showed no failures, so that the significance of the radial redistribution of impurities and fission products is not clear.

Argonne workers have noted that uranium arsenide (UAs) has a face-centered cubic structure with a lattice parameter of 5.777 A; it melts at 2450°C and is completely soluble in all proportions in UP and US.[22]

The vapor pressures of UP and US have been redetermined.[19] A pressure of 0.1×10^{-6} atm was obtained at 1943°K for UP and at 1923°K for US. A pressure of 1×10^{-6} atm was obtained at 2100°K for UP and at 2070°K for US. The properties of UP have been collected and reviewed by Baskin.[60] (W. Chubb)

Synthesization of UC

Studies at The Carborundum Company[61] show the feasibility of preparing UC by utilizing a coprecipitation technique. In these experiments $UO_2(NO_3)_2 \cdot 6H_2O$ and sucrose were dissolved in distilled water, and then the carbon- and metal-bearing materials were coprecipitated by evaporating the water at 100°C.

The dried residue was reacted at 1700°C for 5 hr under a flowing argon atmosphere. A heating cycle of 100°C/hr to 600°C and then 750°C/hr from 600 to 1700°C was used. Results indicate that the variation in the oxygen content of the original $UO_2(NO_3)_2 \cdot 6H_2O$ can cause difficulty in controlling the carbon content of the final UC product. The objective of this work is to extend this technology to the preparation of (U,Pu)C fuels for fast reactors.

A Canadian patent[62] describes a process for pressing and sintering powder fuel pellets of uranium oxide, carbide, nitride, or silicide. Each pellet has a projection and recess on opposite ends in the form of a truncated cone. When loaded into the tube, the projection on one pellet fits into the recess of its neighbor in the tube, thus preventing lateral movement so that a column of pellets acts like a rigid rod.

(D. S. Acuncius)

Fuel–Water Reactions

The effects of temperature, relative humidity, and *p*H on the rate of the uranium + water reaction

$$U + 2H_2O \rightarrow UO_2 + 2H_2$$

have been studied in detail between 35 and 240°C by British researchers.[63] Linear rates of corrosion and hydrogen evolution are obtained at different temperatures, and the derived activation energies vary from 12 to 17 kcal/mole, depending on the batch of uranium. Figure I-10 illustrates some kinetic data obtained by these investigators and shows the effect of temperature on the reaction. The influence of water-vapor pressure on reaction rate is complicated by the change in form of the dependence with different batches of uranium. Gravimetric studies at constant humidities yielded linear corrosion-time plots, from which vapor pressure-rate relations were obtained (Fig. I-11). It is interesting to compare these linear oxidation rates with those reported by Argonne[64] at high temperatures discussed on page 14 of *Reactor Materials*, 10(1). The Argonne workers report parabolic rather than linear rates at temperatures greater than 600°C. Hydrogen apparently has no effect on the reaction.

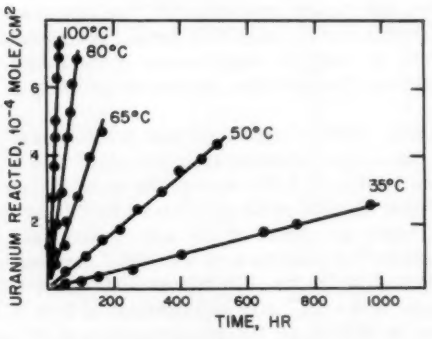

Fig. I-10 Corrosion of uranium by water vapor (relative humidity = 100%) in a sealed system.[63] Identical results are obtained under immersion conditions. Plots of hydrogen evolution (10^{-4} half-mole/cm^2) against time are almost coincident.

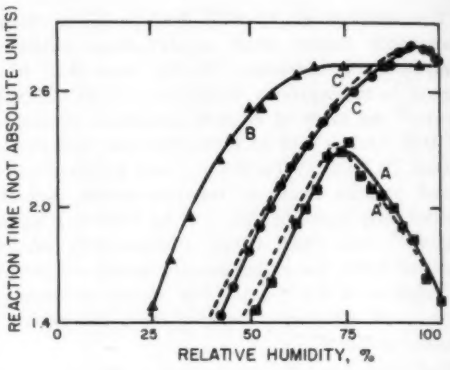

Fig. I-11 Variation of uranium–water reaction rate[63] with water-vapor pressure at 80°C. A, sample 1 (rod); B, sample 2 (foil); C, sample 3 (rod); data from hydrogen evolution. A', C', gravimetric data.

The linear rates of oxidation for uranium immersed in solutions at various *p*H values are shown in Fig. I-12. The oxidation rates in the presence of acetic, nitric, and sulfuric acids are equivalent at equivalent *p*H values, and a similar equivalence applies in the alkaline region with sodium hydroxide, potassium hydroxide, and analine. Thus the oxidation rates depend upon the balance of hydrogen-ion and hy-

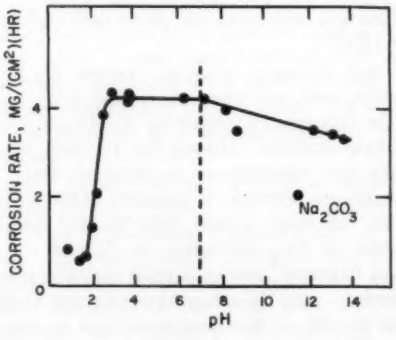

Fig. I-12 Variation of uranium–water reaction rate[63] with pH at 100°C.

droxide-ion concentrations and not upon the other species present. The corrosion rate in the presence of sodium carbonate is exceptional. Furthermore, uranium samples were immersed in water and exposed to gamma irradiation from a ^{60}Co source. Although the samples received approximately 72 Mrads at 30°C, the corrosion rate was not enhanced by the irradiation.

Parallel studies have been made of the uranium hydride + water system. The data are consistent with an oxide product $UO_{2.06\pm0.02}$, containing 2 to 9 wt.% uranium hydride in a protected form. On the basis of these results, a reaction mechanism is proposed for the uranium–water reaction involving OH^- ion diffusion and formation of uranium hydride as a partial intermediate. The reaction scheme suggested is

$$H_2O \rightarrow H^+ \text{ (hydrated)} + OH^- \text{ (at oxide surface)}$$

$$\left.\begin{aligned} U &\rightarrow U^{4+} + 4e^- \\ OH^- &\rightarrow O^{2-} + H^+ \\ H^+ + e^- &\rightarrow H^0 \end{aligned}\right\} \text{concomitantly at the uranium–uranium oxide interface}$$

H^0 is very reactive and may attack uranium or diffuse to the solid interface

$$3H^0 + U \rightarrow UH_3$$

Electrons, or positive holes, can diffuse through the oxide

$$e^- + H^+(\text{hydrated}) \rightarrow H^0$$

and molecular hydrogen will be evolved at the solid–gas interface

$$2H^0 \rightarrow H_2$$

In this reaction scheme uranium hydride is a partial product of uranium oxidation and would be expected to react with water to give hydrogen and uranium dioxide

$$2UH_3 + 4H_2O \rightarrow 2UO_2 + 7H_2$$

In a companion paper[65] the rate and products of the uranium + water + oxygen reaction were investigated. The results indicate that oxygen reduces the corrosion rate 30- to 100-fold and is consumed during the reaction. Although the oxygen is converted to water, it does not react directly with the uranium. Only traces of hydrogen are involved except under condensation conditions. A mechanism for the reaction is postulated, again involving the diffusion of hydroxyl ions. Hydrogen, nitrogen, and carbon dioxide have little or no effect on the uranium + water reaction.

(J. M. Genco)

Basic Studies of Irradiation Effects in Fuel Materials

Metals

Strain rates, strains, and stresses resulting from irradiation growth and swelling in long, cylindrical, solid fuel elements in unsteady-state conditions were determined analytically.[66] From the simple diffusion equation for a nonequilibrium reactor system, an exact solution for neutron-flux distribution was found in the form of products of Bessel functions by exponential time functions. From the heat-conduction equation with an internal heat source in unsteady state, a solution for temperature distribution in the fuel elements was obtained. A physicomechanical analysis for the fuel elements was carried out with some basic assumptions concerning the properties, fabrication, end conditions, and yield conditions of the fuel and cladding materials.

At Harwell[67] it has been found that the inert gases produced in nuclear materials during irradiation precipitate readily as small bubbles, and, because of their insolubility, the subsequent behavior of the gases is determined by the behavior of these bubbles. Thus their behavior determines both how much gas is released and the swelling that is produced by the gas retained. It is shown that bubbles can migrate bodily under the influence of various driving forces and by various mechanisms, and that, in most practical cases, directed migration due to temperature gradients, stress gradients, and moving dislocation lines or grain boundaries is more important than Brownian motion, except in short furnace anneals. Analysis of the various driving forces shows that small bubbles are dominated by the behavior of dislocation lines, but as the size of the bubbles increases, the temperature gradient becomes more important. Thus it is important for the temperature gradient to be known.

It has been found[68] that, in spite of the growing recognition that the motion of inert gases in ion-bombarded solids constitutes a solid-state probe of potentially wide applicability, the relevant diffusion theory has been to some extent neglected. The present work attempts to extend this theory. Use is made of the equation for true diffusion,

$$\partial C_1/\partial t = (D/\lambda^2)(\partial^2 C_1/\partial x^2)$$

the equation for single-jump diffusion, $dC_1/dt = -k' C_1$, as well as the modified equation of Hurst and Gaus,

$$\partial C_2/\partial t = (D/\lambda^2)(\partial^2 C_2/\partial x^2) - (D/L^2\lambda^2)C_2$$

where the final term takes permanent trapping into account. Various geometries and types of diffusion appropriate for ion bombardments are considered,

namely, the plane source (for very low or very high bombardment energies and for amorphous targets), the peaked or "xe^{-x}" distribution (for low-mass, polycrystalline targets), the exponential or "e^{-x}" distribution (for high-mass, polycrystalline targets and for bubble motion), the homogeneously labeled sphere (for high-energy bombardments of fine powders), and single-jump diffusion (for gas release of the type "damage diffusion" or stage I). Expressions are given for analyzing integral depth distributions, measurements of cumulative gas release, and measurements of the rate of gas release.

In Sweden[69] the emission of uranium atoms from the surface of electropolished disks of uranium metal irradiated to about 2.3×10^{16} fissions/cm^3 at a pressure of 10^{-5} torr has been measured. The atoms emitted were collected on catcher foils, and the amount collected was determined by fission counting. The number of uranium knock-ons ejected by a fragment has been calculated. The number of uranium atoms emitted per escaping fission fragment was found to be about 43, which is of the same order of magnitude as the number of uranium knock-ons ejected by a fragment. Other ejection mechanisms, e.g., evaporation of material in thermal spikes, seem to be of little importance.

Ceramics

At Bettis Atomic Power Laboratory[70] the theory of the movement of pores in solids due to various driving forces such as thermal gradients, stress gradients, moving grain boundaries, and moving dislocations has been developed from first principles and compared with previous treatments. The pertinent equations are then employed to develop a scheme of fission-gas swelling in oxide fuels. The resulting scheme is too complex for analytical treatment, and a computer analysis is under way. The scheme assumes the effects of dislocations, grain boundaries, and thermal gradients to be the dominant factors. The quantitative analysis is presented for the migration of fabricated pores in a cylindrical oxide-fuel element by a vapor transport mechanism, with the thermal gradient serving as the driving force. The present analysis, however, presents a fully quantitative treatment that is in good accord with the limited experimental data available which are of reasonable accuracy. The migration of fission-gas bubbles by a surface diffusion mechanism, again with the thermal gradient providing the driving force, is developed quantitatively to provide one possible model of fission-gas release, and here again the results are in good agreement with the limited experimental data available.

A digital computer program (CYGRO-2)[71] provides a method of structural analysis for an oxide-fueled, metal-clad rod-type fuel element in a pressurized environment. Stresses and strains are determined in a cross section of fuel and cladding undergoing thermal expansion and irradiation growth. Elastic, plastic, and creep parameters are used to calculate the effects of temperature, pressure, solid-fission-product growth, and gas-bubble expansion. The axially symmetric fuel may have radial zones and nonfissionable areas.

An analytical FORTRAN IV program (FIGRO) was developed at Bettis[72] for analysis of fuel-volume swelling and calculation of temperatures in bulk-oxide cylindrical fuel elements. The fuel pellet may be solid or annular or may contain two radial zones. Oxide-fuel thermal conductivity is a function of temperature, depletion, and porosity; fuel swelling is a function of temperature, depletion, hydrostatic pressure, and fissioning rate. As a boundary condition for the heat-conduction equation, either the cladding surface flux or the temperature at the inside radius of the fuel may be specified.

In Sweden[73] the emission of uranium atoms from the surface of sintered disks of UO_2 has been measured over the range 5×10^{15} to 7×10^{16} fissions/cm^3 in air at a pressure of about 5×10^{-3} torr and also in air, argon, and nitrogen over the pressure range 10^{-5} to 760 torrs for irradiations to about 3×10^{16} fissions/cm^3. The atoms emitted were collected on catcher foils, and the amount collected was determined by fission counting. The number of uranium knock-ons ejected by a fragment has been calculated. At 10^{-5} torr the number of uranium atoms emitted per escaping fission fragment was found to be about 9, which is of the same order of magnitude as the number of uranium knock-ons ejected by a fragment. Other ejection mechanisms, e.g., evaporation of material in thermal spikes, seem to be of little importance. At high oxygen pressures the emission of uranium atoms increases considerably. This is probably due to radiation oxidation of UO_2 caused by the fragments. The results are discussed in the light of our present knowledge of fission-fragment track formation.

The mean range in UO_2 of fission products of mass 140 was found to be 7.37 ± 0.05 mg/cm^2 by direct gamma spectrometric determination of the fraction of ^{140}La escaping from the surface of the disks. (F. A. Rough)

References

1. L. Baker, Jr., and J. D. Bingle, Kinetics of Oxidation of Uranium Between 300 and 625°C, *J. Nucl. Mater.*, 20: 11-21 (July 1966).
2. J. J. Holmes, Multiprocess Creep in Uranium Deduced From Literature Data, *Amer. Soc. Metals, Trans. Quart.*, 59: 575-576 (1966).
3. R. J. Jackson and A. E. Calabra (Eds.), Advances in Metallography, USAEC Report RFP-658, Dow Chemical Co., Rocky Flats Division, Oct. 20, 1966.
4. H. C. Kloepper, Jr., Some Observations on the Electron Metallography of Uranium, USAEC Report MCW-

1501, Mallinckrodt Chemical Works, Uranium Division, Aug. 1, 1966.
5. W. C. Stoeker and J. W. Starbuck, Uranium Texture Evaluation Studies, 1963–1966, USAEC Report MCW-1504, Mallinckrodt Chemical Works, Uranium Division, Aug. 1, 1966.
6. S. N. Buckley, Irradiation Growth in Uranium, British Report AERE-R-5262, August 1966.
7. R. G. Schierding and L. A. Fergason, Phase Studies of the Uranium–Iron–Silicon Ternary System with the Electron Microprobe, USAEC Report MCW-1502, Mallinckrodt Chemical Works, Uranium Division, Aug. 1, 1966.
8. R. G. Schierding and L. A. Fergason, Phase Studies of the Uranium–Aluminum–Iron System with the Electron Microprobe, USAEC Report MCW-1503, Mallinckrodt Chemical Works, Uranium Division, Aug. 1, 1966.
9. R. B. Russell, The Uranium–Aluminum–Iron Constitution Diagram, USAEC Report NMI-2813, Nuclear Metals Division of Textron Inc., June 30, 1964.
10. M. F. Nolan, Mechanical Properties of Dilute Uranium Alloys at Elevated Temperatures, USAEC Report MCW-1505, Mallinckrodt Chemical Works, Uranium Division, Aug. 1, 1966.
11. G. Oestberg, B. O. Haglund, L. Boerje, and L. Storm, Isothermal Transformation of γ Phase Adjusted Uranium in the β Range, *J. Microscop.*, 5: 21-30 (February 1966).
12. R. Carlander, Examination of EBWR Core-IA Fuel, USAEC Report ANL-6832, Argonne National Laboratory, June 1966.
13. J. A. Fellows, Seven Years of Uranium Alloy Development, 1959/1966, USAEC Report MCW-1510, Mallinckrodt Chemical Works, Uranium Division, July 29, 1966. (Classified)
14. M. F. Nolan, Beta-to-Alpha Transformation Characteristics of Some Dilute Uranium Alloys, USAEC Report MCW-1506, Mallinckrodt Chemical Works, Uranium Division, Aug. 1, 1966.
15. G. Petzow and A. O. Sampaio, Phase Equilibria in Uranium–Cobalt–Iron Alloys in the Partial Range $U–UCo_2–UFe_2$, Portugese Report LFEN-39, 1965.
16. G. Petzow and A. O. Sampaio, The System $U–UMn_2–UAl_2–UFe_2$ (in German), *Z. Metallk.*, 57: 625-632 (August 1966).
17. Union Carbide Corporation, Nuclear Division, Y-12 Development Activities Progress Report, November 1965–January 1966, USAEC Report Y-1558, Nov. 29, 1966. (Classified; material cited is unclassified)
18. Argonne National Laboratory, Fuels and Materials Development Program Quarterly Progress Report for Period Ending September 30, 1966.
19. Argonne National Laboratory, Reactor Development Program Progress Report, September 1966, USAEC Report ANL-7255, Oct. 26, 1966.
20. W. N. Miner, Stability of Delta-Phase Plutonium–Gallium Alloys, USAEC Report LA-DC-7934, Los Alamos Scientific Laboratory, July 18, 1966.
21. E. S. Bomar and P. E. Potter, The Compatibility of Plutonium Carbides with Silicon Carbide, British Report AERE-R-5214, June 1966.
22. Argonne National Laboratory, Reactor Development Program Progress Report, August 1966, USAEC Report ANL-7249, Sept. 23, 1966.
23. Argonne National Laboratory, Reactor Development Program Progress Report, October 1966, USAEC Report ANL-7267. Nov. 22, 1966.
24. J. H. Davies and P. E. Novak, Diffusion of Plutonium and Uranium in Oxide Fuel at 2400°C, USAEC Report GEAP-4877, General Electric Company, Vallecitos Atomic Laboratory March 1966.
25. W. L. Lyon and W. E. Baily, The Solid-Liquid Phase Diagram for the $UO_2–PuO_2$ System, USAEC Report GEAP-4878, General Electric Company, Vallecitos Atomic Laboratory, December 1965.
26. W. C. Pritchard and R. L. Nance, Studies on the Formation of Pu_2O_3 in the Sintering of PuO_2, USAEC Report LA-3493, Los Alamos Scientific Laboratory, December 1965.
27. G. Dean, C. Pelou, and D. Beugnies, Sintering of $(U,Pu)O_2$ Pellets, Report EURFNR-96F (translated from French Report CEA-R-2737), May 1965.
28. S. Takeuchi, T. Honma, T. Satow, and T. Hirai, Th–ThC Phase Diagram, *Trans. Jap. Inst. Metals*, 7: 59-67 (January 1966).
29. S. Peterson (Comp. and Ed.), Metals and Ceramics Division Annual Progress Report for Period Ending June 30, 1966, USAEC Report ORNL-3970, Oak Ridge National Laboratory, October 1966.
30. W. C. Francis and R. A. Moen (Eds.), Annual Progress Report on Reactor Fuels and Materials Development for FY 1966, USAEC Report IDO-17218, Phillips Petroleum Company, November 1966.
31. G. P. Pancer, R. B. Holden, and D. H. Gurinsky, Studies on a Fuel for an Ordered Bed Reactor, USAEC Report BNL-10521, Brookhaven National Laboratory, December 1966.
32. General Atomic, Division of General Dynamics Corp., unpublished, 1966.
33. General Atomic, Division of General Dynamics Corp., unpublished, 1966.
34. R. G. Wymer and D. A. Douglas, Jr., Comps.), Status and Progress Report for Thorium Fuel Cycle Development for Period Ending December 31, 1965, USAEC Report ORNL-4001, Oak Ridge National Laboratory, October 1966.
35. Oak Ridge National Laboratory, unpublished, Oct. 6, 1966.
36. Oak Ridge National Laboratory, unpublished, Dec. 6, 1966.
37. D. L. Keller, Progress Relating to Civilian Applications During July Through September 1966, USAEC Report BMI-1784, Battelle Memorial Institute, Oct. 1, 1966.
38. *Thermal Conductivity of Uranium Dioxide*, Technical Reports Series, No. 59, International Atomic Energy Agency, Vienna, 1966 (STI/DOC/59).
39. Fission-Gas Release Symposium, Gatlinburg, Tenn., June, 1965, *Nucl. Appl.*, 2(2): 116-181 (April 1966).
40. O. Gautsch and C. Mustacchi, Knock-Out Coefficient of Sintered Uranium Dioxide, Euratom Report EUR-3058.e, August 1966.
41. T. G. Godfrey, J. A. Woolley, and J. M. Leitnaker, Thermodynamic Functions of Nuclear Materials: UC, UC_2, UO_2, ThO_2, and UN, USAEC Report ORNL-TM-1596, Oak Ridge National Laboratory, October 1966.
42. S. Yajima, H. Furuya, and T. Hirai, Lattice and Grain-Boundary Diffusion of Uranium in UO_2, *J. Nucl. Mater.*, 20: 162-170 (1966).
43. H. N. Barr and L. A. Sundquist, Method of Making Hollow Spherical Particles, U. S. Patent No. 3,270,098, to USAEC, Aug. 30, 1966.
44. K. Winter, Effect of Some Oxide Additives on the Sintering of Uranium Dioxide, *Silikat Tech.*, 11: 358-363 (November 1965).
45. J. J. Fargo, Fabrication of Thin Uranium Dioxide Plates for Nuclear Energy Fuel Elements, *INTERPACE Tech. J.*, 1: 13-16 (January 1964).
46. R. Boucher, P. Barthelemy, and C. Milet, Études sur les Carbures d'Uranium et de Plutonium Coulés, *Mem. Sci. Rev. Met.*, 63: 543-554 (June 1966).
47. F. Anselin and P. Barthelemy, Sur l'Existence d'une Phase Monoclinique $UMoC_{2-x}$ dans le Systeme Ternaire Uranium, Molybdene, Carbone, *Bull. Soc. Franc. Mineral. Crist.*, 89: 132-133 (1966).
48. R. A. Potter, T. G. Godfrey, and J. M. Leitnaker, Precipitates in Uranium Nitride, *Amer. Ceram. Soc. Bull.*, 45(9): 822 (1966).
49. Bureau of Mines, Albany Metallurgy Research Center, Quarterly Metallurgy Progress Report Number 31, April 1–June 30, 1966, USAEC Report USBM-RC-1249.

50. H. Uchikoshi and B. Ishii, personal communication, October 1966.
51. General Electric Company, Nuclear Materials and Propulsion Operation, High-Temperature Materials Program Progress Report No. 61, USAEC Report GEMP-61. Sept. 30. 1966.
52. B. A. Webb and N. R. Koenig, Method for Controlling the Composition of Uranium Carbide and Nuclear Fuel Element Thereof, U. S. Patent No. 3,202,586, to USAEC, Aug. 24, 1965.
53. Argonne National Laboratory, Proceedings of the Conference on Safety, Fuels, and Core Design in Large Fast Power Reactors, Argonne, Ill., October 11–14, 1965, USAEC Report ANL-7120.
54. R. F. Stoops and J. V. Hamme, Method for Stabilizing Uranium Monocarbide, U. S. Patent No. 3,208,818, to USAEC, Sept. 28, 1965.
55. R. Lorenzelli, A. Martin, and R. Schickel, Reaction of Uranium and Plutonium Carbides With Nitrogen, French Report CEA-R-2997, March 1966.
56. J. E. Frank, R. E. Forrester, and J. S. Buck, Irradiation Behavior of Unalloyed Hypostoichiometric Uranium Carbide, Experiment AI 3-11 and Review, USAEC Report NAA-SR-11440, Atomics International, July 15, 1966.
57. R. D. MacDonald, W. G. Mathers, A. M. Tachis, and J. E. May, SAP Clad Uranium Carbide Fuel Elements, Canadian Report AECL-2571, May 1966.
58. F. W. Albaugh, S. H. Bush, J. J. Cadwell, D. R. de Halas, and D. C. Worlton, Battelle–Northwest, unpublished, August 1966.
59. Battelle–Northwest, Ceramics Research and Development Quarterly Report, July–September 1965, USAEC Report BNWL-198.
60. Y. Baskin, Properties of Uranium Monophosphide, *J. Amer. Ceram. Soc.*, 49: 541-546 (October 1966).
61. C. H. McMurtry and K. M. Taylor, Studies of the Preparation of Mixed Carbide Fuel Utilizing Coprecipitation, Quarterly Progress Report No. 1, May 23–August 30, 1966, The Carborundum Company.
62. R. Hauser, R. Rambourg, and B. Givbert, Canadian Patent No. 725,277, Jan. 4, 1966.
63. M. Mc D. Baker, L. N. Less, and S. Orman, Uranium + Water Reaction–Part I. Kinetics, Products, and Mechanism, *Trans. Faraday Soc.*, 62(5): 2513-2524 (1966).
64. R. E. Wilson, C. Barnes, Jr., R. Koonz, and L. Baker, Jr., Isothermal Reaction of Uranium with Steam Between 400 and 1600°C, *Nucl. Sci. Eng.*, 25: 109-115 (1966).
65. M. McD. Baker, L. N. Less, and S. Orman, Uranium + Water Reaction–Part II. Effect of Oxygen and Other Gases, *Trans. Faraday Soc.*, 62(5): 2525-2530 (1966).
66. B. M. Ma, Radiation Growth and Swelling Analysis for Cylindrical Fuel Elements During a Positive Reactor Period, *Nucl. Sci. Eng.*, 26: 99-109 (September 1966).
67. R. S. Barnes and R. S. Nelson, Theories of Swelling and Gas Retention in Reactor Materials, Report AERE-R-4952, June 1965.
68. R. Kelly and H. Matzke, The Application of Diffusion Theory to Inert-Gas Motion in Ion-Bombarded Solids (Diffusion Theory for Discrete Media, Part III), *J. Nucl. Mater.*, 20: 171-183 (Mar. 14, 1966).
69. G. Nilsson, Ejection of Uranium Atoms From Electropolished Foils of Uranium Metal by Fission Fragments, *J. Nucl. Mater.*, 20: 231-235 (Apr. 25, 1966).
70. F. A. Nichols, Behavior of Gaseous Fission Products in Oxide Fuel Elements, USAEC Report WAPD-TM-570, Westinghouse Electric Corporation, Bettis Atomic Power Laboratory, November 1966.
71. C. M. Friedrich and W. H. Guilinger, Jr., CYGRO-2: A FORTRAN IV Computer Program for Stress Analysis of the Growth of Cylindrical Fuel Elements with Fission Gas Bubbles, USAEC Report WAPD-TM-547, Westinghouse Electric Corporation, Bettis Atomic Power Laboratory, November 1966.
72. I. Goldberg, L. L. Lynn, and C. D. Sphar, FIGRO: FORTRAN IV Digital Computer Program for the Analysis of Fuel Swelling and Calculation of Temperature in Bulk-Oxide Cylindrical Fuel Elements, USAEC Report WAPD-TM-618, Westinghouse Electric Corporation, Bettis Atomic Power Laboratory, December 1966.
73. G. Nilsson, Ejection of Uranium Atoms From Sintered UO_2 by Fission Fragments in Different Gases and at Different Gas Pressures, *J. Nucl. Mater.*, 20: 215-230 (Apr. 25, 1966).

Section II

Reactor Materials

Moderator Materials

Graphite

New information on the ability of graphite to absorb strain by plastic deformation under irradiation was reported by British investigators.[1] A number of polycrystalline graphites in the form of rings restrained from shrinkage at the inner bore were irradiated at approximately 400°C to peak fast-neutron doses of about 18 and 37×10^{20} neutrons/cm^2. The results indicate that at least 0.6% plastic strain can be absorbed in tension without cracking, even when strain is applied for part of the time at rates two to three times the normal irradiation-induced shrinkage rate.

Additional creep data have been obtained by Oak Ridge researchers[2] and, combined with previous data, present a generalized creep behavior for graphite over the temperature range 150 to 1000°C. The data, plotted in Fig. II-1, support the relation

$$K = A\,\dot{\gamma}/\sigma_y$$

where K = creep coefficient
A = accommodation factor
$\dot{\gamma}$ = shear rate due to anisotropic growth ($\dot{G}_c - \dot{G}_a$)
σ = yield strength of the crystallites
$\dot{G}_c$, $\dot{G}_a$ = growth rates in the c and a directions, respectively

The author presents the following comments regarding use of this relation to extrapolate the data of Fig. II-1 to other graphite grades.

The shear rate $\dot{\gamma}$ of graphite can be derived from measurements made on pyrolytic graphites through estimates of polycrystalline-graphite growth rates. The accommodation factor A primarily reflects the degree of accommodation by microcracks and, in general, the void volume in the graphite. It is not necessarily constant and is expected to vary with temperature and neutron exposure. The variation of A with temperature should not be very large; however, A should exhibit a rather significant increase as microcrack closure occurs. The closure of microcracks requires an exposure of approximately 10^{22} neutrons/cm^2; thus the value of A will be essentially constant for at least half this exposure. The value of the yield strength or flow stress σ_y of the crystallites will undoubtedly vary under irradiation and with irradiation temperature. The value of σ_y, like that of A, will not vary with temperature, however, as significantly as $\dot{\gamma}$, the shear rate.

The creep-rate coefficient should therefore strongly reflect the variation of $\dot{\gamma}$ with temperature. This is demonstrated in Fig. II-1, where the creep-rate coefficient exhibits a minimum around 350°C. The creep-rate coefficient K is not exactly proportional to the shear rate $\dot{\gamma}$ because of the variations of A and σ_y.

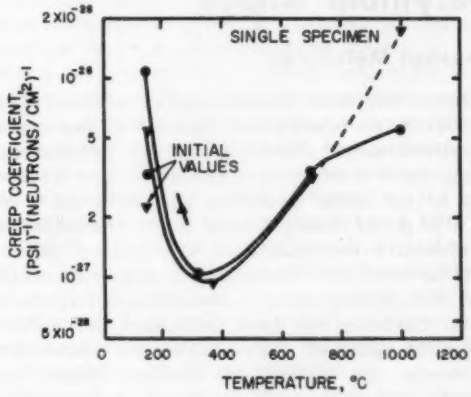

Fig. II-1 The effect of temperature on the creep coefficient of graphite under irradiation.[2] ▲, AGOT; ●, EGCR-type AGOT; ▼, CGB.

The value of A would be essentially independent of the graphite grade; thus the effect of σ_y on the creep-rate coefficient can be demonstrated by a comparison of various grades at the same temperature. In regard to the discrepancy in correlation of the test result at 1000°C for the CGB grade, the author notes that the material demonstrated a one-third decrease in its modulus of elasticity, unlike previously tested grades, and that the test result requires confirming.

British investigators[3] report the use of eddy-current methods capable of revealing surface cracks in graphite and of presenting the information in a way that can be linked to a specification defining crack length and depth. Eddy-current methods used previously have been plagued by serious problems of interpretation. By the reported procedures, using a

frequency of 200 kc/sec and a quantized facsimile record, cracks opening to the graphite surface were clearly resolved from the background signals due to local microstructural variations.

The low-temperature thermal conductivity of polycrystalline graphite increases more quickly with temperature than does the specific heat, the conductivity varying as $T^{2.5}$ to $T^{3.8}$ and the specific heat as T^2. This dependence is not to be expected in a region where boundary scattering is believed to be dominant, and the conductivity should vary as T^2. Kelly[4] has reported the calculation of the average velocity of the out-of-plane vibrations as a function of temperature, using Komatsu's model of the lattice dynamics of graphite, which partially accounts for the observed temperature dependencies.

(M. C. Brockway)

Beryllium and Beryllium Alloys

Physical Metallurgy

Brush Beryllium is investigating the effect of high purity on the mechanical behavior of fine-grained beryllium sheet.[5] Powder-metallurgy techniques are being used to maintain a fine grain size; however, one of the major problems is maintaining a high level of purity while producing a fine-grained powder. Preliminary information on this contract indicates that the fabrication methods being employed are capable of controlling purity in powder-metallurgy beryllium. Oxidation has been minimized by employing argon of sufficient purity during the comminution, screening, die loading, and pressing steps. Grain growth rate appears to be higher because of the absence of inclusions; however, improved pressing characteristics permit the use of lower temperatures for consolidation. Microstructures of these low-oxide pressings and sheets appear extremely clean, being similar to those of ingot-source beryllium. Although the microstructures are relatively free of oxide inclusions in these powder-metallurgy materials, the grain sizes are relatively fine.

London and Stone are studying the mechanical properties of distilled and zone-refined beryllium at Franklin Institute.[6] To overcome difficulties in consolidating the distilled material, they are constructing an electron-beam-melting unit to aid in this part of their investigation. Impure single-crystal material has been prepared to study the effects of purity. Two such crystals have been tested in microstrain compression. At room temperature the crystals failed at a compressive stress of 280,700 psi with no detectable plastic strain. Fracture occurred largely on basal and prism planes. Fracture at 208°C was on a pyramidal plane.

An unusual twin-precipitate interaction in beryllium occurring during recrystallization has been reported.[7] Upon passing through a network of MBe_{13} precipitate particles, the twins undergo a severe constriction resulting in a sausagelike appearance. This type of constriction inhibits the twinning work of deformation and may be regarded as a strengthening mechanism.

Corrosion

The chemical behavior of beryllium metal exposed to a launch-pad-abort fire environment has been investigated by Thompson Ramo Wooldridge.[8] The purpose of the investigation was to study the toxic-beryllium-compound particles or smoke that would become airborne under these conditions. The pure combustion-gas species investigated were oxygen, nitrogen, H_2O, NO, CO, and CO_2. At temperatures below the melting point of beryllium, water vapor is predominantly more reactive than the others; above 2000°F (1093°C) the reactions with oxygen also become important. The other combustion-gas species are of relatively little importance in terms of reactions that generate significant concentrations of airborne contamination. In an oxygen-rich H–O flame, beryllium components heated over 2400°F (1316°C) are likely to ignite and burn in the vapor phase with the release of large amounts of beryllium oxide smoke. This reaction can convert a significant fraction of the beryllium present to smoke. Below 2000°F (1093°C) relatively little airborne contamination is expected unless a large-scale explosion follows a fire of long duration. In general, the degree of interaction between flame environment and beryllium components increases rapidly with increasing beryllium temperature, water vapor, and/or oxygen, and the total pressure of the environment.

Material compatibility and corrosion investigations were conducted to determine the extent of corrosion in the beryllium reflector of the Argonne Advanced Research Reactor.[9] Since aluminum and stainless-steel components were also of interest, couples of these materials with beryllium were also studied. Exposures were made at 200°F (93°C) in water flowing at 44 ft/sec in a closed loop. Corrosion rates were 1.1 to 2.8 mils/year, depending on the ratio of exposure area to water volume. Beryllium was attacked uniformly, with no pitting or localized attack. Very little localized attack was noted in the aluminum and stainless-steel couples; a few pits were seen, but these were less than 1 mil in depth. It was concluded that the corrosion rates were acceptable for the application.

Fabrication

Denny and Meyer have described techniques for the production of fine beryllium wire.[10] The preferred

source of material for fabrication stock was vacuum-cast ingot because of the low nonmetallic inclusion content. Cast ingots were extruded to $\frac{3}{8}$-in.-diameter rod and then drawn at 750 to 800°F (399 to 427°C) with 12.5% reduction per pass. Speeds up to 200 ft/min were used. Major changes in the microstructure were noted as a result of processing the beryllium. The annealed extrusions had an equiaxed grain structure with an average grain size of 48 μ, and conversion of this material to 0.005-in.-diameter wire yields a grain nominally 2 μ in diameter and 6 μ long. The authors indicated that stress relieving must occur during working since no intermediate anneals are used. Properties of 0.005-in.-diameter wire are listed in Table II-1.

Table II-1 MECHANICAL PROPERTIES OF 0.005-IN.-DIAMETER BERYLLIUM WIRE[10]

Condition	Ultimate tensile strength, 1000 psi	Yield strength (0.2% offset), 1000 psi	Elongation, in 10 in., %
As drawn	174.0	137.5	6.3
30 min, 1000°F	132.9	123.2	6.6
30 min, 1200°F	115.3	77.7	13.9
30 min, 1400°F	91.7	49.6	9.0

The Beryllium Corp.[11] reported on a manufacturing process developed to vacuum-cast sound beryllium ingots up to 6 in. in diameter and 12 in. long. Empirical equations were developed which showed a relation between soundness of the ingot and heat-transfer characteristics of the mold. The sound ingots were produced by inducing longitudinal heat transfer with a water-cooled copper plug in the end of the mold. Ingots cast from high-purity melt stock were more susceptible to stress cracking on cooling than those made from regular-purity stock. Beryllium ingot material was successfully upset forged in heavy steel jackets up to 75% at temperatures as low as 1375°F (746°C). The resulting product showed only slight improvement in mechanical properties. Ingots were also extruded into mill shapes in the 1650 to 1950°F (899 to 1066°C) temperature range. Reductions of 12:1 to 25:1 resulted in sound extrusions with improved properties and very little preferred orientation.

Extrusions, forgings, and as-cast ingots were converted into sheet by rolling in the temperature ranges of 1100 to 1200°F (593 to 649°C) and 1450 to 1650°F (788 to 899°C). Special solutionizing and precipitation treatments were used prior to fabrication to produce consistently sound sheet in the low-temperature range. Extruded slabs were the preferred starting stock since they could be rolled successfully in both temperature ranges. Residual cold work in sheet rolled in the lower temperature range gave higher tensile properties and lower elongations. On the other hand, sheet fabricated in the higher temperature range showed greater formability.

A pamphlet summarizing the available machining data for beryllium metal has been compiled by Snider and Kahles.[12] This pamphlet gives machining-data charts with explicit specifications for each machining process.

The National Aeronautics and Space Administration has issued a series of technical memoranda concerning the fabrication of beryllium. The first volume is a reprint of a report written for the Redstone Scientific Information Center by Gerds and Boulger at Battelle.[13] This report, which has already been reviewed, covers a survey of technology in beryllium fabrication from 1960 to 1964. Volume II covers forming techniques for beryllium alloys. The problem of forming structural components from sheet products is detailed. Time–temperature relations are established for the forming of straight bends, compound curved channels, joggles, and hemispherical segments. Examples showing flow of material and resultant dimensional changes are given. Also, this report shows the feasibility of using extreme forming operations on cross-rolled beryllium sheet.

Metal-removal techniques are the subject for Volume III of this series. The proved production techniques for drilling, routing, and abrasive-wheel cutting of both beryllium sheet and plate are reviewed, as well as the production techniques for precision machining of hot-pressed block and extruded rod. An investigation of chemical-milling rates as a function of solution strengths is described. Electrical-discharge machining power and frequency parameters and electrode materials are correlated with the resulting metal-removal rates, surface finishes, and machining times. Metallographic techniques were used for comparisons and failure analysis.

Volume IV of this series covers surface-treatment techniques used in the fabrication of beryllium structures. One section of this report covers removal of surface contaminants incurred during normal shop handling. This would include removal of fingerprints, lubricants, dust, etc., resulting from normal working of the structures. Another part of this report discusses the chemical removal of surface oxides for adhesive bonding and plating. In the case of bonding, the cleaning agent must be compatible with the bonding process and must not contain compounds which would inhibit proper curing of the bonding material. After etching to clean the surface, an activating strike is normally employed prior to final plating. Procedures for zinc, copper, and nickel plating are given. Also described are procedures followed to prevent surface damage during shop operation.

The effects of thermal treatments on the properties and dimensional stability of formed beryllium sheet are reported in Volume V. It was found that relief of residual stresses could be more readily accomplished at 1025°F (553°C) rather than at the

more commonly used 1350°F (732°C). Rapid cooling after thermal treatment was not a recommended production process since it has a deleterious effect on both the properties and contour of formed sheet. Annealing at 1150°F (621°C) for 8 hr results in more consistent properties and behavior than similar treatments at 1350°F (732°C). The topic for Volume VI in the series was joining techniques. This document is concerned primarily with mechanical fastening and adhesive bonding. It was concluded that high-strength mechanical fasteners can be used for fabrication of beryllium structures. Adhesives are not necessary in conjunction with mechanically fastened joints; however, satisfactory adhesive joining of beryllium was accomplished on a laboratory scale. In both cases it was demonstrated that these techniques could be used to produce sound joints. Preliminary evaluations of brazing and diffusion bonding were made. Brazing is the more advanced technique of the two, although the authors recommended that both techniques be developed further since there are few established production techniques for either of these procedures.

Hauser and coworkers at Battelle have reported on the electron-beam welding of beryllium.[14] This report covers half of a 2-year program on the subject. Procedures have been investigated for welding 0.020-, 1/16-, 1/8-, and 1/4-in.-thick sheet. The factors examined for their effect on weld quality were beam voltage, current, diameter, travel speed, preheat temperature, surface preparation, mechanical restraint during welding, and material composition. In the thicker sheets, undercutting and surface roughness of the welds were major problems in developing satisfactory welding procedures. Lower welding speeds and power densities, multiple-pass welds, and the addition of filler metal alleviated the undercutting and roughness problems. Beryllium oxide films were found to form on the welds. Undercutting, roughness, and porosity in the welds tended to increase with the BeO content of the base metal. For a given set of conditions, the quality of welds in the low-oxide (0.69 wt.% BeO) sheet was significantly better than that in the high-oxide (1.93 wt.% BeO) material.

Preheating was necessary to prevent cracking when restraint was used in butt-welded sheets, and higher temperatures were required as this restraint was increased. Distortion during welding was determined to be about the same as in welding aluminum or stainless steel. Traverse shrinkage and longitudinal bowing were the primary means of distortion measured. Multiple-pass welds at lower power densities produced more distortion than did single-pass welds at higher densities.

Bend tests on welded sheet indicated that the ductile-to-brittle transition temperature was about twice that for the base metal, being 1200°F (649°C) as compared to 535°F (280°C). Limited testing on 1/16- to 1/8-in.-thick-welded sheet gave joint efficiencies of 55 to 75% in the range of −40 to 800°F (−40 to 427°C). Loss in properties was attributed to the relatively large grain size of the weld.

Radiation Damage

A machine was designed and constructed to deliver repeated compressive impact blows to small beryllium specimens. Velocity of impacts was measured by photoelectric cells, whereas deformation was measured by strain gauges. Both irradiated and nonirradiated samples were tested, and curves defining energy input as a function of deformation were obtained.[15] As a comparison, standard Izod-impact and Rockwell-hardness tests were made on similar samples taken from the irradiated beryllium. Data were related to fast-neutron exposure. Relations were derived between compressive-impact, Rockwell-hardness, and Izod-impact data. Extrapolation of the trends to a point of minimum residual impact resistance indicated a critical total exposure range of 3.8 to 8.5×10^{21} neutrons/cm^2.

Analysis

Union Carbide Nuclear Division reported[16] techniques for analysis of beryllium for carbon in the combined, free, and adsorbed forms. Separate techniques were used to analyze for carbon in each of these three forms. Combined carbon was converted to methane by the following reaction:

$$Be_2C + 2H_2SO_4 \rightarrow 2BeSO_4 + CH_4\uparrow$$

The methane was then swept into a gas chromatograph for measurement. The interstitial or free carbon was filtered from the dissolved sample, ignited to CO_2, and measured in a Leco conductometric cell by the reaction

$$Ba(OH)_2 + CO_2 \rightarrow BaCO_3\downarrow + H_2O$$

Adsorbed carbon (CO_2 on surface) was removed by heating the sample at 1025°C and measuring the evolved CO_2 by the same technique.

General

Proceedings from the Grenoble Conference on Beryllium Metallurgy (1965) have recently been published.[17] Data are presented on beryllium purification and analysis and on its reaction with other metals. Results of studies on beryllium lattices and the structure of beryllium point defects are listed. Information is also included on mechanical properties of single- and bicrystal beryllium, properties of polycrystalline beryllium, and the manufacture and properties of wrought beryllium products. The proceedings consisted of two main lectures and 60 papers, approximately half in French and the remainder in English. (H. D. Hanes)

Beryllium Oxide

Additional information on the stability of BeO to high irradiation exposure, 4 to 9×10^{21} neutrons/cm^2 ($E_n \geq 1$ Mev), at 1000°C was reported by General Electric researchers.[18] The data indicate that fine-grained BeO can be irradiated at 1000°C to exposures near 10^{22} neutrons/cm^2 ($E_n \geq 1$ Mev) with volume expansion of 3 to 5% and good retention of strength. A significant difference in volume changes was exhibited between high- and low-density specimens. The volume of the high-density (~2.9 g/cm^3) specimens increased approximately linearly with exposure at a rate of roughly 0.5 to 0.6% per 10^{21} neutrons/cm^2. The volume changes of low-density (~2.6 g/cm^3) specimens appeared to be approaching a saturation level at about a 3% increase. Figures II-2 and II-3 illustrate these differences in volume expansion.

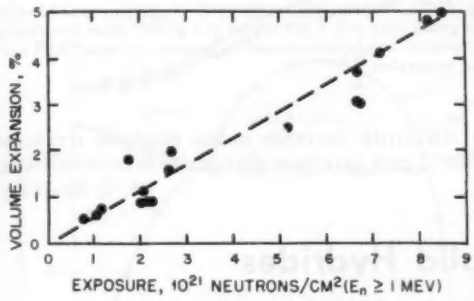

Fig. II-2 Volume expansion as a function of exposure in BeO specimens with a grain size of ~5 μ and a density of 2.9 g/cm³ irradiated at 1000°C (Ref. 18).

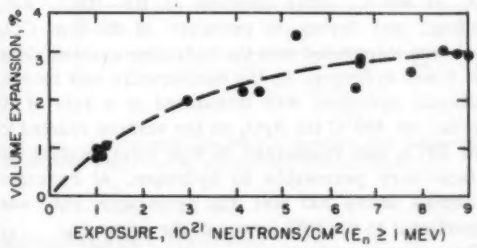

Fig. II-3 Volume expansion as a function of dosage in BeO specimens with a grain size of ~5 μ and a density of 2.6 g/cm³ irradiated at 1000°C (Ref. 18).

Crystalline expansion, on the basis of density measurements of crushed samples, was only 0.6 to 1.0%. Thus most of the total sample expansion was attributed to accumulation of helium bubbles at the grain boundaries.

Irradiation-induced volume expansion also varied with grain size. The large-grained BeO (≥ 17 μ) tended to expand more than the small-grained material.

Open-porosity changes were not pronounced in fine-grain-size materials at intermediate exposures, but appreciable increases occurred in all the materials at the highest exposure. The increases appeared to be roughly proportional to the original density of the material, ranging from 3 to 4% in 2.9 g/cm^3 material to 12 to 13% in 2.6 g/cm^3 material. Such changes, in materials irradiated at low temperatures, would be indicative of extensive microcracking and would be accompanied by marked decreases in strength. Since the fine-grained materials in the 1000°C temperature tests did not show appreciable strength changes, apparently some annealing occurred in the grain boundaries. Such annealing was also indicated by the fact that, in some instances, open porosity increased in the first irradiation (~1×10^{21} neutrons/cm^2, $E_n \geq 1$ Mev) but decreased during irradiation to higher exposures.

The Young's moduli ranged from 50 to 90% of those for unirradiated material and were generally from 85 to 90% for the fine-grained materials. The larger decrease in large-grained material was attributed to some degree of microcracking.

Good strength retention was exhibited by the fine-grain-size materials. The strength of the 5-μ-size high- and intermediate-density materials was equal to or greather than that of material in the unirradiated condition. The small-grain-size materials of 2.6 g/cm^3 density, which appeared to be optimum relative to expansion characteristics, lost 20 to 40% of their strength in the unirradiated condition. In general, the strength change in the fine-grain-size materials was relatively small for the exposure increment between 2 and 9×10^{21} neutrons/cm^2. In contrast, the strength of 17-μ grain-size AOX and UOX–MgO materials continued to decrease with increasing exposure.

Helium bubbles in the grain boundaries of the high-exposure samples were apparently not grossly different from those at lower exposure. There reportedly was an increase in the average size of the bubbles, with many having well-defined crystallographic shapes and maximum sizes of about 0.5 μ, plus indications of bubble coalescence. Bubbles appeared more numerous in the larger-grain-size materials.

Transmission micrographs of high-exposure samples provided further details on intragranular voids, which were first apparent at exposures of about 10^{21} neutrons/cm^2. Maximum widths and lengths observed for such voids were approximately 1000 and 3000 A, respectively. Minimum sizes ranged down to the resolution limit of the microscope. Such voids in BeO irradiated to high exposures were presumed to be composed of vacancies trapped by the helium formed in the $(n,2n)$ and (n,α) reactions with beryl-

lium and to represent reservoirs of considerable quantities of helium within the crystalline lattice.

The researchers also reported new thermal-diffusivity measurements, together with previous data for unirradiated and irradiated BeO.

Data were reported on the variation of diffusivity with crystallographic orientation of unirradiated BeO. Extruded samples of UOX–MgO–BeO provided material having preferential c-axis orientation in the direction of the specimen longitudinal axis. The extent of such orientation was roughly 5, 50, and 80% for grain sizes of 5, 20, and 60 μ, respectively. The measured decrease in diffusivity with increasing grain size indicated that the thermal diffusivity of BeO is roughly 10% less in the crystallographic c-direction than in the a-direction at 300°C.

The effect of BeO density on diffusivity was reported for material in the 4- to 6-μ grain-size range. These data, illustrated in Fig. II-4, were best fitted by two curves for densities greater than or less than approximately 2.7 g/cm^3. The authors suggest that pore shapes may account for the two curves. The naturally occurring pores in the higher density materials may be laminar or cylindrical in shape. The artificially induced (by resin burnout) pores in the two lowest density materials may be nearly isometric.

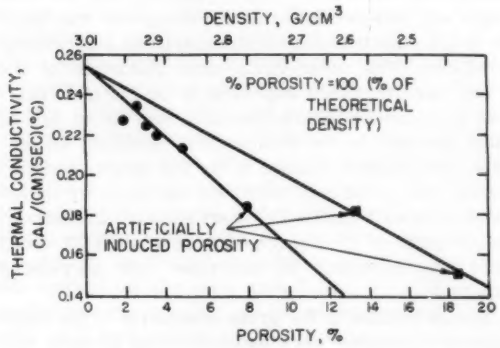

Fig. II-4 Dependence of thermal diffusivity of BeO on specimen on density.[18] Measurements at 300°C.

Thermal-diffusivity measurements on irradiated material indicated that, for an approximately constant volume expansion, the diffusivity decrease was larger for decreasing irradiation temperature. Figure II-5 graphically summarizes data for unirradiated, irradiated, and annealed samples. The irradiation-induced decrease in diffusivity was attributed to phonon scattering by the interstitial defect clusters and loops; the magnitude of the decrease was qualitatively proportional to the number but not the size of the loops formed at the different irradiation temperatures. It was believed that some contribution to

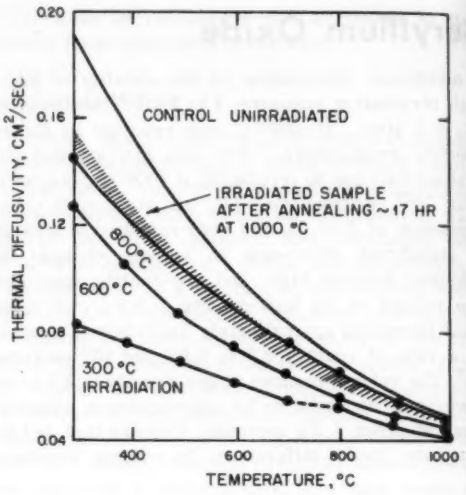

Fig. II-5 Thermal diffusivity of BeO specimens with about 5-μ grain size and a density of 2.9 g/cm^3 after irradiation at various temperatures and exposures to about 0.7% volume expansion.[18]

the diffusivity decrease in the specimen irradiated at 300°C may have been attributable to microcracking.

(M. C. Brockway)

Solid Hydrides

Zirconium Hydride

A technique for increasing the hydriding rate of zirconium by cleaning the surface in situ has been developed at Culcheth.[19] The method is based on the removal of the ZrO_2 surface film by reaction of CCl_4 at 400°C. After pickling in $HF–HNO_3–H_2O$, washing, and drying, a pressure of 50 mm CCl_4 vapor was introduced into the hydriding system, along with 5 mm hydrogen. As the temperature was raised, additional hydrogen was introduced at a rate of 10 ppm/hr. At 400°C the ZrO_2 on the surface reacted to form $ZrCl_4$ and volatilized in this form, making the surface very permeable to hydrogen. At hydrogen pressures above 300 mm, the permeation rate was proportional to the fifth power of the pressure.

Zirconium hydride specimens clad with Fe–25 wt.% Cr–4 wt.% Al have been subjected to full reactor power in a helium–air atmosphere, as part of the General Electric program.[20] The tests have operated routinely for 3000 hr at 650°C.

Lanthanum Hydride

The phase relations in the La–H system have been determined at Iowa State.[21] The phase diagram obtained is shown in Fig. II-6. The dotted lines in the

diagram indicate phase boundaries that were not definitely established in this study but were drawn from consideration of the thermodynamics of the system. The addition of hydrogen increased the melting point of lanthanum and decreased the fcc-to-bcc transformation temperature from 860°C to a eutectoid at 773°C at a composition of 23.5 at.% hydrogen. The solubility of the hydride in fcc lanthanum ranged from 2.83 at.% at 375°C to 21.3 at.% hydrogen at 773°C. The enthalpy of solution was calculated to be 5.76 ± 0.17 kcal. Above 773°C the solubility of lanthanum hydride in bcc lanthanum increased rapidly, and complete solubility was found at temperatures above 960°C. Hydrogen depressed the low-temperature transformation in lanthanum by 27°C.

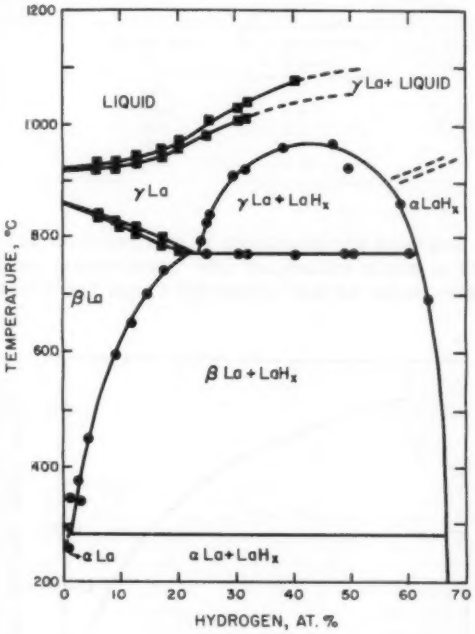

Fig. II-6 Lanthanum–lanthanum hydride phase diagram.[23] ■, thermal analyses; ●, isothermal equilibration.

Miscellaneous Hydrides

An investigation of the ternary system Zr–H–N at Atomics International[22] has shown that the compound $ZrN \cdot ZrH_2$ has a hexagonal structure, with $a_0 = 3.303$ A and $c_0 = 5.501$ A. The density of the compound was found to be 6.42 g/cm^3.

The first in-pile test of fueled yttrium hydride clad with Mo–50 wt.% Re was successfully operated for 1866 hr at a control temperature of 850°C by General Electric.[20] The six specimens appeared to be in the as-fabricated condition after this exposure.

Sound, crack-free buttons of vanadium hydride and of vanadium–18 wt.% titanium hydride have also been produced at General Electric.[20] The N_H of the vanadium hydride was 2.55 and that of the alloy hydride was 5.72; the respective densities were 5.84 and 5.81 g/cm^3.

The first modulus-of-rupture test of irradiated titanium hydride having an N_H of 7.4 showed that its strength (14.7 kg/mm^2) at room temperature was identical to the strength of the unirradiated control specimen.[20] The irradiation test was for 1120 hr in air at 490°C to 0.2×10^{20} fast neutrons/cm^2.

(H. H. Krause)

References

1. J. E. Brocklehurst, A. A. McFarlane, and B. S. Gray, The Effect of Tensile Restraint on Graphite Specimens Irradiated in BR-2, British Report TRG-Report-1279, June 29, 1966.
2. S. Peterson (Comp. and Ed.), Metals and Ceramics Division Annual Progress Report for the Period Ending June 30, 1966, USAEC Report ORNL-3970, Oak Ridge National Laboratory, October 1966.
3. R. S. Sharpe, S. Aveyard, and W. L. Hodgkinson, A Quantized Eddyfax Technique Applied to the Inspection of Reactor-Grade Graphite, British Report AERE-R-5240, August 1966.
4. B. T. Kelly, The Basal Plane Thermal Conductivity of Graphite and the Velocity of Out-of-Plane Waves, British Report TRG-Report-1313, Aug. 1, 1966.
5. B. B. Lympamy, J. J. Theodore, and W. W. Beaver, Research on Effects of High Purity in Wrought Polycrystalline Beryllium Sheet, Third Progress Report, March 1–June 30, 1966, The Brush Beryllium Co., July 8, 1966.
6. G. London and G. Stone, Characterization of the Mechanical Properties of Distilled and Zone Refined Beryllium, September 15, 1965–March 14, 1966, Franklin Institute.
7. R. H. Katz and J. Greenspan, Twin-Particle Interaction in Beryllium, *Acta Met.*, 14: 1124-1126 (September 1966).
8. V. E. Blake, An Experimental Investigation of the Behavior of Beryllium Metal in Simulated Launch-Pad Abort Environments, Report Sandia 82-6211, Thompson Ramo Wooldridge Inc., July 1965.
9. J. C. Griess and J. L. English, Materials Compatibility and Corrosion Studies for the Argonne Advanced Research Reactor, USAEC Report ORNL-4034, Oak Ridge National Laboratory, November 1966.
10. J. P. Denny and G. E. Meyer, Beryllium Ingot Wire, *Wire Wire Prod.*, 41(10): 1640-1641, 1712-1713 (October 1966).
11. G. E. Meyer, Casting and Hot Working of Sound, Large Diameter Beryllium Ingots, Report AFML-TR-65-361, The Beryllium Corp., September 1965.
12. R. E. Snider and J. F. Kahles, Machining Data for Beryllium Metal, Report AFMDC-66-3, Metcut Research Associates, Inc., June 1966.
13. National Aeronautics and Space Administration, George C. Marshall Space Flight Center, The Fabrication of Beryllium, Report NASA-TM-X-53453, July 1966:
    Vol. I, A Survey of Current Technology
    Vol. II, Forming Techniques for Beryllium Alloys
    Vol. III, Metal-Removal Techniques
    Vol. IV, Surface Treatments for Beryllium Alloys
    Vol. V, Thermal Treatments for Beryllium Alloys
    Vol. VI, Joining Techniques for Beryllium Alloys
14. D. Hauser, H. W. Mishler, R. E. Monroe, and D. C. Martin, Electron-Beam Welding of Beryllium, Report

AFML-TR-66-215 (AD-488047), Battelle Memorial Institute, July 1966

15. J. L. Hesse, Impact and Hardness Properties of Irradiated Beryllium, Thesis, New Mexico State University, 1966.
16. F. W. Postma, Jr., and G. E. Walden, Determination of Free, Combined, and Adsorbed Carbon in Beryllium, USAEC Report Y-1556, Union Carbide Corporation, Nuclear Division, Oct. 14, 1966.
17. *Conference Internationale sur la Metallurgie du Beryllium*, Grenoble, France, May 17–20, 1965, Presses Universitaires de France, 1966.
18. General Electric Company, Nuclear Materials and Propulsion Operation, High-Temperature Materials Program Progress Report No. 61, USAEC Report GEMP-61, Sept. 30, 1966.
19. J. Winton, Method for Gas-Hydriding Zirconium Alloys at 400°C, British Report TRG-Report-1255, May 20, 1966.
20. General Electric Company, Nuclear Materials and Propulsion Operation, High-Temperature Materials Program Progress Report No. 60, USAEC Report GEMP-60, Aug. 15, 1966.
21. D. T. Peterson and J. A. Straatmann, Lanthanum–Lanthanum Hydride Phase System, *J. Phys. Chem.*, 70(9): 2980-2984 (September 1966).
22. Atomics International, Annual Technical Progress Report, AEC Unclassified Programs, Fiscal Year 1966, USAEC Report NAA-SR-12010, Aug. 31, 1966.

Section III

Reactor Materials

Nuclear Poisons

Gadolinium

Chinese workers determined the Mo–Gd phase diagram[1] and found a peritectic at 2457 °C. Gadolinium was found to be sparingly soluble in tungsten, as indicated below:

Temperature, °C	Wt.% gadolinium in tungsten
2400	1.1
2200	0.4
2000	0.3
1800	0.2
1600	0.15

The oxidation rate of gadolinium was measured by Mound researchers,[2] with the results shown in Fig. III-1. It had been found earlier that the initial oxidation obeys a parabolic relation in the temperature range 530 to 900 °C. The activation energy for oxidation was calculated to be 34 kcal/mole.

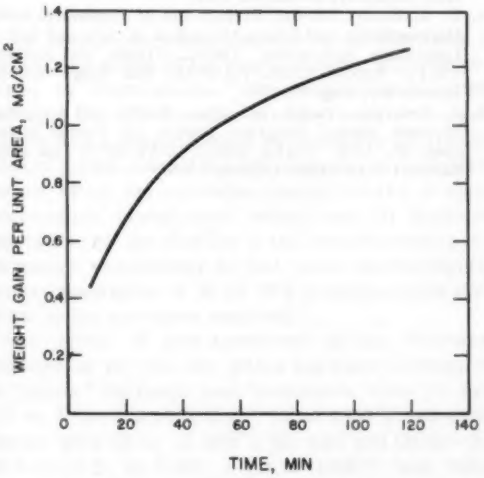

Fig. III-1 Oxidation of gadolinium at 900°C, 150 torrs oxygen.[2]

(M. Kangilaski)

Dispersion and Nonmetallic Poison Materials

Boron and Boron Compounds

Workers at the National Reactor Testing Station[3] are developing a method for controlling the dispersion of burnable poisons in fuel cores. The burnable poison, natural B_4C, was dispersed in the amount of 7 wt.% as −325-mesh particles in aluminum and rolled into foil 0.003 to 0.004 in. thick. This foil was then positioned between two half thicknesses of a 22 wt.% U–Al fuel alloy and rolled by the standard procedure. The boron content of the five elements described varied from 2.78 to 3.35 g, as determined by reactivity measurement. Although a more precise control of boron content is desired, the plates were sound after irradiation in the Engineering Test Reactor to an average ^{235}U burnup of 30%. Further refinements in the procedure and more extensive irradiation testing are required in this area.

Rare Earths

Microspheres of the lanthanide oxides have been prepared by the sol-gel method at Oak Ridge.[4] Gel microspheres are converted to oxide microspheres by drying in vacuum for several hours at 100 to 125 °C, heating to 500 °C in vacuum to decompose the residual nitride, and then air sintering at temperatures to 1500 °C. The Eu_2O_3 microspheres shrink by a factor of 1.69 on the diameter during the sintering operation to produce a crystal density of 95 to 98% of theoretical. The crystallite sizes range from the order of 300 A for the Pr_6O_{11} sintered at 1100 °C to 750 A for the Eu_2O_3 sintered at 1450 °C. The microsphere crush strengths ranged from 200 g for 120-μ-diameter spheres to 1.5 to 2.5 kg for 450-μ-diameter spheres. The crushing strengths of the Eu_2O_3 microspheres, heated to 1450 °C to obtain the monoclinic crystal form, were not as high as those of other lanthanide oxides which did change in crystal form in this temperature range. Chemical analyses of these microspheres or their use in dispersion structures have not been reported. It is anticipated that the incorporation of Eu_2O_3 microspheres in cermets for reactor control rods may be forthcoming.

Oak Ridge[5] has completed the evaluation of three High Flux Isotope Reactor (HFIR)-type control-rod specimens. Two of the rods contained 33 vol.% Eu_2O_3–Al dispersions, and the other, a 38 vol.% $Eu_{5.3}MoO_{11}$–Al dispersion. All three test specimens had the same nominal cladding–core–cladding thicknesses (0.031–0.188–0.031 in.) as the full-size HFIR control-rod plates. The test specimens were irradiated at process-water temperature (60°C) for periods ranging up to 1 year of full-power operation, and this treatment resulted in estimated unperturbed total exposures of up to 2.9×10^{21} thermal neutrons/cm^2 and 1.1×10^{21} fast neutrons/cm^2. Postirradiation examination indicated that both the 33 vol.% Eu_2O_3–Al and the 38 vol.% $Eu_{5.3}MoO_{11}$–Al dispersions were stable during irradiation. Volume changes as given in Table III-1 indicate that the Eu_2O_3 dispersions do not change significantly. The 0.60% change for the $Eu_{5.3}MoO_{11}$–Al dispersion is thought to be an experimental error since this was recorded the first time the samples were removed and checked, and no further change was noted in the later removals.

Table III-1 DIMENSIONAL STABILITY OF Eu_2O_3–Al AND $Eu_{5.3}MoO_{11}$–Al DISPERSIONS AFTER IRRADIATION IN THE ORR AT 60°C (Ref. 5)

Dispersion concentration, vol.%	Specimen burnup		Volume change, %
	Neutrons absorbed per original europium atom	Neutron absorptions/cm^3	
33 Eu_2O_3	0.19	1.6×10^{21}	+0.17
33 Eu_2O_3	0.48	4.1×10^{21}	−0.03
38 $Eu_{5.3}MoO_{11}$	0.34	2.9×10^{21}	+0.60

The behavior of cut sections of unirradiated and irradiated specimens tested in water at 100°C for 100 hr is compared in Table III-2. These results demonstrate the water-corrosion resistance of the $Eu_{5.3}MoO_{11}$ compound. As expected, the Eu_2O_3 hydrolyzed. The comparative improvement in the irradiated Eu_2O_3 dispersions can probably be attributed to the fast-neutron-induced hardening of the aluminum matrix. The increase in strength probably acts to retard cracking when the hydrolyzed Eu_2O_3 swells and corrosion penetration into the interior is thereby decreased. (D. E. Lozier)

Table III-2 CORROSION OF IRRADIATED AND CONTROL HFIR-TYPE NEUTRON-ABSORBER PLATES[5]

Poison loading, vol.%	Specimen burnup, neutron absorptions/cm^3	Weight change, %	Thickness change, %
33 Eu_2O_3	Unirradiated	+2.03	+15.2
33 Eu_2O_3	1.6×10^{21}	+0.43	+ 5.1
33 Eu_2O_3	4.1×10^{21}	+0.32	+ 3.2
38 $Eu_{5.3}MoO_{11}$	Unirradiated	+0.02	0
38 $Eu_{5.3}MoO_{11}$	2.9×10^{21}	+0.06	0

References

1. Y. Chuang, C. Li, H. Chuang, and L. Kao, Study of Molybdenum–Gadolinium Phase Diagrams (in Chinese), *Chin Shu Hsueh Pao*, 9: 110-112 (January 1966).
2. Mound Laboratory Isotopic Power Fuels Programs, July–September, 1966, USAEC Report MLM-1362, Oct. 31, 1966. (Classified)
3. W. C. Francis and R. A. Moen (Eds.), Annual Progress Report on Reactor Fuels and Materials Development for FY 1966, USAEC Report IDO-17218, Phillips Petroleum Company, November 1966.
4. C. J. Hardy, Sol-Gel Preparation of Lanthanide Oxide Microspheres and Characterization of Sols and Gels of Lanthanide Hydroxides, Thoria, Urania, and Plutonia, USAEC Report ORNL-TM-1592, Oak Ridge National Laboratory, Aug. 12, 1966.
5. S. Peterson (Comp. and Ed.), Metals and Ceramics Division Annual Progress Report for Period Ending June 30, 1966, USAEC Report ORNL-3970, Oak Ridge National Laboratory, October 1966.

Section IV

Reactor Materials

Cladding and Structural Materials

Corrosion

Corrosion of Zirconium Alloys

AQUEOUS CORROSION

The aqueous-corrosion behavior of Valoy (Zr–2 at.% Cr–0.16 at.% Fe) has been compared with that of Zircaloy-2 at Vallecitos.[1] Results of long-term tests (in excess of 8000 hr) are summarized below:

	Corrosion rate, mg/(dm²)(day)	
	Valoy	Zircaloy-2
300°C water	Same rates	
400°C steam	0.2	1.4
500°C steam	0.8	9.5

Optimum corrosion performance of Valoy was found to be associated with fine, uniformly distributed intermetallics in a strain-free matrix composed of Zr–0.9 at.% Cr.

The in-pile corrosion behavior of the Zircaloys in the borated water of the Saxton reactor has been reported by Westinghouse.[2] The results of the study indicated that (1) Zircaloy-clad fuel rods were compatible with a borated-water environment; (2) irradiation to a total dose of 2×10^{21} neutrons/cm² (>1 Mev) did not affect the corrosion rate of Zircaloy in high-temperature pressurized water; and (3) hydrogen absorption by the cladding in the borated reactor environment was similar to that in out-of-pile experiments (absorption of 20 to 25% of the hydrogen produced by the corrosion reaction).

The effect of heat-treatment on the corrosion behavior of Zr–Cu–Mo alloys has been investigated in Canada.[3] Optimum heat-treatments were (1) Zr–1.0 wt.% Cu–1.5 wt.% Mo, 1 hr at 1000°C and water quench plus 32 hr at 500°C (in air) and (2) Zr–0.5 wt.% Cu–0.5 wt.% Mo, 1 hr at 1000°C and water quench plus 24 hr at 500°C (in air). Weight gains after 400-hr exposure to 1500-psi steam at 400°C were 40 mg/dm² for the former and 50 mg/dm² for the latter heat-treatment. Overaging produced large intermetallic particles in the above alloys, which resulted in cracking in the corrosion film and acceleration of the corrosion rate.

In steam-oxidation studies of zirconium alloys at General Electric,[4] isothermal tests have shown that zirconium, Zircaloy-2, and Valoy exhibit essentially the same oxidation rates in the temperature range 1200 to 1600°C. Oxidation behavior was examined at temperatures ranging from 1200°C to the melting point of the materials.

ORGANIC COOLANTS

The in-reactor and out-of-reactor corrosion behavior of zirconium alloys in organic coolants has been summarized by Whiteshell.[5,6] It was shown that the rate of hydriding of low-nickel Zircaloy-2, Zircaloy-4, and Zr–2.5 wt.% Nb alloy can be held to reasonable limits by maintaining >50 ppm water in the coolant and controlling the amount of chloride contamination. Estimated useful lives in the WR-1 reactor (organic cooled, heavy-water moderated) were found to be (1) 5 years for Zircaloy-4 or Zr–2.5 wt.% Nb as pressure-tube materials and (2) more than 1 year for Zr–2.5 wt.% Nb as fuel cladding.

Imarisio and Cocchi[7] have made a statistical analysis of the effect of surface preparation and environmental factors on the corrosion behavior in terphenyl of Zircaloy-2 and Zr–3 wt.% Nb–1 wt.% Sn. The results of a factorial experiment indicated that the factors of time, temperature, and chlorine concentration and their interactions were all significant; surface treatment (pickled vs. preoxidized) had a negligible effect, whereas water concentration was significant for the Zr–Nb–Sn alloy but not for Zircaloy-2.

(W. E. Berry)

Corrosion of Aluminum Alloys

The fundamental mechanisms of the corrosion of aluminum alloys in water at 200 to 300°C are being studied at Oak Ridge.[8] Alloy additions include Zn, Mg, Cu, Fe, Y, and Be. Within certain concentration ranges, all additives greatly improved the corrosion resistance of aluminum. The marked improvement occurred when a second phase was present. No electrochemical effect could be ascribed to the second phase because the observed reduction in corrosion rate of the several alloys was independent of whether the second phase was anodic or cathodic to the aluminum matrix.

A Norwegian study[9] has concerned the movement of ions through the passive film on aluminum. In room-temperature high-purity water, passivation was found to be due to a 10- to 30-A-thick barrier film adjacent

to the metal surface. The barrier film was an ionic semiconductor in which the transport of both anions and cations determined the corrosion rate. The barrier oxide was found to be unstable in water and was continuously converted to the hydrated bulk oxide. It was concluded that the bulk oxide also was important in the corrosion process because it protected the barrier oxide from the water.

The aqueous-corrosion behavior of several aluminum alloys has been compared by Phillips Petroleum Company.[10] Out-of-pile isothermal tests at 190°C and at a flow rate of 45 ft/sec have shown that the oxide buildup on the 2219 alloy was higher than that on 6061 and X8001 alloys. In-pile tests of fuel plates at 46 ft/sec, 1 to 2.5×10^6 Btu/(hr)(sq ft), and 142 to 206°C, with fuel burnups to 68% (4626 Mwd), revealed maximum oxide buildup of 2.2 mils on the 2219 copper-containing cladding alloy. No copper was found in the loop water after these tests. It was concluded from these studies that the superior strength at elevated temperatures of the 2219 alloy more than offset its higher oxidation rate, and that it appeared attractive as a fuel-cladding material for high-flux aqueous reactors.

The effect of heat-treatment on the aqueous corrosion of electroless-nickel-coated 6061 aluminum is also being studied by Phillips.[11] Specimens were exposed 800 hr to 190°C water flowing at 45 ft/sec. Nondiffusion heat-treatments at 410°C offered the best corrosion resistance, with corrosion rates of 1 to 3 mg/(dm^2)(day) and no evidence of pitting.

(W. E. Berry)

Corrosion of Stainless Steel

Conceptual sketches illustrating the theory of initiation of stress–corrosion cracking in stainless steels and other alloys have been prepared by The Ohio State University.[12] The theory presumes that cracks initiate at anodic sites where active slip planes under applied stress emerge at the surface and rupture the passive oxide film. This mechanism is used to explain the improved resistance to cracking obtained by oxidizing a specimen prior to exposure to a crack-producing environment over that obtained by exposing the specimen directly to the environment.

Westinghouse has determined the distribution, composition, and activity of corrosion products on the stainless-steel cladding of Yankee reactor cores I and II (Ref. 13). The corrosion films were found to be depleted in iron and enriched in chromium and nickel (with respect to 348 stainless steel), whereas the deposits were slightly depleted in nickel and severely depleted in chromium. The in-core corrosion products were determined to have originated mainly at out-of-core sources. It was concluded that the major effect of the corrosion products appeared to be their influence on the thermal and hydraulic characteristics of the fuel assembly. (W. E. Berry)

Corrosion of Nickel-Base Alloys

The account of stress–corrosion cracking of highly stressed Inconel 600 tubes in the Agesta Nuclear Power Station has been published by Swedish scientists.[14,15] The cracks originated on the outside surface which contacted light water at *p*H 10 (LiOH or KOH) and 217°C for approximately 150 days. Cracks were found in crevices and on fully exposed surfaces. Surface contamination at the cracks was found to be limited to 1 μg/cm^2 of fluorine. Subsequent laboratory tests in high-purity water and in 1*M* LiOH at 220°C failed to produce cracks in stressed Inconel 600 samples. Although the cause of cracking was not established, it was recommended that Inconel 600 be vacuum melted to minimize impurities (particularly carbon), that fabrication and operation stresses be minimized, and that crevices and localized boiling be eliminated in the reactor.

Battelle–Northwest[1] has studied the evaporation rates of superalloys Hastelloy X and Haynes 25 in helium. Preliminary results indicate that evaporation rates increase with temperature at 2000 to 2100°F (1093 to 1149°C) and with velocity above 300 ft/sec. Maximum metal-evaporation rates were about 0.07 mil/day. (W. E. Berry)

Corrosion of Miscellaneous Alloys

The long-term corrosion behavior of a number of candidate materials for the High Flux Isotope Reactor (HFIR) has been studied at Oak Ridge.[16] The environment was water adjusted to *p*H 5.0 (HNO_3) at 100°C with flow rates ranging from 0.5 ft/min to 81 ft/sec. Exposure times ranged up to 20,000 hr. Maximum corrosion rates were:

Aluminum alloys	0.2 mil/year (pits 7 mils deep after 14,200 hr)
QMV beryllium	2 mils/year (pits 13 mils deep after 8500 hr)
Nickel	2 mils/year (shallow pitting)
Electroless nickel on 6061 aluminum	19 mils/year (shallow pitting)
Hardened 416 stainless steel	<0.1 mil/year (small blisters)

Hardened 420 stainless steel exhibited stress–corrosion cracking, as did a beryllium sample coupled to 304 stainless steel. Polyformaldehyde plastic almost disintegrated. Aluminum was subject to pitting attack on surfaces contacted by itself, beryllium, nickel, and 304, 420, and 17-4 PH stainless steels. Maximum pit depth was 54 mils for an Al–Ni couple exposed for 5560 hr.

Oak Ridge[17] has also studied the corrosion of the beryllium reflector, 6061-T6 aluminum beam tubes, and 304 stainless-steel fuel cladding under the Argonne Advanced Research Reactor operating conditions (flowing water to 127°C). The corrosion rate of beryllium was found to be between 1.1 and 2.8 mils/year, which would be acceptable. The corrosion be-

havior of 6061-T6 aluminum under high heat transfer was found to be acceptable if the temperature was maintained at 200°F (93°C) or less. The 304 stainless steel exhibited little or no attack after 2000 hr in water at a heat flux of 2.1×10^6 Btu/(hr)(sq ft), but numerous small cracks 0.2 mil deep were observed at a higher heat flux of 4.0×10^6 Btu(hr)(sq ft).

The corrosion resistance of reactor materials is described in a recent Russian publication,[18] which is more than 600 pages in length. Chapter headings are listed below:

I. Stainless Chromium-Nickel Steels
II. Stainless Chromium-Nickel Steels (Stress-Corrosion Cracking)
III. Stainless Chromium Steels
IV. Carbon and Low Alloy Steels
V. Aluminum and Its Alloys
VI. Beryllium, Magnesium, and Their Alloys
VII. Zirconium and Its Alloys
VIII. Titanium, Niobium, and Their Alloys
IX. Protective Coatings

Information obtained since 1960 on the corrosion behavior of titanium and its alloys has been reviewed by the Defense Metals Information Center.[19] Included among the environments were salts, mineral acids, gases, liquid metals, and organic compounds. Considerable attention was given to the problem of stress–corrosion cracking. (W. E. Berry)

Corrosion of Refractory Metals

The Ohio State University[20] has studied the simultaneous internal oxidation and external scale formation of Nb–Zr and Nb–Zr–Re alloys in oxygen at 1000°C. Eleven arc-melted alloys containing up to 40 at.% zirconium and 10 at.% rhenium were used in this investigation. For each binary alloy a constant rate of scale formation was observed at steady state, and the internal-oxidation zone reached a steady-state time-independent thickness. The scaling rate of Nb–10 at.% Zr was about 2.3 times that of unalloyed niobium. With increasing zirconium, the scaling rate was reduced to a value below that of niobium. This behavior was partially attributed to internal oxidation, with the resulting formation of a relatively impervious ZrO_2 precipitate. The morphologies of the ZrO_2 internal oxide were also found to affect the scaling rate. Increasing the zirconium from 10 to 40 at.% reduced the steady-state thickness of the internal-oxidation zones by a factor of 3, which could not be rationalized from an idealized simple model. The steady-state thickness of the internal-oxidation zone in Nb–Zr alloys was reduced by about a factor of 2 by the addition of 2 or 5 at.% rhenium. These additions also caused local enrichment at the metal/scale interface. More adherent and less porous external scales were formed in the higher rhenium alloy and caused a significant reduction in scale formation.

The oxidation of arc-melted and homogenized Nb–V–Ti solid solutions, containing up to 15 wt.% vanadium and 10 wt.% titanium, has been studied in air[21] at 900 to 1200°C. Oxidation rates were linear except in the initial stages. Titanium and vanadium decreased the oxidation rate by up to factors of 2 and 5, respectively, with a Nb–5 wt.% V–10 wt.% Ti alloy being the most resistant. Activation energies for oxidation of these alloys range from 13.8 to 27.5 kcal/mole and appear to be independent of composition.

The oxidation of tantalum in the temperature range 500 to 950°C and at 1- to 60,000-torr oxygen pressure has been reviewed by Stringer.[22] At atmospheric pressure the rate constant increases with temperature in the range 500 to 650°C and 800 to 950°C but decreases slightly in the range 650 to 800°C. The reaction rate depends on the square root of the oxygen pressure at low pressures and high temperatures, but, at lower temperatures, this pressure dependence decreases. On the basis of experimental evidence, it was concluded that in the range 500 to 800°C the rate-controlling process is a reaction at the interface between the atmosphere and an adherent layer of Ta_2O_5 growing on the metal surface. This reaction is preceded by an equilibrium adsorption of oxygen on the interface, the adsorption taking place with dissociation. In the range 800 to 950°C, the overall linear rate is a consequence of diffusion-controlled growth of adherent Ta_2O_5 to a critical thickness, at which the scale fails. The corollary to this conclusion is that the rate of the diffusion process must be strongly oxygen-pressure dependent.

Stringer[23] found that the oxidation rate of tantalum was not always isotropic. Single-crystal spheres were oxidized at 500, 600, 820, and 925°C in 450-torr oxygen. The rate was isotropic at the lower two temperatures. At the higher temperatures the $\{1\,1\,0\}$ faces oxidized more rapidly than the $\{1\,0\,0\}$, and this led to surface faceting of the metal. Scale failure was found to be aided by pore paths over suboxide plates, an effect which could cause the observed rate anisotropy. The habit plane for these plates was found to be $\{1\,0\,0\}_{Ta}$ at 500 to 925°C. It was demonstrated that the pores were produced by oxidation of suboxide plates, and their existence at 800 and 925°C was proven.[24] The apparent calculated tantalum-atom density was compatible with the tetragonal structure for "TaO_z," for which values of z have been reported to range from 0.25 to 2. Other work[25] indicates that the suboxide plates form during cooling from the range 850 to 1100°C. Electron-probe microanalysis suggested a suboxide composition of Ta_4O, although the amount was insufficient for X-ray diffraction analysis.

The oxidation behavior of chromium containing 32 and 44 at.% rhenium has been studied at 700 to 1400°C in oxygen and air by General Electric[26] using thermogravimetric, metallographic, electron-probe, and X-ray analyses. The oxidation reactions observed included the formation of a Cr_2O_3 external scale, a subscale, and volatile rhenium oxides. The scale on Cr–32 at.% Re alloy was quite protective. Deviations from the parabolic behavior of unalloyed chromium

indicated some rhenium loss, probably as Re_2O_7 evolved through scale defects such as cracks. On Cr–44 at.% Re, the Cr_2O_3 scale was porous, and subsequent rhenium loss gave rise to linear kinetics. Air-oxidized samples showed essentially the same kinetics as samples exposed to oxygen. The Cr_2N was not detected in these samples.

In a NASA–Langley investigation,[27] an improved rate equation for the oxidation of molybdenum to MoO_3 above 1500°K has been derived theoretically. This derivation takes into account both chemical and mass-transfer parameters, and the resulting equation should be applicable to any situation where the mass-transfer coefficient of oxygen to a molybdenum surface can be determined. Application to previously reported data using air and O–He mixtures at subsonic velocities gave an activation energy for oxidation of 20.3 ± 0.2 kcal/mole, which agrees well with generally accepted values. A total of 32 molybdenum hemisphere-cylinder specimens were oxidized using a Mach 2.1 heated air stream at a stagnation pressure of 10.5 atm at 1765 to 2120°K. According to Fig. IV-1, the stagnation-point surface temperature and recession rate generally compared with theoretically predicted values to within a factor of 2. A few specimens exhibited recession rates much higher than those predicted, apparently as a result of a sharp rise in surface temperature which caused some melting.

The oxidation of molybdenum containing up to 8 wt.% yttrium has been studied[28] at 600 and 900°C (presumably in air). At 600°C, yttrium had no effect on oxidation rate, and X-ray analysis indicated that the scale was MoO_3 in all cases. At 900°C, yttrium reduced the oxidation rate and resulted in scale with an outer layer consisting of loose $Y_2O_3 \cdot 3MoO_3$ and an inner layer composed of MoO_2 plus traces of yttrium.

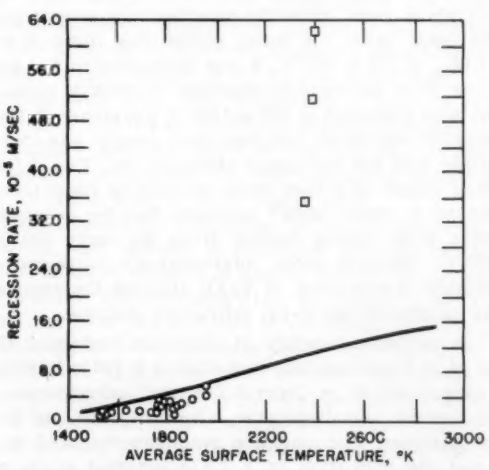

Fig. IV-1 Variation of recession rate of molybdenum with surface temperature.[27] ○, normal oxidation; □, ignition; —, theoretical curve.

Westinghouse[29] conducted a study of the oxidation of polycrystalline tungsten ribbon at 1300 to 2450°K in oxygen at 10^{-5} to 10^{-8} torr. Pressures were measured with a mass spectrometer. The efficiency of carbon removal was found to be reasonable above 10^{-6} torr oxygen at ~2000°K. With carbon removed, the rate of oxygen removal at the tungsten surface was then determined as a function of temperature. Below 2000°K, evaporation of tungsten oxides occurred at predictable rates, but, at higher temperatures, atomic oxygen was produced, making the rate of removal strongly influenced by the specific species present in the entire system. For example, a silver surface reacted with oxygen atoms to give a large apparent increase in the pumping speed at a tungsten surface enclosed in a glass system.

Russian workers[30] have investigated the potentiostatic polarization of molybdenum in 1*N* solution of H_2SO_4 and KOH at room temperature. The passivity region in H_2SO_4 extended from +0.4 to −0.15 volt (presumably with respect to hydrogen) where it adjoins the immunity region. Molybdenum was not passivated in KOH. The electrochemical properties of all known molybdenum oxides were investigated experimentally, and thermodynamic calculations showed that the passivity of molybdenum in acid solution was due to $MoO_{2.65-2.75}$. Molybdenum dissolved at about a constant rate at high anode potentials in acid and alkaline solutions, as permitted by the formation of a multilayered surface film consisting of slight stoichiometric variations of MoO_3.

Fluoride coatings applied from a saturated KHF_2 solution have been reported to offer some oxidation protection of niobium, tantalum, and tungsten.[31] At 800°C the oxidation rates in dry oxygen were reduced by factors of about 2, 4, and 6, respectively.

(B. C. Allen)

IAEA Symposium on Alkali-Metal Coolants

On Nov. 28 to Dec. 2, 1966, the International Atomic Energy Agency (IAEA) sponsored a symposium on "Alkali Metal Coolants — Corrosion Studies and System Operating Experience," with over 100 participants representing 16 countries. Only a few of the approximately 50 papers presented dealt with coolants other than sodium. The proceedings, being published by the IAEA, will constitute a rather complete international state-of-the-art compendium as of mid-1966. Some of the corrosion papers are reviewed briefly here.

The Soviets described[32a] an extensive study of the effects of various parameters on the corrosion of steels by sodium. Measurements made on tabs of assorted metals and alloys exposed in pumped loops fabricated of a steel containing 20 wt.% chromium, 14 wt.% nickel, and 2 wt.% silicon yielded the results shown in Figs. IV-2 to IV-4. These, plus metallographic and mechanical-property studies of sodium-exposed specimens and argon-exposed controls, led

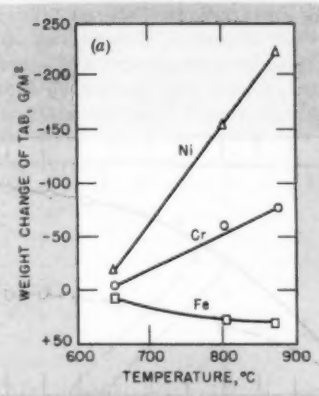

Fig. IV-2 Influence of test conditions on attack of sheet coupons of electrolytic nickel, Armco iron, and cast chromium by flowing sodium during 500-hr exposure in a (20 Cr–14 Ni–2 Si, wt.%) steel loop.[32]

(a) Effect of temperature.
Oxygen in sodium = 30 to 50 ppm
Sodium flow velocity = 0.6 m/sec

(b) Effect of oxygen content in sodium.
Temperature = 800°C
Sodium flow velocity = 0.6 m/sec

(c) Effect of sodium flow velocity.
Temperature = 650°C
—, Oxygen in sodium = 30 to 50 ppm
---, Oxygen in sodium = 300 to 500 ppm

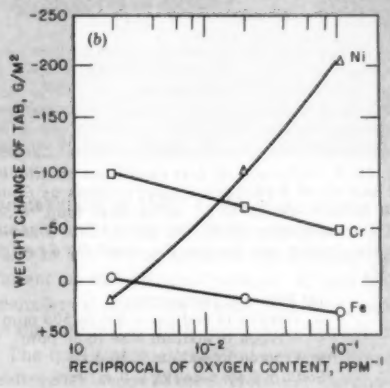

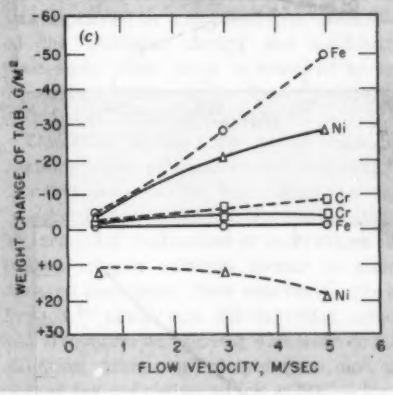

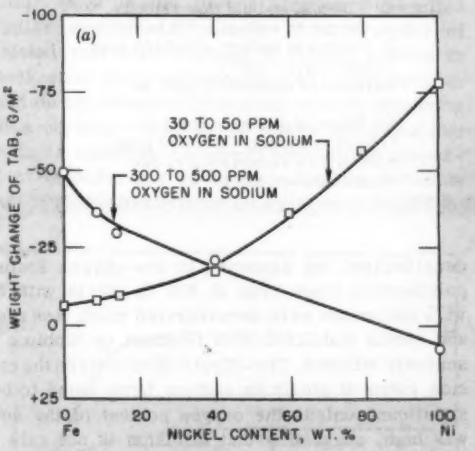

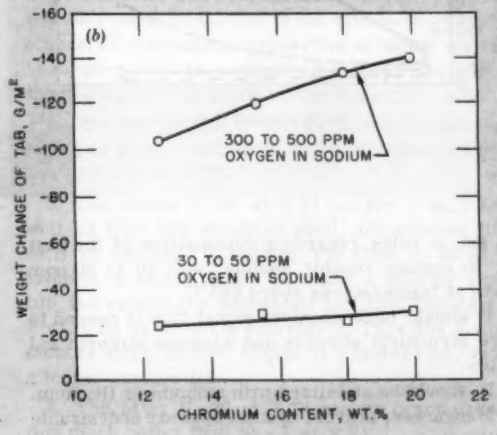

Fig. IV-3 Influence of composition of Cr–Ni steel coupons on attack by flowing sodium during 500-hr exposure in (20 Cr–14 Ni–2 Si, wt.%) steel loop.[32a]

(a) Effect of nickel content.
Chromium content ~16 wt.%
Temperature = 650°C
Sodium flow velocity = 5 m/sec

(b) Effect of chromium content.
Nickel content = 15 wt.%
Temperature = 800°C
Sodium flow velocity = 3 m/sec

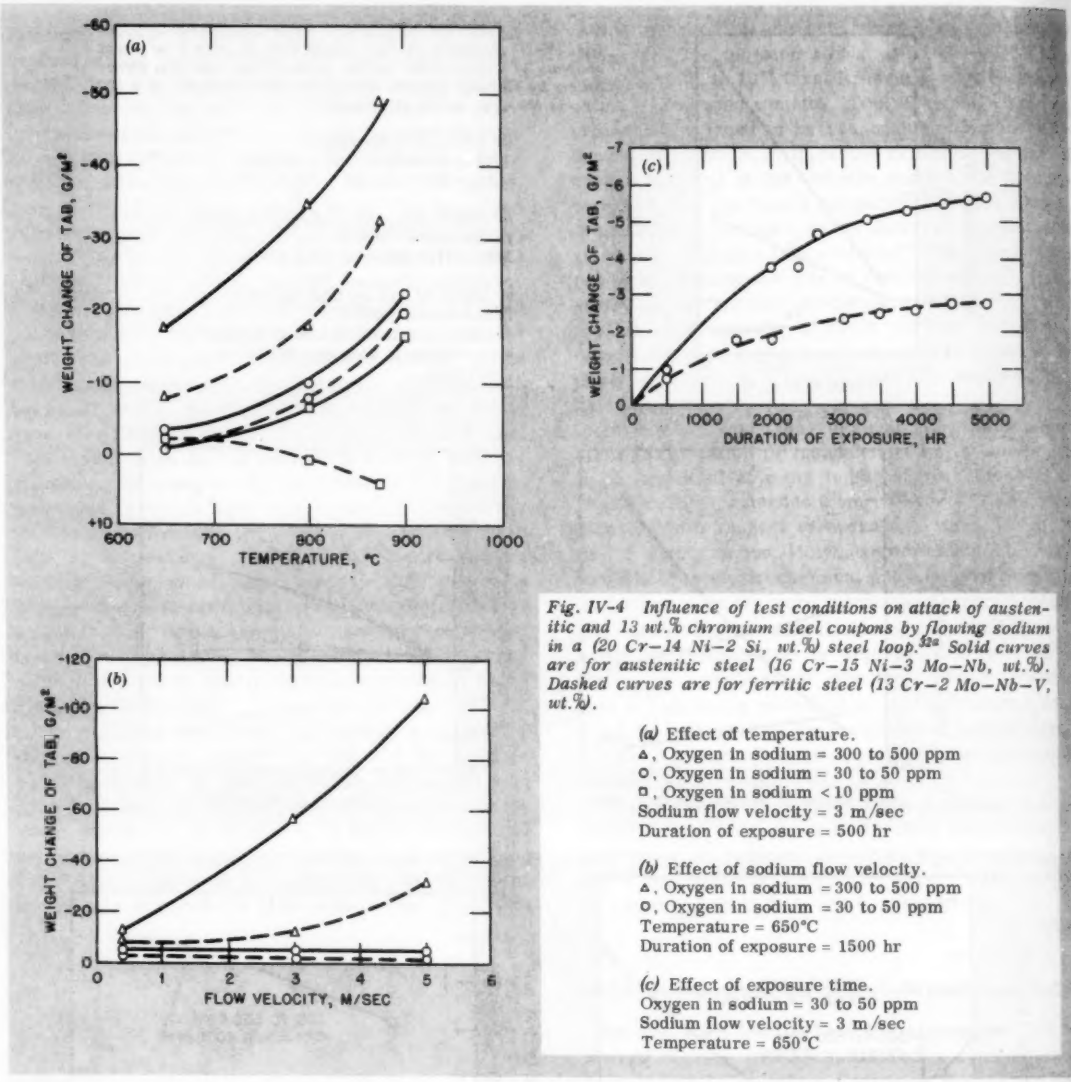

Fig. IV-4 Influence of test conditions on attack of austenitic and 13 wt.% chromium steel coupons by flowing sodium in a (20 Cr–14 Ni–2 Si, wt.%) steel loop.[32a] Solid curves are for austenitic steel (16 Cr–15 Ni–3 Mo–Nb, wt.%). Dashed curves are for ferritic steel (13 Cr–2 Mo–Nb–V, wt.%).

(a) Effect of temperature.
△, Oxygen in sodium = 300 to 500 ppm
○, Oxygen in sodium = 30 to 50 ppm
□, Oxygen in sodium < 10 ppm
Sodium flow velocity = 3 m/sec
Duration of exposure = 500 hr

(b) Effect of sodium flow velocity.
△, Oxygen in sodium = 300 to 500 ppm
○, Oxygen in sodium = 30 to 50 ppm
Temperature = 650°C
Duration of exposure = 1500 hr

(c) Effect of exposure time.
Oxygen in sodium = 30 to 50 ppm
Sodium flow velocity = 3 m/sec
Temperature = 650°C

to a set of rules regarding composition of the best steel to contain reactor sodium (with 30 to 50 ppm oxygen) at temperatures above 650°C:

1. It should have no more nickel than is needed to ensure structural stability and adequate strength and ductility.
2. It should be stabilized with niobium or titanium.
3. Manganese, silicon, and nitrogen are undesirable constituents.
4. It should contain minor additions of molybdenum or tungsten (on the order of 3 wt.%).

A Czechoslovakian study[32b] employing remarkably similar loops yielded conclusions that are consistent with these. It was noted that low-alloy steels were decarburized by exposure to low-oxygen sodium in polythermal loops even at 400°C; steels with 3 to 5 wt.% chromium were decarburized much less readily, and steels stabilized with titanium or niobium were scarcely affected. The effects of velocity on the corrosion rates of steels in sodium were found to be insignificant unless the oxygen content of the sodium was high, suggesting that diffusion is not rate controlling in a pure sodium environment. This agrees exactly with the Soviet findings (cf. Fib. IV-4*b*).

Results of an extended Oak Ridge loop program on the effects of operating conditions on mass transfer of nickel-base alloys and stainless steels in sodium were summarized.[32c] Comparative amounts of cold-

leg deposits after 1000-hr loop tests are shown in Fig. IV-5. Immediately evident is the fact that the nickel-base alloys show no mass transfer below about 1200°F (650°C) and that they are considerably worse than the stainless steels at 1500°F (815°C) and above.

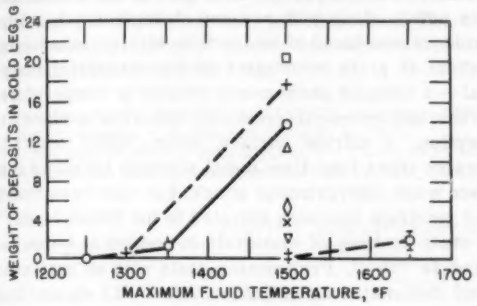

Fig. IV-5 Comparative mass-transfer rates of nickel-base alloys and stainless steels in sodium.[32c] Operating conditions; ΔT, 300°F; flow, 2.5 gal/min; test time, 1000 hr. □, Hastelloy W; +, Hastelloy B; ○, Inconel; △, Inconel X; ◇, 330 stainless steel; ×, 310 stainless steel; ▽, 430 stainless steel; ‡, 347, 316, and 304 stainless steels; ⨯, 316 stainless steel.

At a peak temperature of 1500°F, the mass-transfer rate of Inconel in sodium increases linearly with ΔT in the range 150 to 400°F but seems to be independent of oxygen content of the sodium between 10 and 500 ppm. Mass transfer of stainless steels, however, was found to increase noticeably with increasing oxygen in the sodium. The qualitative agreement between these Oak Ridge findings and those of the Soviets and Czechoslovakians noted above is excellent.

Similar work in the United Kingdom[32d] resulted in similar conclusions; namely, mass transfer of high-nickel materials exposed to flowing sodium in stainless-steel loops is insensitive to oxygen level in the sodium but sensitive to sodium velocity (implying diffusion control), whereas the rate of mass transfer of steels is sensitive to oxygen level and is proportional to velocity only up to some limiting Reynolds number. These latter effects are apparent in Fig. IV-6.

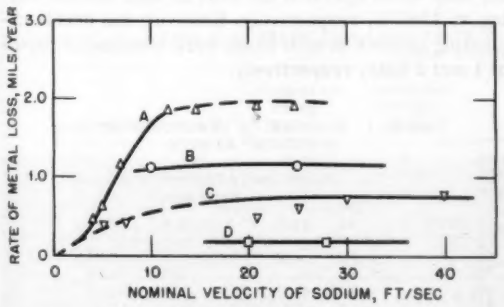

Fig. IV-6 Effect of velocity on the rate of metal loss from various stainless steels (bore diameter constant).[32d] A, 650°C, ~25 ppm O_2. B, 725°C, ~10 ppm O_2. C, 650°C, ~10 ppm O_2. D, 650°C, <5 ppm O_2.

The effect of surface finish on the corrosion of Inconel X-750 and Inconel X-550 by 500, 550, and 600°C flowing sodium (50 cm/sec) was studied in Germany.[32c] Specimens annealed at 1050°C were exposed in a stainless-steel loop for over 1000 hr and then examined for changes in weight, surface geometry, and composition. Two chemical methods (pickling and electropolishing) and three mechanical methods (grinding, polishing, and sandblasting) were used to obtain a range of surface qualities. The oxygen content of the sodium was maintained at <10 ppm. Corrosion in all cases was trivial, the maximum (at 600°C) being equivalent to a uniform surface loss of 10^{-4} mm in 2 years. At 500°C the specimens generally gained weight; at 550 and 600°C they all lost weight. The chemically treated surfaces had better corrosion resistance than the mechanically treated surfaces. This was explained by a microscopic "Beilby" layer formed on the surfaces during the mechanical polishing processes. This layer is believed to absorb sodium or sodium oxide at the lower temperatures and to dissolve at higher temperatures.

Vanadium alloys are being considered as fuel claddings for sodium-cooled fast reactors. It was demonstrated earlier that, when the oxygen content of the sodium is kept at the low levels achievable by hot trapping, corrosion of such alloys is very slight. Higher oxygen contents result in significantly increased corrosion. This was verified in a paper by the French,[32f] along with the fact that, although titanium and zirconium as alloying elements do not improve the situation, aluminum, molybdenum, and chromium decrease the corrosive attack at 600°C for a given oxygen level. Similar work at Argonne, discussed in previous reviews, was summarized[32g] at the symposium, and the results of studies of the effects of sodium exposure on mechanical properties of jacket materials were presented in a separate paper.[32h] Briefly, the conclusions in this latter study are:

1. The application of stress during sodium exposure has a large influence on the mechanical properties of V–20 wt.% Ti.

2. The alloys V–20 wt.% Ti and Nb–1 wt.% Zr, as well as type 304 stainless steel, are affected differently by exposure to sodium. The alloy V–20 wt.% Ti exhibits a higher creep rate and a shorter rupture life, but essentially unchanged ductility. The alloy Nb–1 wt.% Zr is severely embrittled. Type 304 stainless steel is more ductile, creeps at a faster rate, and has a longer rupture life.

3. The alloy V–20 wt.% Ti resists crack propagation much better than Nb–1 wt.% Zr.

4. Both alloys form a brittle oxide case during exposure to oxygen-contaminated sodium. This case cracks during specimen strain.

5. Sheet and tube specimens show the same general creep behavior after exposure to oxygen-contaminated sodium.

In 1963, Atomics International reported[33] the results of a joint study with United States Steel to develop a ferritic alloy as a substitute for 304 stainless steel for use in sodium-cooled reactor systems. The goals were equivalent mechanical properties, resistance to decarburization, fabricability, no postweld heat-treatment requirement for joints, and lower costs. Steels with 2¼ wt.% Cr–1 wt.% Mo–0.6 wt.% V, and with these three constituents plus 0.1 wt.% niobium, were found to be very promising. Reporting on a similar study,[32i] the Germans noted that the addition of vanadium was ineffective in preventing carbon diffusion in ferritic steels at 700°C, and that niobium was a much better carbon stabilizer. However, the precipitated niobium carbide or iron niobide had an adverse effect on the impact properties and yield strength — an effect that could be counteracted by appropriate additions of manganese or nickel to the steel. Ten-ton heats of 2¼ wt.% Cr–1 wt.% Mo steels containing on the order of 1 wt.% niobium and 0.5 wt.% manganese showed satisfactory mechanical properties, workability, and weldability.

A model for the kinetics of carburization of stainless steel exposed to sodium was presented by the British.[32j] They assumed that the equilibrium level of carbon at the steel surface was set by the carbon activity of the sodium, and that a carbon activity gradient exists which extends into the stainless steel, with the growth of the thickness of the carburizing zone controlled by the diffusion of carbon down this gradient. Within this zone, chromium-rich carbide tends to precipitate to bring the local level of dissolved chromium into equilibrium with the local carbon activity, as required by the carbide composition and the law of mass action. With the aid of experimental data on carbon pickup, values for the diffusion coefficient of carbon were calculated on this basis and were found to be in reasonable agreement with extrapolated values for carbon diffusion in chromium-free austenite.

Two papers were presented on experiments designed to study corrosion in the vicinity of a small water leak in a sodium-heated steam generator. The British[32k] noted that damage is concentrated in the ever-widening zone where the sodium–water reaction front impinges on the metal surface, so that a small leak could soon cause extensive damage in adjacent areas. This so-called "tube wastage" was first observed in the Fermi reactor heat-exchanger failure in December 1962 and was also studied in detail by Atomic Power Development Associates.[32m] The latter researchers reported measured wasted-surface temperatures during the reaction of 2200°F (1200°C). In the British study, corrosion rates were found to be very much lower with stainless steel and nickel alloys than with ferritic materials, leading the workers to suggest that the phenomenon is associated with the formation of $(Na_2O)_2FeO$. Iron powder has also been observed in the vicinity of the reaction, which would imply that the double oxide is subsequently reduced, either by the hydrogen produced or by thermal cycling.

Argonne work on the effect of 650°C sodium on reactor-component materials was described.[32n] Severe sensitization of 304 stainless steel, indicating extensive carbide precipitation in the grain boundaries, was noted, along with reduced strength and ductility. Evidence was found of interaction with, or infusion of, sodium at grain boundaries of the structural material — a complex phenomenon related to temperature, stress, and chemical-reactivity effects of surface adsorption. A nitride surface layer, which may adversely affect long-time metal strength but might also discourage intergranular attack, has also been found.

A program has been initiated in the Netherlands[32p] to study fretting of materials in sodium at temperatures to 750°C. Preliminary tests with an austenitic steel designated as X8CrNiMoVNb 16/13 showed that adhesion and subsequent metal transfer occur irrespective of sodium temperature and oxygen content. However, volume wear does not become appreciable except at high oxygen content. At low oxide content, surface deterioration does not lead to the formation of wear debris. There is some indication that the wear process is quite insensitive to sodium temperature.

(E. M. Simons)

Corrosion by Liquid Metals and Fused Salts

CORROSION BY SODIUM

Weight-change data from a 70-day comparison test of six unalloyed metals in static oxygen–refreshed sodium at 650°C are summarized[34] in Table IV-1. It is clear that molybdenum and chromium are quite resistant under these conditions. The vanadium is probably next in resistance, with titanium, niobium, and tantalum demonstrating poor behavior.

Brookhaven[35] is phasing out its program on the evaluation of materials for use in boiling sodium and cesium systems. No corrosion was found in a D-43 (Nb–10 wt.% W–1 wt.% Zr–0.1 wt.% C) thermal-convection loop and in a T-111 (Ta–8 wt.% W–2 wt.% Hf) loop which operated for 3466 hr with sodium boiling at 1260°C, respectively. However, the bubble nucleating devices in both loops were attacked to depths of 1 and 2 mils, respectively.

Table IV-1 BEHAVIOR OF UNALLOYED METALS IN SODIUM[34] AT 650°C

Metal	Weight change, mg/cm², at indicated time, days					
	7.8	14.8	28.0	42.0	56.0	70.0
Cr	−0.04	−0.04	−0.04	−0.04	−0.04	−0.08
Mo	0	0	0	−0.03	−0.03	−0.03
Nb	−0.11	−0.18	−0.63	−1.5	−2.1	−2.5
Ta	−1.5	−3.0	−7.6	−10.1	−11.8	−14.4
Ti	+0.39	+0.33	−0.39	−0.99	−1.7	−2.3
V	+0.18	+0.15	−0.07	+0.11	+0.19	+0.22
O in Na, ppm		10.7	10.3		11.3	9.3

Table IV-2 summarizes the results of 25 capsule tests run with refractory-metal alloys exposed to boiling, refluxing sodium at 1000°C and above for up to 6271 hr. Most of the alloys look promising.

Utilizing a magnetic balance, workers at Culcheth[36] measured the wetting behavior in liquid sodium of alloys based on iron, nickel, and chromium. Their related measurements of density and surface tension of sodium yielded the following:

Density, $g/cm^3 = 0.952 - 2.45 \times 10^{-4} t°C$, from 98 to 440°C
Surface tension, γ, dynes/cm, from 98 to 300°C:
For pure sodium (3 ppm oxygen), $\gamma = 203 - 0.08(t°C - 98)$
For oxide-saturated sodium, $\gamma = 203 - 0.11(t°C - 98)$

Both iron and nickel were found to be completely wetted in pure sodium at 270°C in less than 1 hr. Oxide-contaminated sodium wets iron and nickel at significantly lower temperatures (e.g., 200°C for nickel in oxide-saturated sodium). The rate of wetting of Fe–Ni alloys by oxide-saturated sodium, although not as high as that of either pure metal alone, increased with increasing nickel content of the alloy.

The corrosiveness of pastes of UN, UO_2, UC and sodium was studied at Argonne[37] by examining 304 stainless steel coupons after 1000-hr, 760°C static-capsule exposures. The results, shown in Table IV-3, are consistent with the known behavior of the separate

Table IV-2 RESULTS OF REFLUXING-SODIUM* CAPSULE CORROSION TESTS[35]

Material	Composition, wt.%	Annealing temp.,† °C	Bend radius‡	Capsule material§	Test temp., °C	Test duration, hr	Corrosion results
D-43	Nb–10 W–1 Zr–0.1 C			D-43	1315	3000	No effect
TZM	Mo–0.5 Ti–0.06 Zr			D-43	1315	3000	No effect
FS-85	Nb–28 Ta–10 W–1 Zr			D-43	1315	3000	Microcracking
FS-60	Ta–10 W			D-43	1315	3000	No effect
T-111	Ta–8 W–2 Hf			D-43	1315	3000	Pitting
D-11	Nb–1 Zr	1150	2t	D-43	1000	2000	No effect
D-43	Nb–10 W–1 Zr–0.1 C	1370	2t	D-43	1000	2000	No effect
FS-85	Nb–28 Ta–10 W–1 Zr	1370	2t	D-43	1000	2000	Slight attack and cracking
F-48	Nb–15 W–5 Mo–1 Zr–0.05 C	1370	2t	D-43	1000	2000	No effect
B-66	Nb–5 V–5 Mo–1 Zr	1370	1t	D-43	1000	2000	No effect
Cb-753	Nb–5 V–1 Zr	1150	2t	D-43	1000	2000	Slight cracking
D-14	Nb–5 Zr	1370	3t	D-43	1000	2000	No effect
AS-55	Nb–5 W–1 Zr–0.2 Y–0.06 C	1370	3t	D-43	1000	2000	No effect
S-291	Nb–10 Ta–10 W	1150	1t	D-43	1000	2000	Slight attack
Cb-Ti	Nb–10 Ti	1150	2t	D-43	1000	2000	No effect
W–Re	W–26 Re	1540	3t	D-43	1000	2000	No effect
FS-60	Ta–10 W	1370	3t	D-43	1000	2000	No effect
T-111	Ta–8 W–2 Hf	1540	2t	D-43	1000	2000	~1 mil attack
T-222	Ta–10 W–2.5 Hf–0.1 C	1540	1t	D-43	1000	2000	No effect
TZM	Mo–0.5 Ti–0.08 Zr	¶	1t	D-43	1000	2000	Slight attack
FS-85	Nb–28 Ta–10 W–1 Zr			Seam-welded FS-85 tubing**	1315	6271	Slight attack
T-111	Ta–8 W–2 Hf			Seamless T-111 tubing**	1315	6271	No effect
D-43	Nb–10 W–1 Zr–0.1 C			Seamless D-43 tubing**	1315	6271	No effect
X-34	Nb–5 W–3 Zr–0.1 C			X-34 rod stock**	1315	6271	No effect
TZM	Mo–0.5 Ti–0.06 Zr			TZM rod stock**	1315	6271	Possible attack

*Capsules charged with hot-trapped sodium.
†Annealed 1 hr in vacuum of $< 5 \times 10^{-7}$ torr.
‡180° U-bend; unrestrained; t = specimen thickness.
§D-43 capsules heat-treated 2200°F (1200°C), 1 hr prior to filling.
¶Not annealed; bent in air at 175°C.
**No inserts; capsule served as specimen.

Table IV-3 STATIC CORROSION TESTS OF 304 STAINLESS STEEL BY Na–U CERAMIC PASTES[37]
(Time: 1000 hr; Temperature: 760°C)

Contents of capsule	Coupon wt. change, mg/cm^2	Thickness change, mils	Metallographic observations	Chemical analysis,* wt.% Nitrogen	Carbon
Na	+0.03	0	Sensitized structure†		0.082
Na + Na_2O (4000 ppm)	+0.4	+0.5	Intergranular corrosion		0.049
Na + UC‡ (34 vol.%)	+0.9	+1	Heavy carbide precipitation throughout sample. Surface reaction layer visible		1.6
Na + UO_2§ (42 vol.%)	+0.2	0	Sensitized structure†		0.071
Na + UN¶ (41 vol.%)	−0.3	0	Sensitized structure†	0.113	
Na + UN¶ (40 vol.%)	−0.3	0	Characteristic austenitic twinned structure	0.028	

*Original coupon: nitrogen, 0.045 wt.%; carbon, 0.056 wt.%.
†Carbides precipitated in grain boundaries.
‡Hyperstoichiometric UC (5.2 wt.% C) prepared by the liquid-metal process (Run UC-12, see USAEC Report ANL-6925, p. 98).
§Hydrogen-reduced UO_2.
¶High-density UN prepared by nitridation of uranium shot (Run UN-9A, see USAEC Report ANL-7055, pp. 94-97).

constituents. For example, 760°C sodium attacks 304 stainless steel intergranularly in the presence of Na_2O, and hyperstoichiometric UC will carburize stainless steel. Hypostoichiometric UC should show less interaction with the stainless steel.

CORROSION BY LITHIUM

Beskorovaynyy, Ivanov, and coworkers have published the results of detailed analytical and experimental studies on the behavior of carbon and steels in molten lithium.[38] In a paper dealing with metal–Li–C systems,[38a] the fate of carbon impurities in lithium is predicted from thermodynamic considerations and verified experimentally, using radioactive carbon tracers. Thus Fig. IV-7 would suggest that iron will not reduce Li_2C_2 below about 750°C, whereas, above this temperature, Fe_3C and Li_2C_2 are about equally stable. Similarly, Li_2C_2 is more stable than Mo_2C below about 700°C and more stable at higher temperatures. All the other carbides studied (Cr_7C_3, $Cr_{23}C_6$, NbC, and TaC) were more stable than Li_2C_2 at all temperatures. It was even found that, when carbon-contaminated lithium was heated in contact with an alloy containing several different structural metals, there was a partitioning of the carbon among the metals in accordance with the relative stabilities shown in Fig. IV-7.

On the basis of an extension of this work employing similar techniques, a description of the mechanism of corrosion of carbon steels in lithium was evolved.[38b] Briefly, at temperatures up to 723°C, steels are decarburized by the reaction

$$2Li\ (liquid) + 2Fe_3C\ (solid) = Li_2C_2\ (solid) + 6Fe\ (solid)$$

The Li_2C_2 is dissolved in the surrounding lithium with a net increase in volume, giving rise to stresses and differential plastic strains, which affect the rate of penetration of lithium into the steel.

Corrosion of austenitic stainless steel was investigated in a similar fashion.[38c] The surfaces of austenitic steel specimens tested in lithium in Armco-iron crucibles at 700°C for up to 200 hr were found to be depleted in chromium and nickel, with consequent microporosity and loss of ductility. This was attributed to dissolution of chromium, nickel, and some iron in the lithium, as well as to interaction of the carbon impurities in the lithium with the chromium (in particular). These effects were less severe when stainless-steel crucibles were used in place of Armco iron, since the former presented additional chromium and nickel-bearing surfaces to the lithium.

Yttrium is one of the known deoxidizing agents for lithium. However, work at Argonne[39] showed that pure yttrium disintegrates in lithium at 1200°C in a tantalum capsule, leaving a dark gray crust on the capsule walls. In another test the addition of 2.5 at.% yttrium to lithium did not reduce the corrosion of tantalum at 1200°C. Instead, it actually seemed to accelerate the attack (as compared with the case with no additive). Similar results were obtained when 3.4 at.% sodium was added to the lithium (eutectic composition; m.p., 170.6°C).

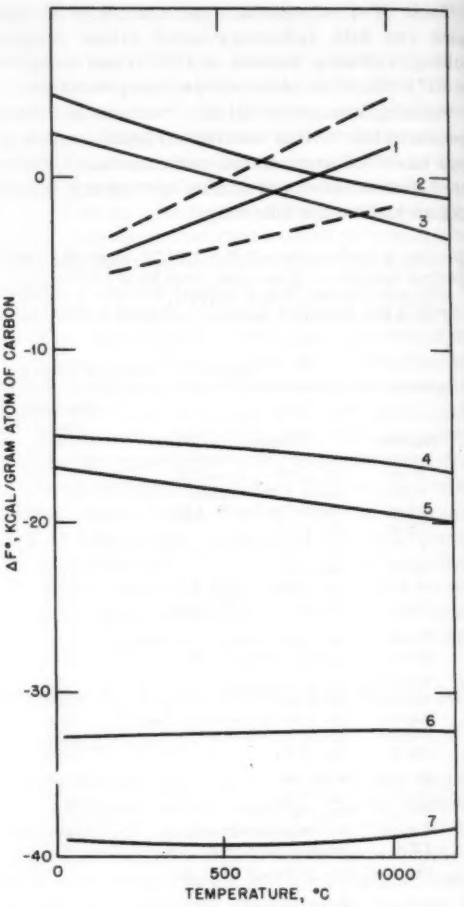

Curve	Reaction
1	Li (liquid) + C (solid) = $\frac{1}{2}Li_2C_2$ (solid)
2	3Fe (solid) + C (solid) = Fe_3C (solid)
3	2Mo (solid) + C (solid) = Mo_2C (solid)
4	$\frac{7}{6}$ Cr (solid) + C (solid) = $\frac{1}{6}$ Cr_7C_3 (solid)
5	$\frac{23}{6}$ Cr (solid) + C (solid) = $\frac{1}{6}$ $Cr_{23}C_6$ (solid)
6	Nb (solid) + C (solid) = NbC (solid)
7	Ta (solid) + C (solid) = TaC (solid)

Fig. IV-7 Free energy of formation of carbides.[38a] (Dashed lines represent uncertainty band in calculation of $\Delta F°$ for lithium carbide).

CORROSION BY POTASSIUM

Six high-temperature commercial brazing alloys (Table IV-4), joining 316 stainless-steel tubes, were

evaluated at Oak Ridge[8] in boiling potassium at 1540°F (840°C) for 6500 hr and 1600°F (870°C) for 4500 hr. Although the potassium leached material from all alloys, leaving subsurface voids, the joint integrity was good after 6500 hr at 1540°F in all but the Nicrobraz 10 joint.

Table IV-4 BRAZING ALLOYS TESTED IN BOILING POTASSIUM[8]

Alloy designation	Composition, wt.%	Brazing temp. °F	Brazing temp. °C
General Electric J8100	71 Ni–19 Cr–10 Si–0.15 C	2125	1165
General Electric J8300	61 Ni–19 Cr–10 Si–10 Mn	2100	1150
Coast Metals 50	93.4 Ni–3.5 Si–1.6 B–1.5 Fe	2000	1095
Coast Metals 52	90.5 Ni–4.5 Si–3.25 B–1.5 Fe	1950	1065
Nicrobraz 50	77 Ni–13 Cr–10 P	1850	1010
Nicrobraz 10	89 Ni–11 P–0.15 C	1850	1010

CORROSION BY CESIUM

Workers at Mine Safety have been engaged in a program[40] to study factors affecting the compatibility of cesium with containment metals. Using weight changes of sleeve-type capsule inserts as a criterion, they ascertained that the tendency to migrate in a polythermal cesium or potassium system was in the order Ni > Fe > Mo > Nb. Their studies showed that varying the temperature gradient, in the range 200 to 500°F (95 to 260°C), had little effect on mass transfer but that raising or lowering the maximum temperature was much more influential.

CORROSION BY BISMUTH

Argonne[37] workers have been investigating the feasibility of thermally regenerative bimetallic electromotive-force cells, using Na–Bi, Na–Pb, Na–Sn, or Li–Sn cells. During regeneration, the cathode metal would be circulated between the regenerator at 800 to 1000°C and the fused-salt electrolyte at about 550°C. In static corrosion tests for 24 to ~100 hr, ferritic materials showed some degree of resistance to liquid bismuth at over 800°C but were not tested in liquid tin because of their high solubility in tin. The following showed promising results in both bismuth and tin: Mo, Ta, W, Mo–30 wt.% W, Mo–50 wt.% Re, and high-purity alumina. The results of thermal-convection loop tests, shown in Table IV-5, show that neither stainless steel nor low-carbon steel is suitable for use with bismuth at 800°C or higher; however, the latter might be used for Na–Bi alloys below 650°C.

CORROSION BY FLUORIDE SALTS

The Oak Ridge Molten Salt Breeder Reactor design requires a graphite-to-Hastelloy N joint which will remain leaktight in contact with 700°C molten fluoride fuel. In the laboratory,[8] a short section of graphite pipe containing fluoride salts sealed in with molybdenum end caps brazed to the graphite with Au–35 wt.% Ni–30 wt.% Mo (ANM-16) withstood 150-psig internal pressure at 700°C during a 500-hr test with no salt penetration into the graphite and no detectable corrosion of the braze. Subsequently, joints of graphite brazed to Mo with Pd–35 wt.% Ni–5 wt.% Cr survived a 700°C corrosion test in $LiF–BeF_2–ZrF_4–Th_4–UF_4$ for 1000 hr with only a slight roughening (<0.5 mil) of the exposed braze surface.

A potential fused-salt fuel for a pulsed reactor was tested at Battelle–Columbus[41] for compatibility with niobium in static isothermal capsules. One capsule containing the UF_4–73 mole % LiF salt mixture was vacuum heated at 1200°C for 350 hr, and another was

Table IV-5 DYNAMIC CORROSION[37] OF STEEL AND STAINLESS STEEL BY Bi, Bi–Na ALLOYS, AND Pb

Test material	Liquid metal	Max. hot-leg temp., °C	Min. cold-leg temp., °C	Time, hr	Results
1020 steel	Bi	550	450	1000	Dissolution, up to 250-μ depth
1020 steel	Bi	800	700	24	Slight dissolution; plugs formed, stopping circulation
1020 steel	Bi	850	450	430	Leak developed;* dissolution of up to 60% of the loop metal at the hot leg
1020 steel	Bi	850	450	279	Leak developed;* dissolution of up to 50% of the loop metal at the hot leg; slight intergranular penetration
1020 steel	20 at.% Na–Bi	850	450	125	Leak developed;* dissolution of up to 50% of the loop metal at the hot leg
1020 steel	30 at.% Na–Bi	650	550	1506†	Slight mass transfer; dissolution of up to 10% of the loop metal at the hot leg
316 stainless steel	Bi	850	450	300	Leak developed;*‡ extensive mass transfer; integranular penetration
316 stainless steel	25 at.% Na–Bi§	650	550	4426†	Extensive mass transfer; dissolution of up to 65% of the loop metal at the hot leg
316 stainless steel	Pb	850	650	706	Plug formed in the cold-leg section

*The leak developed at the entrance section of the hot leg.
†The experiment was terminated at the indicated time.
‡The loop plugged, but, on dissection, a small leak was found.
§The loop was started using 30 at.% Na–Bi as the liquid metal. After 24 hr, bismuth was added until the composition of the liquid metal was 25 at.% Na–Bi.

held at 1500°C for 24 hr. No corrosive attack could be found by metallographic examination of the capsules. (E. M. Simons)

Metal–Water Reactions

Argonne[34] has reported a calculational technique for describing the extent of a metal–water reaction and core heating during a loss-of-coolant accident. This computer program is similar to that previously described by Battelle–Columbus.[42] The FORTRAN computer program, designated CHEMLOC-I, describes the core heating and chemical reaction up to the time of fuel melting. CHEMLOC-I takes into consideration the temperature effects associated with the gas, cladding, and fuel separately; axial and radial heat conduction in the cladding and fuel; radial radiation from cladding to cladding; convection between the cladding and the flowing gas; and axial changes in the hydrogen concentration in the steam.

For the analysis the core is divided into 10 radial zones, each having an equal number of fuel rods. As the steam flows upward through the core, the concentration of hydrogen increases due to chemical reaction between the steam and the cladding. Computer calculations were made for the LOFT reactor using an initial core temperature of 285°C and for an initial core-temperature distribution corresponding to the equilibrium temperature at operating power. Calculations were made for constant or unlimited steam flow rates of 100, 1000, 5000, 7500, and 10,000 lb/hr and for variable steam flow rates starting at 3600 lb/hr and decreasing exponentially with time. Figure IV-8 shows the percent of cladding reacted as a function of time for the various initial core temperatures and steam flow rates. It was concluded from the calculations that convective cooling from constant steam flow rates of 7500 and 10,000 lb/hr was sufficient to avoid extensive heating of the core. (J. M. Genco)

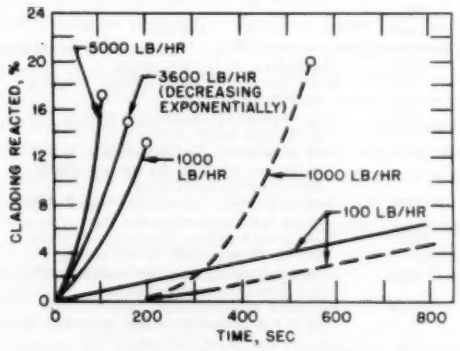

Fig. IV-8 Cladding reacted as a function of time for various temperature and steam conditions.[34] ——, initial temperature 285°C; ——, initial temperature corresponding to operating power; ○, point at which 10% of core is at or above 2800°C. Steam flow rates are as indicated.

Radiation Effects in Nonfuel Materials

Stainless Steels

Researchers at Windscale[43] have examined the tensile behavior of a 20 wt.% Cr–25 wt.% Ni–0.7 wt.% Nb stainless steel, irradiated to a total exposure of 3.5×10^{20} neutrons/cm^2. The tests were conducted at a strain rate of 3×10^{-4}/sec in argon, and the ductilities were compared with those of unirradiated specimens which were held at 750°C for 1300 hr (equivalent to irradiation temperature and time). Photomicrographs showed the formation of differing voids and cracks in the regions of fracture in the materials tested, indicating that grain-boundary cohesion is lowered by irradiation.

The effect of postirradiation annealing in 304L stainless steel is being investigated at Argonne.[34] Specimens prepared from an Experimental Breeder Reactor (EBR-II) fuel jacket, which had been exposed to a maximum total flux of 1.2×10^{22} neutrons/cm^2, were annealed at 900°C for 1 hr and then burst tested at 900°C. The tangential rupture strengths of the irradiated samples were in all instances lower than that of the unirradiated material. The ductilities of the as-irradiated and the irradiated and annealed tube sections were about the same, but were much less than that for the unirradiated tubes.

Harwell[44] workers tested the hypothesis that enhanced precipitation of carbides and nitrides causes radiation-induced loss of high-temperature ductility in stainless steel. Tensile specimens were irradiated to a thermal dose of 1×10^{21} neutrons/cm^2 at 40°C in contact with the moderator of either the Dido or Herald reactors or at 500 to 650°C in a He–Ne mixture in the Pluto or Mol BR-2 reactors. Tensile tests were conducted in air on hard-beam machines with most tests run at 750°C and a few at 650°C. Stress-rupture tests were performed in air at 650°C. Only one of three lots of material showed improved post-irradiation ductility after cold working and annealing to precipitate these compounds; hence the original hypothesis was rejected. It was concluded that fine grain size was responsible for this smaller loss in ductility after irradiation rather than the precipitation of carbides and nitrides.

Three 20 wt.% Cr–25 wt.% Ni austenitic stainless steels irradiated at 650 and 750°C in a thermal-neutron flux and a 316L austenitic stainless steel irradiated at 300°C in a fast-neutron flux were examined by electron microscopy at Culcheth.[45] The 20 wt.% chromium steels (including niobium-stabilized, titanium-stabilized, and unstabilized types) were irradiated to 3.5×10^{20} neutrons/cm^2 (thermal) and 1.5×10^{20} neutrons/cm^2 (fission) in the Dounreay Materials Testing Reactor (MTR) and were tested as tensile specimens at 750°C. The 316L stainless steel

was irradiated in the form of 500-μ-thick disks in the Dounreay Fast Reactor to a dose of 1.5×10^{22} neutrons/cm^2. Small helium bubbles were observed in the three 20 wt.% chromium steels after high-temperature irradiation in a thermal flux and in the 316L steel after annealing. Heterogeneous precipitation of bubbles occurred during irradiation at 650°C, and homogeneous precipitation was produced by an 850°C postirradiation anneal. These processes occurred simultaneously during irradiation at 750°C. The grain-boundary distribution of bubbles were different in the niobium- and titanium-stabilized steels, an effect which was attributed to different distributions of boron. A tensile stress was found necessary for growth of helium bubbles at grain boundaries. The critical helium-bubble size which would grow under high-temperature tensile-stress conditions was believed to be between 100 and 250 A in diameter. These observations lead to the suggestion that high-temperature ductility in irradiated stainless steel can be improved by reducing the segregation of boron at the grain boundaries and by providing fine grain-boundary precipitates to anchor small bubbles and prevent their migration and coalescence.

Low-Alloy Steels

The radiation-induced embrittlement of carbon-steel and low-alloy-steel pressure vessels used for nuclear reactor containment has been the subject of continuing research for a period of years. The measure of this embrittlement has generally been described in terms of the increase in ductile-to-brittle transition temperature (or NDT). More specifically, the NDT is defined[46] as that temperature at or below which a small flow residing in a zone of yield-point loading will initiate rapid brittle failure. The Naval Research Laboratory has attempted to equilibrate damage or radiation-induced embrittlement occurring in two different reactors on the basis of flux spectral differences and distributions of neutron-energy groups within the reactors. The Charpy V-notch transition-temperature behavior for specimens of A350F1 (modified) which were irradiated in the Low Intensity Test Reactor (LITR) was determined. A critical exposure limit was then calculated for the 5M-1A reactor pressure vessel from neutron data obtained in both the SM-1A and LITR reactors. Considering the relative damaging potential of these spectra, it was shown that with neutron energies >0.5 Mev a 67-Mw-year operation of SM-1A could be projected before the neutron-induced NDT increase reached a critical point.

Researchers at Oak Ridge[47] are studying the effect of irradiation on weld-heat-affected zones of ASTM A-212, grade B, pressure-vessel steel. They have reconfirmed earlier findings which showed that heat-affected-zone samples have a higher ductile-to-brittle transition temperature after irradiation and show less recovery from postirradiation annealing than base-plate specimens. Other studies on the tensile properties of this steel after postirradiation annealing demonstrated that recovery of irradiation effects occurred in the temperature interval from 300 to 600°C.

The grain-size dependence of the ductile-to-brittle transition temperature has also been shown, and it was concluded that the transition temperature should increase at a greater rate with increases in yield stress due to radiation hardening.

The effects of irradiation on the room-temperature fatigue properties of SA-212B and SA-302B steels are being investigated at Phillips Petroleum.[48] Of the fatigue properties, only plastic strain range exhibited an effect attributable to irradiation after an exposure of 3.7 and 7.4×10^{17} neutrons/cm^2 ($E > 1$ Mev). It should be noted that, although these are low levels of irradiation, for some materials these exposures are in the range at which significant radiation-induced changes begin to occur.

The Naval Research Laboratory[48] has evaluated metallurgical variables as related to the radiation sensitivity of structural steels. The study included three pressure-vessel steels, A-302B, HY-80, and A-350LF3 with samples taken from both large-tonnage commercial heats and special laboratory heats. Those metallurgical variables evaluated included the identity and quantity of major alloying elements and residual elements, melting, heat-treatment practice, microstructure, and gas content. The results showed that radiation-embrittlement sensitivity was dependent upon heat-treatment practices and greatly dependent upon microstructure. It was found that vacuum melting and control of residual-element content lowered the radiation-embrittlement sensitivity as compared with that of steels produced by conventional open-hearth melting, regardless of the final heat-treatment conditions. Stress-relieving heat-treatments did not alter the irradiation response of A-302B steel. The radiation sensitivity was not influenced by nickel content in the range 3.8 to 8.4 wt.%. The application of this knowledge to the development of a steel with low embrittlement sensitivity was considered realistic and attainable; however, the full assessment of the individual and combined influences of the many variables would require a large experimental effort.

Culcheth[49] researchers have investigated the effect of neutron irradiation on the high-strain fatigue properties of a low-carbon manganese steel and a low-alloy steel. Specimens were tested at room temperature after irradiations to total exposures of 1×10^{19} and 1×10^{20} neutrons/cm^2 (>1 Mev), respectively, in the Dounreay MTR. It was concluded that irradiation to these dosages had a relatively small effect on the room-temperature high-strain fatigue behavior of these materials. At total strain ranges above about 3%, irradiation reduced the number of cycles to failure, whereas, at strain ranges less than 3%, irradiation caused an increase in the number of cycles to failure.

Nickel-Base Alloys

Studies are in progress at Oak Ridge[50] to reduce the irradiation-induced embrittlement at elevated temperatures in Hastelloy N. These studies have shown that titanium additions of 0.4, 0.55, 0.66, and 1.05 wt.% improve the rupture life and rupture ductility at 650°C after irradiation to a thermal-neutron exposure of 2.5×10^{20} neutrons/cm^2 at 650°C. The reduced ductility in irradiated Hastelloy N was believed to be due primarily to helium produced by transmutation of ^{10}B. Therefore, by the addition of titanium, a strong boride former, the ^{10}B should be more uniformly distributed and consequently the concentration of helium at the grain boundaries should be reduced.

Zirconium Alloys

Sections of Zircaloy-2 tube irradiated in the Engineering Test Reactor (ETR) to an estimated exposure of 2.3×10^{21} neutrons/cm^2 ($E > 1$ Mev) have been burst tested at room temperature by Phillips Petroleum.[10] The burst pressures were compared with those required to burst specimens which were from the out-of-pile section. These data showed an increase in ultimate hoop strength from about 90,000 to 110,000 psi as a result of irradiation. Girth measurements at the fracture indicate about 22% increase in diameter. The greatest increase in hydrogen (as indicated by analysis) was found in the out-of-pile section, which went from 20 to about 32 ppm.

Beryllium

Beryllium specimens irradiated to 0.88 and 1.08×10^{21} neutrons/cm^2 (>1 Mev) at 600°C were tested in compression and compared by Phillips Petroleum[10] workers with control specimens annealed at 600°C with simulated reactor shutdowns. Fracture of the unirradiated specimens occurred mainly by a shear mechanism, whereas the irradiated specimens failed mainly by cleavage on planes parallel to the direction of applied load. A slight increase in yield strength was found after irradiation, but a decrease in ultimate strength was noted. This decrease in ultimate strength was attributed to the presence of gas bubbles in the grain boundaries after irradiation. A beryllium–irradiation surveillance program has been started at Phillips to monitor changes in dimensional stability, mechanical strength, and load-carrying capabilities of the ATR reflector beryllium at reactor ambient temperatures. Two grades of hot-pressed, one grade of hot-extruded, and one grade of vacuum-cast beryllium are included in the surveillance program.

Basic Studies of Radiation Effects

Battelle–Northwest[51] has studied the dislocation movement during deformation of a Cu–8 wt.% Al alloy and 99.99% pure copper after irradiation. Foils were irradiated at 40°C in a predominantly thermal-flux reactor and strained to 5.0% maximum. Observations by transmission-electron microscopy showed that moving dislocations produced defect-free channels by interaction with dislocation loops and clusters in the irradiated pure copper, but no interaction was detected in the irradiated and deformed Cu–Al alloy.

Workers at Westinghouse[52] have extended theories, developed initially to explain irradiation behavior in face-centered cubic metals, to the case of neutron embrittlement and subsequent recovery in body-centered cubic metals. The approach combines Seeger's damage theory with Maxin's saturation-effect concept and Cottrell's brittle-fracture theory. It was suggested that annealing of neutron damage occurs by thermally activated motion and coalescence of individual damage zones, through surface diffusion of atoms on the zone interior surfaces.

The change in electrical resistivity has been used as a measure of radiation damage in iron and medium- and high-carbon steels by the Russians.[53] Samples were irradiated at about 70°C to exposures of 2.5×10^{19} neutrons/cm^2 fast flux. The results indicate that carbon content in the range 0.01 to 0.93 wt.% had no great effect on the radiation-induced increase in resistivity. There were, however, variations in the structure of the metals. The greatest increase in electrical resistivity occurred in those samples annealed at 630°C before irradiation. Other studies by the Russians[54] on cast-iron alloys containing metastable phases have shown that these alloys undergo phase transformations when subjected to simultaneous electron radiation and heat-treatment under conditions which normally slow down the process. The depth at which the transformations were observed agreed with the calculated depth of penetration of electrons.

The diffusion of ^{63}Ni into copper over the temperature range 200 to 520°C was compared with that from samples which were simultaneously exposed to alpha irradiation.[55] Whereas the diffusion under only thermal conditions was temperature dependent, the diffusion under thermal conditions plus simultaneous irradiation was independent of temperature. A theoretical model was applied to these results by workers at Ispra[56] where the sink concentrations and concentration of point defects during alpha irradiation were estimated. This model shows that ^{63}Ni atoms diffuse by an interstitial diffusion mechanism during irradiation.

(F. R. Shober)

Selected Metallurgical Aspects of Cladding Materials

Zirconium Alloys

Prestraining of zirconium at 77°K results in significant changes in room-temperature mechanical

properties.[57] At prestrains up to 1%, the room-temperature elongation is increased and the strength decreased. This phenomenon is attributed to prestrain-induced nucleation of numerous fine (1 1 2 1) twins. Prestrains above 1% result in a decrease in elongation and an increase in yield and tensile strength. These effects are illustrated in Fig. IV-9. Structural

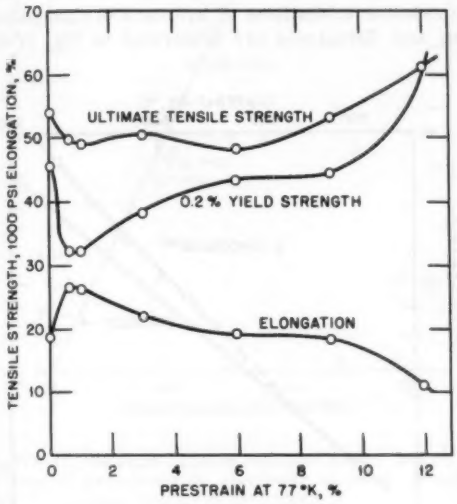

Fig. IV-9 Room-temperature tensile properties of transverse pure zirconium specimens as functions of percent prestrain by cold rolling[57] at 77°K.

changes in zirconium subjected to tension at room temperature have been studied by electron-transmission microscopy.[58] Deformation in annealed zirconium was found to occur by prismatic slip, without the appearance of twins or deflected slip. No stacking faults were produced by the deformation. The appearance of a yield point in high-purity polycrystalline zirconium was found[59] to be favored by fine grain size, air cooling from the recrystallization temperature (instead of water quenching), and testing in the temperature range −20 to 200°C (and possibly higher). However, yield-point appearance could be suppressed by adding 32 ppm hydrogen to zirconium or by increasing its grain size above 0.0076 mm. The thermal-expansion coefficient of zirconium in the *a* direction was found[60] to diminish sharply above 400°C, with a consequent rapid rise of the *c*/*a* ratio. These changes were attributed to possible changes in electronic structure. Figure IV-10 illustrates the thermal conductivity of Zircaloy-4 up to 1500°C, as determined by General Electric workers.[4]

The anisotropy of mechanical properties in alpha-zirconium alloys can be related to the preferred orientation of the material.[61] Figure IV-11 illustrates that the present testing methods, where Izod V-notch

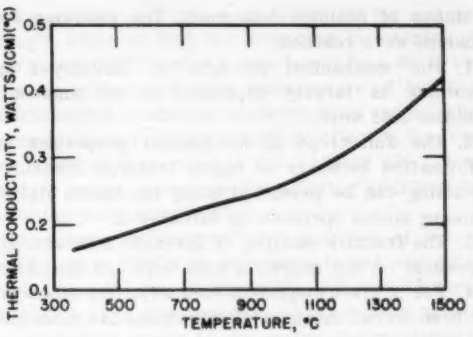

Fig. IV-10 Effect of temperature on thermal conductivity[4] of Zircaloy-4.

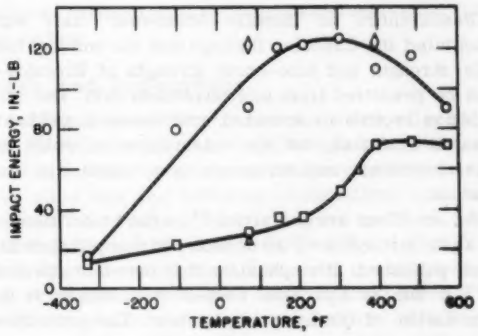

Symbol	Specimen-axis orientation with respect to rolling direction	Notch-axis orientation with respect to plane of the plate
○	Parallel	Perpendicular
□	Parallel	Parallel
△	Perpendicular	Parallel
◇	Perpendicular	Perpendicular

Fig. IV-11 Impact energy of Zircaloy-2 subsize Izod V-notch specimens tested with different rolling directions and notch orientations.[61]

specimens from both the longitudinal and transverse directions to rolling are tested with the notch axis in the normal direction, are inadequate to characterize the material. It is apparent that tests with the axis of the notch in the parallel direction, which is not the usual orientation, result in significantly lower impact resistance.

A thorough investigation of the effect of preferred orientation on the mechanical properties of Zircaloy-2 tubing was performed by Chalk River.[62] Axial-tensile, ring-tensile, and closed-end and free-end burst tests were carried out at room temperature and at 300°C on specimens with a wide range of textures and per-

centages of residual cold work. The following conclusions were reached:

1. The mechanical strength of Zircaloy-2 fuel sheathing is largely dependent on the amount of residual cold work.

2. The anisotropy in mechanical properties and deformation behavior of highly textured Zircaloy-2 sheathing can be predicted using the known slip and twinning modes operative in Zircaloy-2.

3. The fracture ductility of Zircaloy-2 sheathing is dependent on the degree of cold work and on texture.

4. For a given degree of cold work, the tubes with the best overall mechanical properties are those having only radial basal poles.

5. Yield strengths of Zircaloy-2 sheathing in the closed-end and free-end burst tests can be predicted within 7% from the axial-tensile yield strength and Knoop hardness measurements.

Researchers at Battelle–Northwest[63] have substantiated the Canadian findings that the uniaxial tensile strength and tube-burst strength of Zircaloy-2 can be predicted from microhardness data. The correlation applies to annealed, cold-worked, and heat-treated material, but the orientations at which the microhardness measurements are made are important.

An excellent review article[64] on the embrittlement of alpha zirconium by zirconium hydride platelets has been published. It emphasizes that the embrittlement is not due to hydrogen content but, rather, to the orientation of the hydride platelets. The embrittlement was shown to be very sensitive to the rate of loading such that Zircaloy-2 containing hydride platelets might not be brittle in a tensile test but would demonstrate brittle behavior in an impact test. Numerous investigations have been performed to determine the factors that govern the orientation of the hydride platelets in zirconium alloys. The orientation of zirconium hydride platelets in Zircaloys is dependent on crystallographic texture if the sample is annealed and unstressed. Reorientation of the platelets during annealing increases with increased cold work in the metal and with decreasing grain size. Therefore the final orientation of hydride platelets is expected to depend on all three factors.[65,66a]

Different fabrication methods result in different textures in thin-walled Zircaloy-2 tubes.[67] The variation in textures promotes precipitation of hydride platelets in different orientations with respect to the tube. For example, swaged and annealed tubes have the hydride platelets in the circumferential direction, whereas reduced and drawn tubes that are subsequently annealed have the hydrides oriented in the radial direction.[67] It has been shown that the final operation is the most significant in determining the hydride orientation.[68] The radial strain that causes hydrides with a radial orientation is due to an unsupported sinking operation. Annealing that results in recrystallization and grain growth is effective in removing the directionality of fabrication, but is undesirable because of the resulting large grain size. Thus the amount of radially oriented hydride platelets in tubing can be generally minimized by relatively high values of wall reduction.

The solubility of hydrogen was found to be less in Zircaloy-4 than in alpha zirconium, thereby suggesting that the presence of foreign atoms affects the thermochemical behavior of hydrogen in zirconium.[69] The relative solubilities of hydrogen in alpha zirconium and Zircaloy-4 are illustrated in Fig. IV-12,

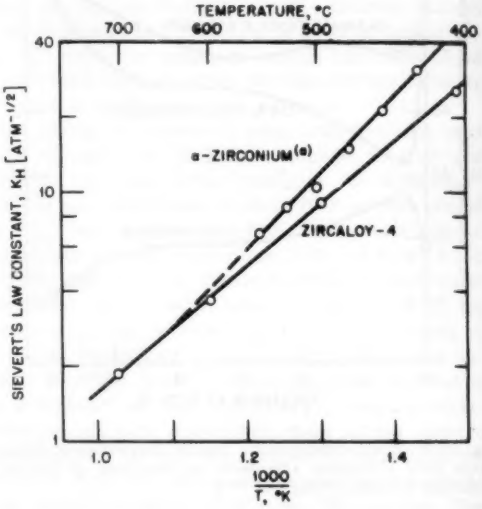

Fig. IV-12 Relative solubilities[69] of hydrogen in alpha zirconium and Zircaloy-4. (a) L. D. LaGrange et al., Journal of Physical Chemistry, 63: 2035 (1959).

which relates the Sievert's law constants to the reciprocal of temperature.

Hydrogen decreases the room-temperature toughness of Zircaloy-2 and Zr–2.5 wt.% Nb, but it has no noticeable effect on fracture toughness at 300 °C. The crack-opening-displacement (C.O.D.) concept which is based on the fact that crack instability occurs when the opening of a crack tip reaches a critical value was applied to this system. In this manner a straight-line relation above a hydrogen content of 400 ppm, as illustrated in Fig. IV-13, was obtained.[70] The crack-opening displacement δ is related to the fracture stress and crack length by

$$\delta = \frac{\pi \sigma^2 a}{E \sigma_y}$$

where σ = fracture stress
a = half-length of crack
E = modulus of elasticity
σ_y = yield stress

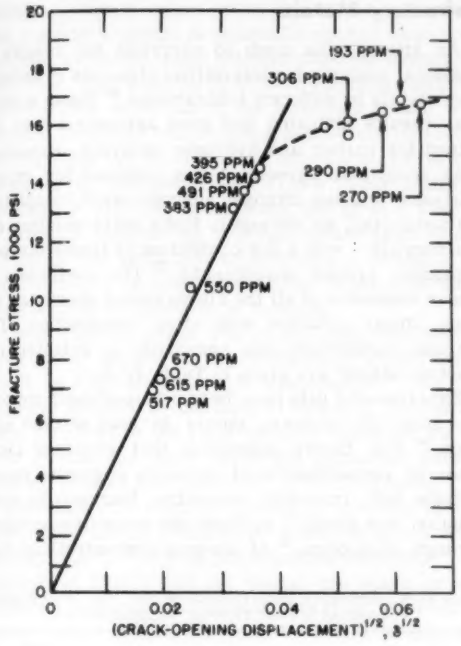

Fig. IV-13 Relation between fracture stress and $\delta^{1/2}$ for Zircaloy-2 pressure-tube specimens at room temperature.[70] Hydrogen contents as indicated.

The critical crack length that is needed for failure decreases with increasing hydrogen content.[71] The effect is most marked around ambient temperature. Figure IV-14 illustrates that at 300°C the hydrogen content has only a minor effect on the critical crack length.

The optimum composition of Zr–Nb alloys has been found to be at least 2.2 wt.% niobium and 1000 to 1200 ppm oxygen.[72] The heat-treatment for optimum strength requires that the quenching be carried out from above 850°C and at a rate faster than 80°C/sec. After quenching, an aging temperature of 500°C is recommended. Additions of neodymium and holmium to zirconium were found to have no effect on the fracture mode of zirconium in the −196 to 100°C temperature range, providing the alloying additions remained in solid solution.[73]

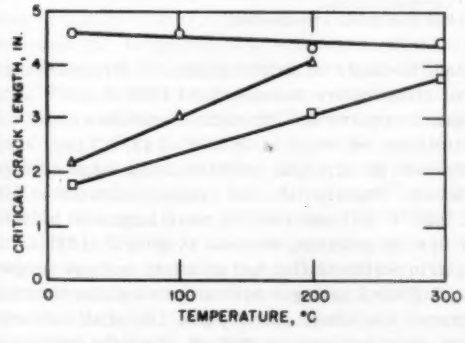

Fig. IV-14 Effect of temperature and hydrogen content on the critical crack length for Zircaloy-2 at a hoop stress[71] of 16,000 psi. ○, <25 ppm hydrogen; △, ~200 ppm hydrogen; □, ~400 ppm hydrogen.

It has been established[74] that a stress of at least 30,000 psi at 300°C is necessary to get significant hydride-platelet orientation in Zr–2.5 wt.% Nb during cooling. A high concentration of basal poles parallel to the applied stress is necessary for reorientation of the hydrides. Reorientation of the hydrides was found to have no significant effect on the room-temperature tensile properties of Zr–2.5 wt.% Nb. The addition of niobium to zirconium was found[75] to increase the degree of hydrogen supersaturation during cooling.

Steels and Superalloys

A British patent was issued for a low-alloy steel that is weldable and can be rolled into 3-in. plate and is thus fabricable into massive pressure vessels.[76] The alloy has the following composition: less than 0.15 wt.% C, 1.0 to 1.2 wt.% Mn, 1.4 to 1.7 wt.% Ni, 0.25 to 0.35 wt.% Mo, 0.08 to 0.13 wt.% V, 0.40 to 0.45 wt.% Cr, and up to 0.25 wt.% Nb, with the balance being constituents that are usual in mild steel. The room-temperature strength and ductility of a high-alloy steel (Fe–8.67 wt.% Cr–8.08 wt.% Ni–1.87 wt.% Si–0.81 wt.% Mn–3.96 wt.% Mo, and 0.28 wt.% C) were considerably improved[77] by straining and aging at 450 to 650°C. The amount of straining was the most influential factor in determining mechanical-property changes, whereas the straining and aging temperatures were less important. Figures IV-15 and IV-16 illustrate the effects of amount of straining at 450°C and aging temperature on room-temperature strength and ductility.

The maximum solubility of nitrogen in 304 stainless steel was found[78] to be 0.125 wt.% at 538°C. Further nitrogen additions resulted in the formation of CrN, Cr_2N, and gamma austenite. Aging of a precipitation-hardening Fe–Cr–Ni alloy containing titanium and aluminum at 750°C for times up to 1400 hr showed that TiC particles promote nucleation of the (Fe,Cr) sigma phase.[79]

Aging at 1000, 1200, 1400, and 1600°F (538, 649, 760, and 871°C) was carried out[80] for times up to 5000 hr on weld metal of Hastelloy X and Hastelloy W and on base metal of Hastelloy X-280 and Haynes Stellite-25. Both of the weld metals were embrittled, but the Hastelloy W appears to have better mechanical properties after prolonged heating. Hastelloy X-280 maintains a ductility of 40% or more when aged and tested at all four aging temperatures, whereas Haynes Stellite-25 maintains a ductility of at least 18% or

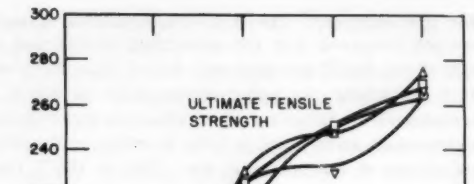

Fig. IV-15 Effect of deformation at 450°C and aging temperature on room-temperature strength of a high-alloy steel.[77] Deformation temperature, 450°C. Aging temperatures: ▽, 450°C; □, 500°C; △, 550°C; ○, 600°C.

more. Cold working of L-605 (Haynes Stellite-25) up to 40% resulted in considerable improvement of room-temperature properties after aging[81] at 1600°F (871°C) for 1000 hr. The prior cold work resulted in formation of Co_2W and M_6C particles throughout the grain rather than at grain boundaries, which was the case for the unworked metal.

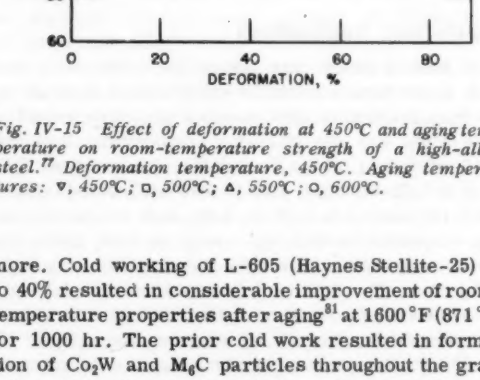

Fig. IV-16 Effect of deformation at 450°C and aging temperature on room-temperature ductility of a high-alloy steel.[77] Deformation temperature, 450°C. Aging temperatures: ▽, 450°C, □, 500°C; △, 550°C; ○, 600°C.

Refractory Metals

An attempt was made to correlate the results of chemical analysis for interstitial elements in refractory metals by different laboratories.[82] These analytical results indicated that good agreement was obtained for carbon and hydrogen analyses, somewhat less acceptable agreement was obtained for oxygen analyses, and the nitrogen analyses were completely untrustworthy. An attempt to find a solid-solution refractory alloy with a low coefficient of linear thermal expansion proved unsuccessful.[83] The coefficient of linear expansion of all the alloys tested showed an almost linear relation with alloy composition. The thermal conductivity and emissivity of selected refractory alloys[8] are given in Table IV-6.

Experimental data have been obtained which support the stage-III recovery theory in cold-worked niobium.[84] The theory postulates that recovery takes place by recombination of randomly migrating interstitials with immobile vacancies. Nitrogen in solid solution was found to increase the room-temperature strength of niobium.[85] At nitrogen concentrations high

Table IV-6 PHYSICAL PROPERTIES OF Nb-, Ta-, AND W-BASE ALLOYS AS A FUNCTION OF TEMPERATURE

Temp., °C	Thermal conductivity, watts/(cm)(°C) Nb–10 wt.% W	Ta–8 wt.% W–2 wt.% Hf	W–26 wt.% Re*	Total hemispherical emittance of W–26 wt.% Re
0			0.310	
100	0.4844	0.420	0.359	0.26
200	0.5099	0.446	0.402	0.28
300	0.5307	0.469	0.440	0.30
400	0.5468	0.487	0.473	0.32
500	0.5625	0.500	0.501	0.35
600	0.5782		0.525	0.37
700	0.5920		0.548	
800	0.6062		0.569	
900	0.6175		0.588	
1000	0.6264		0.605	
1100			0.621	
1200			0.634	
1300			0.648	0.52†
1400			0.660	
1500			0.671	

*Estimated values.
†Based on linear extrapolation.

enough to cause a second phase, no strengthening at room temperature was noted. At 1900°F (1038°C) nitrogen increased the strength of niobium at all concentrations, whereas at 2600°F (1427°C) only minor increases in strength resulted from large nitrogen additions. Rupture life and creep resistance at 1700 and 1900°F (927 and 1038°C) were improved by nitrogen in solid solution, whereas at 2600°F (1427°C) nitrogen in solid solution had no effect on these properties. Sufficient nitrogen to cause a two-phase structure improved the creep and rupture life at all temperatures. Nitrogen content did not affect the ductility of niobium at elevated temperatures.

It has been found that tantalum and niobium pick up hydrogen at elevated temperatures and form brittle

hydrides, which cause crumbling of the material.[86] The hydrogen pickup is especially severe when large thermal gradients exist between different sections of the alloy. The addition of 25 wt.% rhenium results in considerable reduction of the hydrogen uptake when thermal gradients are present at approximately 1500°F (816°C). For the Nb–Re alloy, only 1.0 at.% hydrogen is taken up, compared with 47.6 at.% for unalloyed niobium. In the case of tantalum, the 25 wt.% addition of rhenium reduces the hydrogen uptake from 40.8 to 0.2 at.%. The reduction in hydrogen solubility is attributed to the increase of electron–atom ratio which results from the addition of rhenium.

Oxygen in the range 180 to 1170 ppm was found to have minor effects on the mechanical properties of Nb–5 wt.% Zr alloy at room temperature.[87] The oxygen was present in the form of equiaxed ZrO_2 particles. No effect on the yield strength was found, but the flow stress and work hardening increased linearly with the volume fraction of the ZrO_2 dispersion.

Additions of 0.1 wt.% beryllium to niobium-15 wt.% zirconium alloys resulted in a second phase which strengthens the alloy by precipitation hardening.[88] Annealing at 1650°C did not change the shape or distribution of the second phase in this alloy, whereas the second phase in a Nb–15 wt.% W–3 wt.% Zr alloy was significantly affected by this heat-treatment.

A Nb–Hf base alloy has been developed which has good elevated-temperature properties.[89] This alloy contains additions of yttrium and/or tungsten. An age-hardenable tantalum-base alloy is obtained by dispersing tungsten-coated MoC or WC particles in tantalum containing zirconium or hafnium.[90] The composite is then held at elevated temperature until the carbide coatings are diffused in the alloy.

The yield stress in molybdenum single crystals was found to be independent of orientation above room temperature.[91] However, both yield strength and rate of work hardening were dependent on crystal orientation below room temperature. Minor additions of lanthanum and yttrium had no influence on the onset of recrystallization in molybdenum; however, additions of 0.03 to 0.06 wt.% yttrium or lanthanum sharply increased the temperature at which recrystallization was completed.[92] Additions of 0.1 to 0.2 wt.% zirconium or hafnium increased the recrystallization temperature of molybdenum sheet[93] from approximately 950°C to 1220°C. An addition of 1 wt.% vanadium was found to have a lesser effect on the recrystallization temperature, resulting in an increase[93] to about 1050°C. Effects of rhenium additions on the ductility of molybdenum were determined through electron microscopy and metallography.[94] Generally, the appearance of twinning in body-centered cubic metals coincides with low-temperature brittleness. In molybdenum the addition of rhenium resulted in increased twinning, but the ductility was also increased. Aging studies of Mo–Zr, Mo–Ti, and Mo–Hf were carried out[95] at 1300, 1400, and 1500°C. These alloys contained the interstitial elements of 0.003 to 0.005 wt.% carbon, 0.01 to 0.20 wt.% oxygen, and up to 0.06 wt.% nitrogen. In all three alloys, age hardening was found to be caused by the precipitation of finely dispersed oxides of alloying elements.

The isothermal sections of the Mo–Ti–Zr and Mo–Nb–Zr phase diagrams have been determined[96] at 1200°C. Besides the body-centered cubic ternary terminal solid solution and a ternary Lave's phase, no intermediate phases were found. In general appearance, the two systems were very similar. A thorough investigation of the Mo–Nb–Cr system has been performed by Russian investigators.[97] Isotherms have been determined at 1000, 1115, 1225, 1275, 1350, and 1550°C by use of X-ray diffraction and differential thermal analysis.

Annealing of tungsten in pure argon and krypton, rather than in vacuum, was found to improve its elevated-temperature mechanical properties.[98] The recrystallization temperature of tungsten specimens annealed in inert gases was 100 to 200°C higher than that for specimens annealed in vacuum. No explanations were offered for this difference.

The mechanism of decomposition within the spinoidal boundary in the W–Cr system was investigated.[99] The decomposition was found to follow a nucleation and growth mechanism when the quenched alloy was aged, rather than the classical spinoidal decomposition.

Fibered composites of tungsten with individual additions of zirconia, yttria, hafnia, and thoria or the refractory compounds (HfB, HfC, HfN, and TaC) were produced by elongating a sintered composite at 4200°F (2316°C) by extrusion.[100] In some cases it was found that the reinforcing particles had dissolved during the extrusion operation and then reprecipitated. In general, these additions resulted in rupture lifetimes 25 to 50 times that of recrystallized tungsten at 2500 to 3500°F (1370 to 1930°C). Maximum strengthening was obtained with about 8 to 10% fiber additive.

Miscellaneous

A thorough survey[101] has been made of deformation characteristics of beryllium, refractory metals, and superalloys. Mechanisms are covered from both a theoretical and a practical approach, so that fundamental reasons are given for actual material behavior. The following subjects are covered in the report: theory of plasticity; high-velocity forming; work-hardening mechanisms in metals; shear forming and spinning of metals; friction and wear in metal-deformation processes; rod, wire, and tube drawing; and applications of static high pressure to the forming of metals by hydrostatic extrusion.

Application of stress during strain aging of iron, niobium, and tantalum results in increases in the upper yield strength, lower yield strength, and yield-point elongation, whereas the tensile strength and

damping capacity are not affected.[102] The cause of yield-point strengthening is believed to be the rearrangement of dislocations, rather than stress-enhanced diffusion.

A British patent for a creep-resistant, fine-grained magnesium alloy has been issued.[103] The alloy has the following composition: 0.05 to 0.3 wt.% Al, 1.0 to 1.7 wt.% Si, up to 0.1 wt.% Be, up to 0.4 wt.% Ca, up to 0.25 wt.% Mn, up to 0.1 wt.% Zn, and the balance Mg. The addition of 0.5 wt.% zirconium to aluminum results in finely dispersed Al_3Zr particles, which increase the recrystallization temperature of aluminum.[104] Figure IV-17 illustrates that the recrystallization temperature is further increased by annealing at 500°C. (M. Kangilaski)

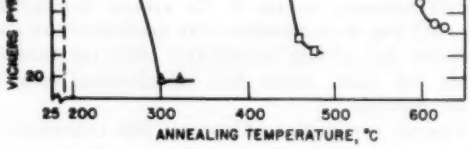

Fig. IV-17 Room-temperature hardness after 66% deformation and annealing for 1 hr at the specified temperature.[104] △, superpurity aluminum; □, Al—0.5 wt.% Zr; ○, Al—0.5 wt.% Zr annealed for 6 hr at 500°C before deformation.

Selected Mechanical Properties of Cladding and Structural Materials

Stainless Steels

French investigators[105] are studying the influence of carbon concentration on the mechanical properties of austenitic stainless steels of the 18-10 type prepared from pure metals. Three alloys were prepared as follows:

Alloy A with 20 ppm carbon
Alloy B with 80 ppm carbon
Alloy C with 600 ppm carbon

The structural states were considered in determining mechanical properties: the austenitic structure obtained by hyperquenching, and the austeno—martensitic structure obtained by cooling the preceding structure in liquid nitrogen. Strengths of the two states are shown in Tables IV-7 and IV-8, respectively. Carbon has practically no effect on the properties of very pure 18-10 steel, at least up to a concentration of the order of 100 ppm. However, pure steel containing 600 ppm carbon behaves like commercial 18-10 steel.

A statistical evaluation of the results of creep tests on six heats of type 304 stainless steel and two heats of type 316 stainless steel at 1250 and 1350°F (675 and 760°C) has been completed by Atomics International.[106] Correlation coefficients ranged from 0.90 to 0.97 (a coefficient of 1.0 would indicate perfect reproducibility of creep properties between heats).

The creep behavior of niobium—stabilized 318 stainless steel was determined in vacuum at 650°C for stress levels of 15, 20, and 30 kg/mm² at Argonne.[107] The as-received tubing conformed to ASTM Specification A-269 for unfired pressure vessels with regard to heat-treatment and surface finish. The strain-vs.-time curves for this material before and after exposure to steam are given in Fig. IV-18 (*A*, *B*, and *C*). Specimens in the as-received condition ruptured at the indicated strains, whereas the exposed specimens went to much higher strains. The increase in ductility and decrease in creep strength after exposure are attributed to decarburization by the steam. The creep behavior of 318 stainless steel at 650°C and 15 kg/mm² stress is compared with that of 316 stainless steel in Fig. IV-18 (*D*).

Table IV-7 MECHANICAL CHARACTERISTICS OF STEELS IN THE AUSTENITIC STATE[105]

Mechanical properties	Alloy A	Alloy B	Alloy C	Commercial 18-10 steel	High-purity 18-10 steel
Ultimate tensile strength, kg/mm²	46.4	49.5	66.2	64	53
Elastic limit, kg/mm²	10.8	11.8	19.2	23	11
Elongation, %	38	35.2	44.2	48.2	46.7

Table IV-8 MECHANICAL PROPERTIES OF STEELS IN THE AUSTENO—MARTENSITIC STATE[105]

Mechanical properties	Alloy A	Alloy B	18-10 steel of high purity
Ultimate tensile strength, kg/mm²	64.4	60.1	67.5
Elastic limit, kg/mm²	26.4	20.1	23
Elongation, %	28.4	30.9	23

Refractory Metals

Investigators at Oak Ridge found[47] that the resolved lower yield stress of niobium decreased with an increasing number of electron-beam floating-zone passes during zone purification. The lowest yield stress obtained was 1.2 kg/mm² for Du Pont niobium as shown in Fig. IV-19.

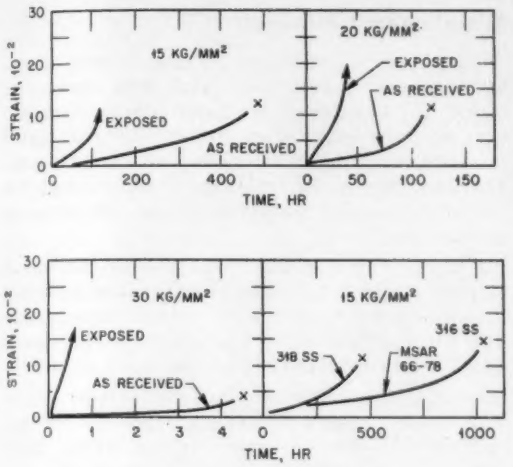

Fig. IV-18 Creep of 318 stainless steel at 650°C and indicated stress level.[107] A, B, and C provide a comparison of creep before and after exposure to steam at 0.42 kg/mm² pressure and 650°C for 350 days. D provides a comparison of 318 and 316 stainless steels in creep at 650°C and 15 kg/mm² stress.

Variations in the mechanical properties of niobium caused by nitrogen additions, in amounts to give single- and two-phase structures, were investigated at both room and high temperatures at the Naval Research Laboratory.[108] Nitrogen in solid solution raised both the room-temperature hardness and the tensile strength. Increasing the nitrogen content to give two-phase structures produced no additional strengthening, however. At elevated temperatures the effect was different in that, with an increase in nitrogen content, there was a continued rise in tensile strength through the two-phase region. The creep-rupture strength of niobium was improved by nitrogen in solution at temperatures slightly below 0.5 of the melting temperature, whereas above this temperature the strength was unaffected. This change in the nitrogen effect with temperature appears to be related to a concurrent change in the mechanism controlling creep. An increase in the nitrogen content of two-phase alloys produced strengthening throughout the 1700 to 2600°F (927 to 1427°C) test range. Ductility was high for all alloys at elevated temperatures and, except for a high-nitrogen alloy, also at room temperature.

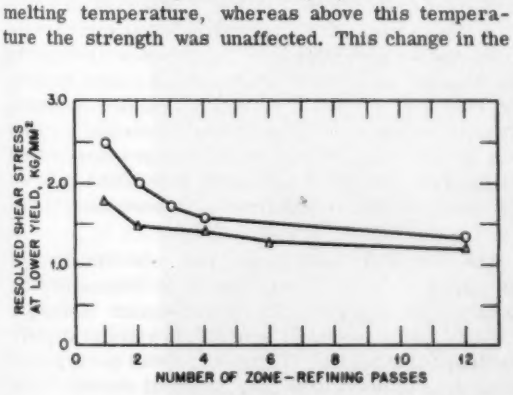

Fig. IV-19 Resolved shear stress at the lower yield point as a function of the number of floating-zone passes for niobium from two sources.[47] ○, Wah Chang niobium; △, Du Pont niobium.

The properties and behavior of niobium-base alloys containing 55 wt.% niobium, 39.5 wt.% titanium, and 5.5 wt.% aluminum were investigated by the Russians.[109] Rolled specimens (reduced 34 to 40%) were aged (400 to 800°C for 3 hr) or annealed at 1000°C and then aged. Aging sharply increased the hardness and strength of both as-rolled and annealed specimens, with the maximum effect being produced by aging at 600 to 650°C. The microstructure of tempered strain-hardened alloys consisted of a finely dispersed heterogeneous mixture of solid solution and, apparently, the $(NbTi)_3Al$ compound. In stress-relaxation tests at 500°C, the initial stress of 43.5 kg/mm² in as-rolled and aged specimens dropped about 19%. The as-rolled alloy had a tensile strength and elongation of 90.5 kg/mm² and 7%, respectively, and, after aging at 725°C, 120 kg/mm² and 7%, respectively. Aging the as-annealed alloy increased the strength from 67 to 95 kg/mm² and decreased ductility from 25 to 3%. This alloy has a modulus of elasticity of about 1200 kg/mm². The alloy is recommended as an age-hardenable, nonmagnetic, corrosion-resistant material with a stable modulus of elasticity for springs operating at elevated temperatures in aggressive media.

The ductile-to-brittle transition temperature of Nb–V alloys with 2, 4, 6, and 8 wt.% vanadium were investigated at Knolls[110] in the temperature range −253 to 100°C. The transition temperature of notched tensile bars was arbitrarily defined as that temperature where the reduction in area was 35%. This was increased by the addition of vanadium to niobium, the relation being linear up to 6 wt.% vanadium. The temperature range over which the alloys change from ductile-to-brittle behavior varied directly with vanadium content. When tested in the unnotched condition, these alloys did not undergo a ductile-to-brittle transition as defined in this study, nor did they become notch sensitive at temperatures of −196°C. Notched specimens were tested at crosshead motions of 0.025 and 2.0 in./min to study the strain-rate sensitivity of Nb–V alloys. Most of the data indicated that the mechanical properties of Nb–V alloys were insensitive to strain rate. The addition of 500 ppm nitrogen and 1500 ppm oxygen to Nb–2 and 4 wt.% V alloys caused pronounced increases in the ductile-to-brittle transition temperature of the Nb–V alloy. Nitrogen was found to be more potent than oxygen as a strengthener. The influence of both nitrogen and hydrogen on mechanical properties was greater in the alloys with higher vanadium content.

The stress-rupture properties of 5-mil-diameter tungsten wire were determined for rupture times up to about 200 hr at testing temperatures from 1200 to 2500°F (649 to 1371°C). Results at Lewis Research Center[111] showed that the rupture properties were superior to those reported for other forms of tungsten, other refractory metals, and superalloys in this temperature range. The onset of primary recrystallization, observed between 1800 and 2000°F (982 and 1093°C), was indicated by a decrease in microhardness, a decrease in ductility, and a coarsening of grain size. The strength superiority of the wire over the other materials was maintained beyond the onset of primary recrystallization.

Southern Research[112] has issued a report describing an evaluation program performed to obtain preliminary design data for tungsten and TZM sheet produced in the Refractory Metal Sheet Rolling Program. A comprehensive listing of properties at different temperature levels is included. Properties presented include tensile, notch-tensile, compression, bearing, shear, creep, thermal stability, weld-joint efficiency, recrystallization temperature, bend-transition temperature, density, thermal expansion, thermal conductivity, and specific heat.

Tensile properties were determined at Argonne[34] for V–15 wt.% Ti–7.5 wt.% Cr as a function of temperature and at a constant strain rate of 2×10^{-4}/sec. Results are shown in Fig. IV-20. The largest decrease

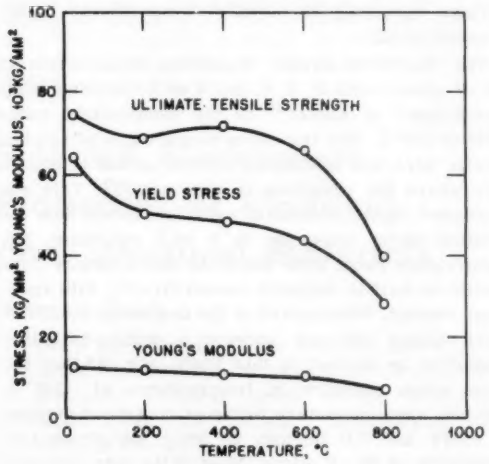

Fig. IV-20 Short-time tensile properties[34] of V–15 wt.% Ti–7.5 wt.% Cr annealed at 850°C for 1 hr (strain rate, 2×10^{-4} sec^{-1}).

in strength occurs between 600 and 800°C (~0.4 to 0.5 T_m), which is within the recovery range for this alloy. The autographic load-elongation curves at 200 and 400°C exhibited a "sawtooth" shape, which is typical of strain-aging behavior.

Miscellaneous Materials

The properties of Haynes 25 alloy (L-605), a non-heat-treatable cobalt-base alloy with chromium, nickel, and tungsten as the major alloying elements, have been summarized at Atomics International[113] from what they consider to be the best available data. The alloy has good high-temperature strength but suffers from poor machinability and difficulties in primary fabrication.

A report has been issued by workers at General Electric, Vallecitos,[114] which summarizes published fracture-mechanics data for a number of commonly used alloys. Types of alloys covered include pressure-vessel steels and turbine/generator-rotor steels.

Resonant-transverse-vibration fatigue tests of constant strain amplitude were carried out by the British[115] on the magnesium alloys ZR55, ZR57 (both Mg–Zr), MN70 (Mg–Mn), and AL80 (Magnox) in the strain range 4×10^4 to 3×10^{-3} at frequencies of 150, 1000, and 8000 cps at 400°C. A method is described by which the inelastic component of the strain may be evaluated from measurements of the resonant frequency of the fatigue specimens. Results are used to show that the fatigue life of the alloys can be expressed in the form $\epsilon p\, T^n = C$, where ϵp is the inelastic strain range, T is the time to failure, and n and C are constants independent of frequency. Tests on AL80 showed[13] that fatigue service in air or in argon is more damaging than fatigue service in CO_2 (Ref. 116). The difference first becomes apparent in tests lasting over 100 hr and then becomes progressively greater for tests of longer duration.

(J. A. DeMastry)

Ceramic Technology

Workers at General Electric[66b] observed orientation effects when beryllia prepared by calcining beryllium sulfate was extruded. The grains were found to be oriented with the crystallographic c-axis lying in or near the extrusion direction. Neither extruded rods made from beryllium hydroxide-derived beryllia nor isostatically pressed rods prepared from either of the two powders investigated were found to be so oriented. Similar orientations have been observed in some commercially prepared alumina.

The diffusion coefficients for self-diffusion of oxygen in Y_2O_3 and Er_2O_3 have been determined by workers at Ames.[117] The experimental technique involved measurement of weight-gain rates of slightly reduced oxide in air. (Tests performed in oxygen at pressures up to $^2/_3$ atm gave identical results.) The model employed is that of penetration of oxygen into a sphere of uniform initial concentration from a constant, inexhaustible supply. Calculated values of the diffusion coefficient were reported:

For Y_2O_3 (1000 to 1500°C),

$$D = 7.24 \exp(-58{,}640/RT) \text{ cm}^2/\text{sec}$$

For Er_2O_3 (850 to 1250°C),

$$D = 1.22 \exp(-47{,}830/RT) \text{ cm}^2/\text{sec}$$

Workers at Douglas[118] have investigated the chemical bonding of zirconia with monofluorophosphoric acid. Previous investigators had found that addition of this acid to stabilize zirconia produced chemically bonded ZrO_2 at 200°C. Investigation indicated that the reactions proceeded as follows:

1. The H_2PO_3F undergoes hydrolysis, yielding H_3PO_4 and HF.
2. HF reacts exothermically with ZrO_2, forming ZrF_4, an intermediate reaction product.
3. Upon heating, H_3PO_4 yields $H_4P_2O_7$ and H_2O.
4. ZrF_4 reacts exothermically with $H_4P_2O_7$, forming ZrP_2O_7, the bonding agent.

Similar reactions were encountered between MgO and H_2PO_3F.

McHugh, Walen, and Humenik, Jr.,[119] reported on their work on dispersion-strengthened Al_2O_3. Finely divided molybdenum particles served to inhibit grain growth during sintering. Specimens sintered in vacuum had densities approaching 98% of theoretical, with an average grain size of about 2 μ. Average strengths over 80,000 psi were reported.

(H. D. Sheets)

Nonfuel Refractories

The preparation and property evaluations of several refractory carbide materials have been studied by Russian investigators. Krushinskii[120] has examined the effects of temperature in the preparation of WC on the formation of hard phases. The change in WC properties was found to depend on the temperature of preparation (1400 to 1800°C). It was shown that an increase in temperature improves the structure and properties of systems with nonuniform distribution of the carbide phase. Chaporove, Rybalchenko, and Vrzheshch[121] examined the effects of additions of 0 to 20 wt.% Cr_2C_3 on the physical and mechanical properties of TiC–65 wt.% WC. It was observed that additions of Cr_2C_3 increased scaling resistance and electrical resistance without noticeably affecting the hardness, modulus of elasticity, and other properties.

Suzuki[122] has reported some property variations in sintering WC–10 wt.% Co alloys as functions of particle size and binder composition. The hardness and electrical resistivity of the alloys were found to decrease with increasing carbon content and grain size. The strength of the alloys was also dependent on the binder composition and grain size. The lattice parameters of the binder phase and the magnetic saturation of the alloys were independent of grain size; however, the stability of the low-carbon alloys at high temperatures was strongly affected by grain size.

Several researchers have examined the elastic properties of various refractory carbides. Brown, Armstrong, and Kempter[123] determined the elastic properties of polycrystalline transition-metal monocarbides. Table IV-9 summarizes these properties

Table IV-9 ROOM-TEMPERATURE ELASTIC PROPERTIES AND ELECTRICAL RESISTIVITY OF FOUR POLYCRYSTALLINE TRANSITION-METAL MONOCARBIDES[126]

Material	Elastic properties, 10^{12} dynes/cm²			Poisson's ratio	Specific electrical resistance, μohm-cm
	Young's moduli	Shear moduli	Bulk moduli		
$HfC_{0.967}$	4.61	1.95	2.42	0.18	24.6
$NbC_{0.984}$	4.88	1.98	3.00	0.22	49.1
$TaC_{0.994}$	5.37	2.16	3.44	0.24	25.6
$WC_{1.001}$	4.23	2.63	3.29	0.18	17.8

as determined at 23°C; the data were corrected to theoretical density.

The Young's moduli for the carbides of Ti, U, Cr, Zr, Nb, and Mo and for tungsten are presented by Russian[124] workers on samples with near stoichiometric compositions. It was found that the Young's modulus of carbides depends on the quantity of $s + d$-electrons in the metal atom in the Ti, U, and Cr and Zr, Nb, and Mo series. It is assumed that a similar dependence takes place in the tungsten, tantalum, and hafnium series which would permit estimating the values of Young's modulus of tantalum and hafnium carbides.

Chang and Graham[125] discuss the differences in the elastic behavior of the Group IV, transition-metal carbides and the monocarbide of uranium in reference to their different electronic structures. The plastic constants of zirconium and titanium carbide were determined at low temperatures, using a pulsed-ultrasonic phase-comparison technique.

Russian investigators[126] examined a series of zirconium carbide alloys containing 0.1 to 68 wt.% carbon. Compacts were produced by vacuum sintering pure zirconium (99.5%) and carbon at 2000°C, with subsequent arc melting in an inert atmosphere. Alloys were also produced by the direct arc melting of solid 99.8% pure zirconium and carbon. On the basis of physicochemical analyses, a phase diagram was constructed. Two-phase alloys containing 0.05 to 5.4 wt.% carbon consisted of grains of zirconium carbide and the alpha phase, which is a supersaturated solid solution of carbon in zirconium formed by the $\beta \rightarrow \alpha$ transformation. Alloys with a carbon content ranging from 6.0 wt.% to that of zirconium carbide (11.63 wt.% carbon) consisted of a solid solution of zirconium in the carbide. With a further increase in carbon content, free carbon was

precipitated both as eutectic and as primary carbide grains. The solubility of carbon in beta zirconium at 1100°C was less than 0.1 wt.%, whereas, in alpha zirconium at 820°C, it was 0.3 wt.%. The microhardness of cast and quenched zirconium alloys increased with increasing carbon content, reaching a maximum of 2150 kg/mm^2 at a composition corresponding to that of zirconium carbide. Further increases in the carbon content decreased the microhardness because of the appearance of free carbon in the form of both a eutectic and primary grains.

Studies of elevated-temperature deformation of NbC–C composites at constant time and pressure have shown an increase in resistance to deformation as NbC content increases and with additions of niobium metal.[8] Varcum-resin-binder additions improved material flow during hot pressing, but also caused a significant decrease in the resistance to deformation. At a constant vol.% carbide, the deformation curves for NbC and TaC were very similar. Iron contamination at the level of 3000 ppm increased the total cumulative deformation considerably at lower temperatures.

The thermal-expansion characteristics of NbC–graphite composites were measured to 2500°C by Miccioli.[127] Presintered NbC–graphite material was hot pressed into test bars at 2150°C and 4500 psi. The mean coefficient of thermal expansion and the percentage of permanent deformation as functions of original length were related to both graphite content and sample orientation (hot-pressed direction) as shown in Figs. IV-21 and IV-22, respectively. A high-temperature inversion, observed for NbC, was also observed for the composite system. Both the inversion and the measured deformation behavior appear to be orientation dependent.

Russian investigations[128] have shown that the wettability of the refractory compounds (carbides, borides, and nitrides) by metals is directly connected with the character of their chemical interaction, as well as with the direction of primary migration (transfer) of elements between the melt and the refractory compound. The wettability of the refractory compound by the melt can be regulated by the introduction of additions to one of the contacting materials, thus intensifying or weakening the migration of chemically interacting atoms in the necessary direction. Avgustinik[129] has presented a review of literature data and information on high-temperature reactions between metals and borides, carbides, oxides, and nitrides. The information is concerned mostly with chemical reactions between the refractory materials and the transition metals. It was noted that the high-temperature reactions were predominantly chemical.

Workers at the Lewis Research Center[130] have reported on the reactions of several carbides, nitrides, and borides in various liquid media, such as acid solutions of HCl, HF, and H_2CrO_4 and the liquids H_2O_2 and fused KOH. Semiquantitative analyses of the reaction products included mass-spectrographic determinations of the evolved gases. A hypothesis was presented from the solution-chemistry study on the nature of bonding in the refractory materials. In general, TiC, ZrC, and SiC were practically inert in strong aqueous acids (HCl) and strong aqueous bases (NaOH) to 100°C. The ZrC reacted with HF, whereas both ZrC and TiC were attacked by strong acid solutions of oxidizing agents. The SiC was found inert to all aqueous solutions tested. All of the tested carbides were attacked by molten KOH. The diborides of titanium and zirconium were more reactive to strongly acid solutions than the cor-

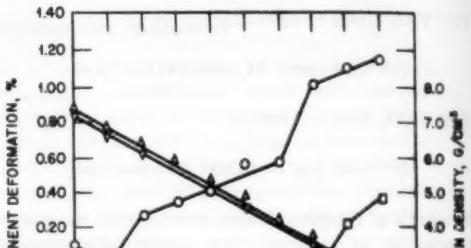

Fig. IV-22 Permanent deformation as a function of NbC–graphite composition and orientation to the hot-pressing direction.[127] ||: ○ and △, permanent deformation and density, respectively; ⊥: □ and ▽, permanent deformation and density, respectively.

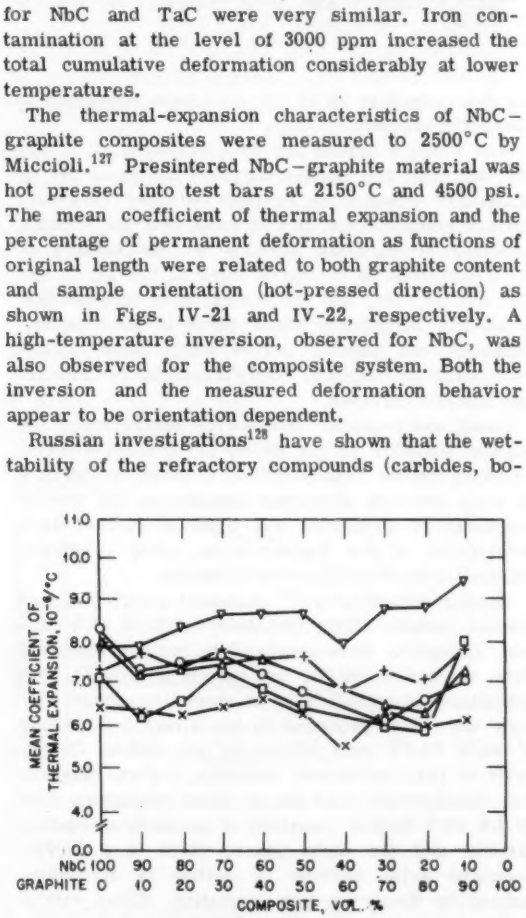

Fig. IV-21 Thermal-expansion coefficients as a function of NbC–graphite composition and orientation to the hot-pressing direction.[127] ⊥: □, 27–1000°C; △, 27–1500°C; ○, 27–2000°C; ||: ×, 27–1000°C; +, 27–1500°C; ▽, 27–2000°C.

responding carbides and nitrides. Both reduced metal–salt solutions such as $CuSO_4$ to corresponding free metals. Copper was noted to deposit on zirconium and titanium diborides when the latter were exposed to an acidified $CuSO_4$ solution at 23°C for 72 hr. There appeared to be no reactions of either TiN or ZrN with acid solutions of $CuSO_4$. The TiN was slightly attacked by concentrated H_2SO_4 at 100°C and readily attacked by hot aqueous HF containing an oxidizing agent such as $HgCl_2$. Both TiN and ZrN reacted with hot 6*M* H_2SO_4 plus 0.5*M* CrO_3, 1*M* H_2SO_4 plus 1*M* H_2O_2, and molten KOH.

Berkowitz-Mattuck[131] has reported the high temperature (1200 to 2000°K) oxidation of zone-melted ZrB_2 and HfB_2 at oxygen partial pressures of 1 to 700 torrs in helium. Parabolic rate behavior was observed. For ZrB_2 above 1400°K, an activation energy of 77 ± 5 kcal/mole was determined. Below 1400°K the activation energy was much lower and the mechanism of oxidation was different, probably because of the presence of B_2O_3 in the condensed phase. Below 1300°K the parabolic rate constant appears to be directly proportional to the oxygen partial pressure; at 1830°K the rate constant is independent of oxygen pressure. For HfB_2 in the range 1480 to 1870°K, an activation energy of 47 ± 4 kcal/mole was observed. Around 1970°K—the transition temperature for the monoclinic-to-tetragonal phase change in HfO_2—there was a sharp increase in the rate of oxidation. The parabolic rate constant for total oxygen consumption increases as the 0.4 ± 0.1 power of the oxygen partial pressure at 1630 and 1760°K. (W. C. Chard)

References

1. R. L. Dillon, US–UK Libby–Cockcroft Technical Exchange Coolant Corrosion of Reactor Materials, USAEC Report BNWL-CC-846, Battelle–Northwest, Oct. 1, 1966.
2. D. R. McClintock, In-Pile Experience with Zircaloy-Clad Fuel Rods in Borated PWR Environment, *Trans. Amer. Nucl. Soc.*, 9(1): 32-33 (June 1966).
3. C. F. Dixon and H. M. Skelly, Effect of Heat Treatment on the Corrosion Behavior of Two Zirconium–Copper–Molybdenum Alloys, USAEC file No. NP-16239, Canadian Department of Mines and Technical Surveys, Mines Branch, March 1966.
4. General Electric Company, Nuclear Materials and Propulsion Operation, High-Temperature Materials Program Progress Report No. 61, USAEC Report GEMP-61, Sept. 30, 1966.
5. J. Boulton, Use of Zirconium Alloys in Organic Coolants, Canadian Report AECL-2619, September 1966.
6. J. Boulton, S. R. Hatcher, and R. E. Hollies, The Use of Zirconium Alloys in Organic Coolants, *Trans. Amer. Nucl. Soc.*, 9(1): 45-46 (June 1966).
7. G. C. Imarisio and M. Cocchi, Statistical Techniques and Analysis in Corrosion Measurements of Zr Alloys in Terphenyls, Report EUR-2997.e, European Atomic Energy Community, 1966.
8. S. Peterson (Comp. and Ed.), Metals and Ceramics Division Annual Progress Report for Period Ending June 30, 1966, USAEC Report ORNL-3970, Oak Ridge National Laboratory, October 1966.
9. K. Videm, Fundamentals of the Corrosion of Super Pure Aluminum in Water, Norwegian Report KR-88 (CONF-660514-2), February 1966.
10. W. C. Francis and R. A. Moen (Eds.), Annual Progress Report on Reactor Fuels and Materials Development for FY 1966, USAEC Report IDO-17218, Phillips Petroleum Company, November 1966.
11. Phillips Petroleum Company, Nuclear Technology Branches Quarterly Report, January 1–March 31, 1966, USAEC Report IDO-17192, August 1966.
12. R. W. Staehle, A Study of the Mechanism of Stress Corrosion Cracking in the Iron–Nickel–Chromium Alloy System, USAEC Report COO-1319-42, Ohio State University Research Foundation, Aug. 30, 1966.
13. L. F. Picone and G. R. Taylor, Chemical Evaluation of Yankee Core I Fuel Cladding Corrosion Products, USAEC Report WCAP-6072, Westinghouse Electric Corporation, Atomic Power Division, August 1966.
14. B. Groenwall, L. Ljungberg, W. Huebner, and W. Stuart, Intercrystalline Stress Corrosion Cracking of Inconel 600 Inspection Tubes in the Agesta Reactor, Swedish Report AE-245, August 1966.
15. S. Sandstroem (Ed.), Operating Experience at the Agesta Nuclear Power Station, Swedish Report AE-246 and Suppl., September and October 1966.
16. J. L. English and J. C. Griess, Dynamic Corrosion Studies for the High Flux Isotope Reactor, USAEC Report ORNL-TM-1030, Oak Ridge National Laboratory, September 1966.
17. J. C. Griess and J. L. English, Materials Compatibility and Corrosion Studies for the Argonne Advanced Research Reactor, USAEC Report ORNL-4034, Oak Ridge National Laboratory, November 1966.
18. A. I. Gromova et al., *Corrosion Resistance of Reactor Materials*, Atomizdat, Moscow, 1966.
19. J. D. Jackson and W. K. Boyd, Corrosion of Titanium, Report DMIC-Memo-218, Battelle Memorial Institute, Defense Metals Information Center, Sept. 1, 1966.
20. R. A. Rapp and G. N. Goldberg, Oxidation of Nb–Zr and Nb–Zr–Re Alloys at 1000°C, *Trans. AIME*, 236: 1619-1628 (1966).
21. D. A. Prokoshkin, E. V. Vasil'eva, and F. M. Lazarev, Kinetics and Activation Energy of Oxidation of Alloys of the Nb–V–Ti System, *Zh. Prikl. Khim.*, 39: 323-327 (February 1966).
22. J. Stringer, Rate-Controlling Processes in the High-Temperature Oxidation of Tantalum, paper presented at the Electrochemical Society Meeting, Philadelphia, Pa., Oct. 10 to 14, 1966.
23. J. Stringer, The High-Temperature Oxidation of Tantalum Single Crystals, to be published in *J. Less-Common Metals*.
24. J. Stringer, Void Formation During the Oxidation of Tantalum, *J. Less-Common Metals*, 11: 111-118 (1966).
25. L. M. Adelsberg, G. R. St. Pierre, and R. Speiser, On the Origin and Identity of the Oxide Platelets Observed in Tantalum After Oxidation, *Trans. AIME*, 236: 1363-1366 (1966).
26. C. S. Tedmon, Jr., High-Temperature Oxidation of Ductile Chromium–Rhenium Alloys, *J. Electrochem. Soc.*, 113: 769-773 (August 1966).
27. D. R. Schryer and G. D. Walberg, A Theoretical and Experimental Investigation of the Oxidation of Molybdenum at Temperatures at Which Its Trioxide Is Volatile, Report NASA-TR-R-232, National Aeronautics and Space Administration, Langley Research Center, March 1966.
28. I. Cheng, Y. Yin, and H. Li, Effect of Yttrium on High-Temperature Oxidation of Molybdenum, *Chin Shu Hsueh Pao*, 9: 107-109 (January 1966).
29. J. H. Singleton, The Interaction of Oxygen with Hot Tungsten, USAEC Report TID-23122, Westinghouse Research Laboratories, May 5, 1966.

30. A. A. Pozdeeva, E. I. Antonovskaya, and A. M. Sukhotin, Passivity of Molybdenum, *Corros. Sci.*, 6: 149-158 (March–April 1966).
31. T. R. Bhat and I. A. Kahn, Retardation of Oxidation Rates of Niobium, Tantalum, and Tungsten by Fluoride Coating, *J. Less-Common Metals*, 11: 290-292 (1966).
32. International Atomic Energy Agency Symposium on Alkali Metal Coolants—Corrosion Studies and System Operating Experience, held at Vienna, Austria, Nov. 28–Dec. 2, 1966:
    a. N. P. Agapova, A. G. Ioltukhovskiy, and V. V. Romaneev, Behavior of Stainless Steel in Sodium in the 600–900°C Temperature Range, Paper SM-85/51, Kurchatov Institute, Moscow.
    b. G. Ilinchev, The Effect of Certain Factors on the Corrosion of Structural Materials in Liquid Sodium, Paper SM-85/3, Research Institute for Protection of Materials, Prague.
    c. J. H. DeVan, Corrosion of Iron- and Nickel-Base Alloys in High-Temperature Sodium and NaK, Paper SM-85/32, Oak Ridge National Laboratory.
    d. A. W. Thorley and C. Tyzack, The Corrosion Behavior of Steels and Nickel Alloys in High Temperature Sodium, Paper SM-85/18, Reactor Materials Laboratory, Culcheth.
    e. H. U. Borgstedt, G. Drechsler, and G. Frees, The Influence of the Surface Quality on the Liquid Sodium Corrosion of Nickel Alloys, Paper SM-85/12, Kernforschungzentrum, Karlsruhe.
    f. L. Champiex, R. Darras, and J. Sannier, Corrosion of Vanadium and Vanadium Alloys in Liquid Sodium, Paper SM-85/7, Center of Nuclear Studies, Saclay.
    g. S. Greenberg, W. E. Ruther, and H. A. Levin, Corrosion of Vanadium-Base Alloys in Sodium at 550 to 750°C, Paper SM-85/20, Argonne National Laboratory.
    h. F. L. Yaggee and E. R. Gilbert, Effect of Sodium Exposure on the Mechanical Properties of Potential Fuel Jacket Alloys at 550–700°C, Paper SM-85/21, Argonne National Laboratory.
    i. E. Baerlecken, K. Lorenz, E. Kranz, and D. Schlegel, Development of a Low-Alloy Ferritic Steel for High-Temperature Sodium Service with Special Regard to Carbon Transport, Paper SM-85/44, Thyssen Rohrenwerke AG, Dusseldorf.
    j. C. S. Campbell and C. Tyzack, A Preliminary Model for the Carburisation of Stainless Steel at High Temperatures in Sodium Containing Carbon at Unit Activity, Paper SM-85/19, Reactor Materials Laboratory, Culcheth.
    k. R. A. Davies, J. A. Bray, and J. M. Lyons, Corrosion of Steels in the Vicinity of a Sodium–Water Reaction, Paper SM-85/15, Dounreay Experimental Reactor Establishment.
    m. H. O. Muenchow and W. L. Chase, An Investigation of Tube Wastage Caused by Small Leaks of Water in Sodium-Heated Steam Generators, Paper SM-85/24, Atomic Power Development Associates, Inc.
    n. F. A. Smith, E. S. Sowa, E. L. Kimont, and C. R. Sutton, 650°C Sodium Free-Surface, Stress, and Wear Effects on Reactor Component Metals, Paper SM-85/22, Argonne National Laboratory.
    p. A. W. J. deGee, C. P. L. Commissaris, E. G. Chirer, and A. J. Bogers, Equipment for the Study of Wear Under Conditions of Oscillatory Relative Motion in Liquid Sodium, Paper SM-85/39, Metal Research Institute TNO, Delft.
33. W. J. Anderson, G. S. Sheffield, and A. J. Birkle, Development of Ferritic Steels for High-Temperature Sodium Service. Part II, USAEC Report NAA-SR-7544, Atomics International, Nov. 30, 1963.
34. Argonne National Laboratory, Reactor Development Program Progress Report, October 1966, USAEC Report ANL-7267, Nov. 22, 1966.
35. J. R. Weeks (Comp.), Brookhaven National Laboratory, unpublished, 1966.
36. B. Longson and A. W. Thorley, The Wetting Behaviour of Some Alloys Based on Iron, Nickel, and Chromium in Liquid Sodium, British TRG-Report-1291, July 14, 1966.
37. Argonne National Laboratory, Chemical Engineering Division Semiannual Report, July–December 1965, USAEC Report ANL-7125, May 1966.
38. V. S. Yemel'yanov and A. I. Yevstyukhin (Eds), *Metallurgy and Metallography of Pure Metals* (in Russian), No. 5, Moscow, 1966.
    a. N. M. Beskorovaynyy, V. K. Ivanov, and M. T. Zuyev, Carbon Behavior in Metal-Liquid-Lithium-Carbon Systems, pp. 130-150 (pp. 1-20 in English translation JPRS-37, 701).
    b. N. M. Beskorovaynyy and V. K. Ivanov, Corrosion Mechanism of Carbon Steels in Lithium, pp. 151-162 (pp. 21-32 in English translation JPRS-37, 701).
    c. N. M. Beskorovaynyy, V. K. Ivanov, and V. V. Petrashko, Corrosion of Chromium–Nickel Stainless Steel in Lithium, pp. 163-172 (pp. 33-41 in English translation JPRS-37, 701).
39. W. D. Wilkinson (Ed.), Fuels and Materials Development Program Quarterly Progress Report for Period Ending September 30, 1966, Argonne National Laboratory.
40. F. Tepper and J. Greer, Factors Affecting the Compatibility of Liquid Cesium with Containment Metals, Report AFML-TR-66-280, MSA Research Corp., June 1966.
41. D. L. Keller (Comp.), Quarterly Progress Letter Report to Sandia Corp. on Development of a Fuel System for a Fast Flux Pulse Reactor for Period Ending Oct. 31, 1966, Battelle Memorial Institute, Nov. 16, 1966.
42. D. N. Sunderman, D. L. Morrison, J. A. Gieseke, R. L. Ritzman, C. T. Walters, and J. M. Genco, An Evaluation of the Applicability of Existing Data to the Analytical Description of a Nuclear-Reactor Accident, USAEC Report BMI-X-10154, Battelle Memorial Institute, Jan. 1, 1966.
43. R. Summerling, Formation of Intergranular Voids and Cracks in an Irradiated Austenitic Steel Tensile Tested in the Temperature Range 650 to 850°C, *Nature*, 211: 512-514 (July 30, 1966).
44. P. C. L. Pfeil and P. J. Barton, The Effect of Prior Cold Work and Heat Treatment on the Tensile Ductility of Neutron-Irradiated 20 Wt.% Cr–25 Wt.% Ni: Nb Steel, British Report AERE-R-5291, September 1966.
45. A. F. Rowcliffe, G. J. C. Carpenter, H. F. Merrick, and R. B. Nicholson, An Electron Microscope Investigation of the High-Temperature Embrittlement of Irradiated Stainless Steels, British TRG-Report-1283, July 8, 1966.
46. C. Z. Serpan, Jr., and L. E. Steele, Neutron Spectral Considerations Affecting Projected Estimates of Radiation Embrittlement of the Army SM-1A Reactor Pressure Vessel, Report NRL-6474, Naval Research Laboratory, Aug. 12, 1966.
47. P. Patriarca (Comp.), Oak Ridge National Laboratory, unpublished. December 1966.
48. J. R. Hawthorne and L. E. Steele, Initial Evaluations of Metallurgical Variables as Possible Factors Controlling the Radiation Sensitivity of Structural Steels, USAEC Report NRL-6420, Naval Research Laboratory, Sept. 29, 1966.
49. D. S. Wood and E. R. Johnson, Effect of Irradiation on the High-Strain Fatigue Behavior of a Low-Carbon High-Manganese and a Low-Alloy Steel, British Report TRG-Report-1277, June 29, 1966.
50. Oak Ridge National Laboratory, unpublished, Dec. 6, 1966.

51. J. L. Brimhall and B. Mastel, Deformation Structure of Neutron-Irradiated Copper–Aluminum Alloy, *Appl. Phys. Lett.*, 9: 127-128 (Aug. 1, 1966).
52. F. A. Nichols, Theory of Radiation Embrittlement and Recovery of Radiation Damage in Ferritic Steels, *Phil Mag.*, [8] 14: 335-342 (August 1966); also USAEC Report WAPD-T-1865.
53. S. R. Veljkovic, A. Scepanovic, and V. Stefanovic, Radiation Damage in Steel with Medium and High Carbon Content, *Bull. Boris Kidric Inst. Nucl. Sci.*, 17: 77-88 (April 1966).
54. V. A. Shalashov, Singularities in Radiation-Thermal Treatment of White Cast Iron, *Metalloved. Term. Obrabotka Metal.*, No. 7: 65-67 (July 1966).
55. H. P. Bonzel, Influence of Surface Structure and Purity of Copper Samples and of Alpha Irradiation on the Diffusion of ^{63}Ni in Copper, Report AED-DISS-65-298, 1965.
56. W. Schuele, Contribution to the Enhanced Diffusion of ^{63}Ni in Alpha-Irradiated Pure Copper, Report EUR-2968.e, European Atomic Energy Community, Nov. 15, 1965.
57. R. E. Reed-Hill and E. P. Dahlberg, Some Effects of Prestrain at 77°K on the Mechanical Properties of Zirconium at Room Temperature, *Electrochem. Technol.*, 4(7-8): 303-307 (July–August 1966).
58. J. Pollard and L. P. Rzepski, Observation of Zirconium Foil Specimens Under the Electron Transmission Microscope. Study of Plastic Deformation, *Mem. Sci. Rev. Met.*, 63: 473-480 (May 1966).
59. D. Weinstein, Yield Point Occurrence in Polycrystalline Alpha-Zirconium, *Electrochem. Technol.*, 4(7-8): 307-312 (July–August 1966).
60. J. C. Couterne and G. Cizeron, Determination des Coefficients Principaux d'Expansion Thermique du Zirconium, *J. Nucl. Mater.*, 20: 75-82 (1966).
61. M. L. Picklesimer, Deformation, Creep, and Fracture in Alpha Zirconium Alloys, *Electrochem. Technol.*, 4: 289-300 (July–August 1966).
62. K. P. Steward and B. A. Cheadle, The Effect of Preferred Orientation on the Mechanical Properties and Deformation Behaviour of Zircaloy-2 Fuel Sheathing, Canadian Report AECL-2627, August 1966.
63. R. G. Wheeler and D. R. Ireland, Multiaxial Plastic Flow of Zircaloy-2 Determined from Hardness Data, *Electrochem. Technol.*, 4(7-8): 313-317 (July–August 1966).
64. C. E. Coleman and D. Hardie, Hydrogen Embrittlement of α-Zirconium: A Review, *J. Less-Common Metals*, 11: 168-185 (September 1966).
65. J. J. Kearns and C. R. Woods, Effect of Texture, Grain Size, and Cold Work on the Precipitation of Oriented Hydrides in Zircaloy Tubing and Plate, *J. Nucl. Mater.*, 20: 241-261 (1966).
66. J. W. Colby (Ed.), Papers Presented at the X-Ray Preferred Orientation Meeting Held at National Lead Co. of Ohio, December 5 and 6, 1963, Report NLCO-946:
    a. P. L. Rittenhouse and M. L. Picklesimer, Effect of Preferred Orientation and Stress on the Directional Precipitation of Hydrides in Zircaloy-2, pp. 79-102.
    b. L. H. Sjodahl and S. F. Bartram, Measurement of Orientation in Extruded BeO, pp. 107-117.
67. T. Okada, H. Hirano, and N. Kunimoto, Texture and Microstructure of Thin-Walled Zircaloy-2 Tubes, *Electrochem. Technol.*, 4(7-8): 365-374 (July–August 1966).
68. E. D. Hindle and G. F. Slattery, Influence of Processing Variables on the Grain Structure and Hydride Orientation, *J. Inst. Metals*, 94: 245-249 (July 1966).
69. E. A. Gulbransen, A. R. Pebler, and K. F. Andrew, Hydrogen Reactions with Alloys of Zirconium and the Metals Vanadium, Chromium, Iron, Cobalt, Nickel, Copper, Molybdenum, and Niobium, USAEC Report WERL-3203-5, Westinghouse Research Laboratories, Sept. 7, 1966.
70. G. W. Parry, The Effect of Hydrogen on the Fracture Toughness of Zircaloy-2 and Zirconium–2.5 Wt.% Niobium, Canadian Report AECL-2622, August 1966.
71. A. Cowan and K. J. Cowburn, Critical Crack Length Measurements in Hydrided Zircaloy-2 Pressure Tubes, British Report TRG-Report-1262, June 6, 1966.
72. J. Winton and R. A. Murgatroyd, The Effect of Variation in Composition and Heat Treatment on the Properties of Zirconium–Niobium, *Electrochem. Technol.*, 4(7-8): 358-365 (July–August 1966).
73. F. J. Zanner, R. M. Vermett, and W. R. Clough, Studies on the Tensile Fracture Characteristics of Zirconium and Zirconium–Rare Earth Solid Solution Alloys, *Electrochem. Technol.*, 4(7-8): 317-322 (July–August 1966).
74. G. W. Parry, Stress Reorientation of Hydrides in Cold-Worked Zirconium–2.5 Wt.% Niobium Pressure Tubes, Canadian Report AECL-2624, August 1966.
75. D. E. Coates, Hydrogen Supersaturation in Zirconium and Zirconium–2.5 Wt.% Niobium, Canadian Report AECL-2599, July 1966.
76. A. Cowan and R. W. Nichols, Improvements Relating to Low Alloy Steels, British Patent 1,034,424, June 29, 1966.
77. D. Fahr, Strengthening Mechanisms of Ultra-High-Strength Austenitic Steel, USAEC Report UCRL-16922, University of California, Lawrence Radiation Laboratory, June 1966.
78. Virginia Polytechnic Institute, The Influence of Nitrogen Additions on Phase Relationships in AISI Type 304, Summary Report 438-A, USAEC–Euratom Report EURAEC-1716, August 1966.
79. M. H. Lewis, Precipitation of (Fe, Cr) Sigma Phase from Austenite, *Acta Met.*, 14: 1421-1428 (November 1966).
80. D. R. Ireland, The Effects of Aging on Dissimilar Metal Welded Joints with Multipass Welding of Hastelloy X and Hastelloy W Filler Metal, USAEC Report BNWL-290(Pt. 1), Battelle–Northwest, July 1966.
81. G. D. Sandrock and L. Leonard, Cold Reduction as a Means of Reducing Embrittlement of a Cobalt-Base Alloy (L-605), Report NASA-TN-D-3528, National Aeronautics and Space Administration, Lewis Research Center, August 1966.
82. D. L. Chase, Comparison of Chemical Analyses of Refractory Alloys, DMIC-Report-220, Battelle Memorial Institute, Defense Metals Information Center, Sept. 10, 1965.
83. K. S. Pradantseva and N. A. Soloveva, Thermal Expansion of the Solid Solutions of Refractory Metals of the IV, V, and VI Groups of the Periodic System, *Metalloved. Term. Obrabotka Metal.*, No. 6: 41-44 (1966).
84. L. Stals, J. Nihoul, and R. Gevers, Analytical Study of Isochronal Annealing of Cold Worked Niobium, *Phys. Status Solidi*, 15: 717-723 (June 1, 1966).
85. J. Stoop and P. Shahinian, The Effect of Nitrogen on the Tensile and Creep-Rupture Properties of Niobium, *Amer. Soc. Metals, Trans. Quart.*, 59: 411-426 (September 1966).
86. J. R. Stephens and R. G. Garlick, Compatibility of Tantalum, Columbium, and Their Alloys with Hydrogen in the Presence of Temperature Gradient, Report NASA-TN-D-3546, National Aeronautics and Space Administration, Lewis Research Center, August 1966.
87. R. J. E. De Bruyne, Influence of Oxygen on Mechanical Properties of Nb–5 Percent Zr Alloys, USAEC Report IS-T-92, Ames Laboratory, May 1966.
88. E. S. Bartlett and E. F. Bradley, Niobium Alloys Containing Beryllium, *J. Less-Common Metals*, 11: 219-220 (1966).
89. S. A. Worcester, R. T. Torgerson, and W. A. Baginski, Columbium–Hafnium Base Alloys with Yttrium Additions, U. S. Patent 3,266,892, Aug. 16, 1966.

90. D. D. Foley, Production of Age Hardenable Tantalum Based Alloys, U. S. Patent 3,265,540, to American Radiator and Standard Sanitary Corp., Aug. 9, 1966.
91. F. Guin and P. L. Pratt, Effects of Orientation on the Yielding and Flow of Molybdenum Single Crystals, *Phys. Status Solidi*, 15: 539-552 (June 1, 1966).
92. V. P. Gol'tsev, Effect of Lanthanum and Yttrium on the Recrystallization of Molybdenum, *Dokl. Akad. Nauk SSSR*, 166: 71-73 (Jan. 1, 1966).
93. V. P. Gol'tsev, Effects of Vanadium, Titanium, Hafnium, and Zirconium on Recrystallization of Molybdenum, *Vesti Akad. Navuk BSSR, Ser. Fiz.-Tekh. Navuk*, 4: 53-56 (1965).
94. Y. I. Demkin, The Nature of Plasticity in Molybdenum–Rhenium Alloys, *Dokl. Akad Nauk SSSR*, 116: 71-73 (Jan. 1, 1966).
95. V. P. Gol'tsev, Investigation of the Aging Kinetics of Molybdenum-Base Alloys, *Dokl. Akad. Nauk SSSR*, 10: 385-387 (1966).
96. Y. Chuang, C. Tang, and H. Chuang, The Isothermal Sections at 1200°C of the Equilibrium Diagrams of the Systems, Mo–Ti–Zr and Mo–Nb–Zr (in Chinese), *Chin Shu Hsueh Pao*, 9: 63-71 (January 1966).
97. V. N. Svechnikov and G. F. Kobzenko, Pnase Equilibrium Diagram in the Chromium–Niobium–Molybdenum System, *Fazovye Prevrashcheniya v Metallakh i Splavakh*, pp. 147-158, Institute of Physics of Metals, Academy of Sciences, Ukrainian SSR, Kiev, 1965.
98. Yu. M. Alexandrova, L. N. Alexandrov, and V. D. Eliseevc, Influence of Inert Gases on Tungsten Recrystallization, *Fiz.-Khim. Mekh. Mater.*, 2: 327-332 (1966).
99. D. Porter, Decomposition of Chromium–Tungsten Solid Solution, USAEC Report UCRL-16619, University of California, Lawrence Radiation Laboratory, January 1966.
100. M. Quatinetz, J. W. Weeton, and T. P. Herbell, Investigation of Extruded Tungsten Composites Containing Fibered or Reacted Additives, *Int. J. Powder Met.*, 2(2): 51-64 (April 1966).
101. F. W. Boulger, A. F. Gerds, W. A. Glaeser, H. J. Henning, and A. T. Hopper, Survey of Current Knowledge of the Deformation Characteristics of Beryllium, the Refractory Metals, and the Superalloys, Report AD-630427, Battelle Memorial Institute, Feb. 10, 1966.
102. E. A. Almond and D. Hull, Effect of Stress on Strain Aging, *Phil. Mag.*, 14(8): 515-529 (September 1966).
103. P. A. Fisher and P. D. Demaine, Improvements in or Relating to Magnesium Base Alloys, British Patent 1,034,227, June 29, 1966.
104. V. de L. Davies, The Effect of Fine Disperse Al_3Zr on the Recrystallization of Aluminum, *J. Inst. Metals*, 94: 191-192 (May 1966).
105. G. Chaudron, Preparation and Properties of Stainless Steels, USAEC–Euratom Report EURAEC-1678, Centre National de la Recherche Scientifique, Sept. 28, 1966.
106. Atomics International, AEC Unclassified Programs. Quarterly Technical Progress Report, July–September 1966, USAEC Report NAA-SR-12175, Nov. 25, 1966.
107. Argonne National Laboratory, Reactor Development Program Progress Report, September 1966, USAEC Report ANL-7255, Oct. 26, 1966.
108. J. Stoop and P. Shahinian, Effects of Nitrogen on Tensile and Creep-Rupture Properties of Niobium, *Amer. Soc. Metals, Trans. Quart.*, 59: 411-426 (September 1966).
109. A. K. Boresova and B. G. Belon, Spring Niobium-Base Alloy with Stable Elasticity Modulus at High Temperatures, *Metalloved. Term. Obrabotka Metal.*, No. 6: 10-11 (1966).
110. C. D. Calhoun, Ductile-to-Brittle Transition of Niobium–Vanadium Alloys as Affected by Notches, Strain Rate, Nitrogen, and Oxygen, USAEC Report KAPL-3119, Knolls Atomic Power Laboratory, April 1965.
111. D. L. McDanels and R. A. Signorelli, Stress-Rupture Properties of Tungsten Wire from 1200 to 2500°F, *Metals Eng. Quart.*, 6(3): 51-58 (August 1966).
112. Southern Research Institute, The Mechanical and Thermal Properties of Tungsten and TZM Sheet Produced in the Refractory Metal Sheet Rolling Program. Part I, Report AD-638631, Aug. 31, 1966.
113. J. W. Ramsey, The Design Properties of Haynes Alloy No. 25 (L-605), USAEC Report NAA-SR-Memo-11680, Atomics International, October 1965.
114. M. B. Reynolds, Fracture Toughness of Some Engineering Alloys, USAEC Report GEAP-5014, Vallecitos Atomic Laboratory, March 1966.
115. R. W. Suhr, High Frequency Fatigue Life of Some Magnesium Alloys Used in Fuel Element Applications, *J. Nucl. Mater.*, 20: 94-103 (July 1966).
116. L. E. Raraty and R. W. Suhr, Correlation of the Fatigue Properties of Magnox AL80 in Terms of the Plastic Strain Range, *J. Inst. Metals*, 94: 292-300 (August 1966).
117. A. F. Voigt (Ed.), Reactor Materials Development Quarterly for Division of Reactor Development, July–September 1966, USAEC Report IS-RD-7, Ames Laboratory.
118. V. Edlin, Interim Report on the Bonding Reaction Mechanism in Chemically Bonded ZrO_2. Phase 2, USAEC file No. NP-16047, Douglas Aircraft Co., Inc., Aug. 10, 1964.
119. C. O. McHugh, T. J. Walen, and M. Humenik, Jr., Dispersion-Strengthened Aluminum Oxide, *J. Amer. Ceram. Soc.*, 49(9): 486-491 (September 1966).
120. A. N. Krushinskii, Investigation of the Effect of the Temperature of Obtaining WC on the Formation of Hard Alloys with Nonuniform Distribution of the Carbide Phase, *Porosh. Met., Akad. Nauk Ukr. SSR*, No. 7: 73-75 (July 1966).
121. I. N. Chaporove, R. V. Rybalchenko, and E. Y. Vrzheshch, Preparation of Carbides (Ti, W, Cr)C and a Study of Their Properties, *Porosh. Met., Akad. Nauk Ukr. SSR*, No. 7: 76-83 (July 1966).
122. H. Suzuki, Variations in Some Properties of Sintered Tungsten Carbide–Cobalt Alloys with Particle Size and Binder Composition, *Trans. Jap. Inst. Metals*, 7: 112-117 (April 1966).
123. H. L. Brown, P. E. Armstrong, and C. P. Kempter, Elastic Properties of Some Polycrystalline Transition-Metal Monocarbides, *J. Chem. Phys.*, 45: 547-549 (1966).
124. I. N. Frantsevich and A. B. Lyashchenko, Young's Modulus of Carbides of Some Transition Metals, *Porosh. Met., Akad. Nauk Ukr. SSR*, No. 7: 73-75 (July 1966).
125. R. Chang and L. J. Graham, Low-Temperature Elastic Properties of ZrC and TiC, *J. Appl. Phys.*, 37: 3778-3783 (September 1966).
126. Y. Gedin et al., Investigations of Alloys of the Zr–C System, *Met. Metalloved. Chistykh Metal., Sb. Nauch. Rabot*, No. 5: 25-32 (1966).
127. B. R. Miccioli, Thermal Expansion Behavior of Niobium Carbide–Graphite Composites, *Amer. Ceram. Soc. Bull.*, 45: 670-673 (July 1966).
128. G. A. Yasinskaya, Wettability of Refractory Carbide, Boride, and Nitride by Molten Metal, *Porosh. Met., Akad. Nauk Ukr. SSR*, No. 7: 53-56 (July 1966).
129. A. I. Avgustinik, Reactions of Oxides and Carbides with Metals, USAEC Report UCRL-Trans-10044 [from *Zh. Vses. Khim. Obshchest. im. D. I. Mendeleeva*, 10: 512-518 (1965)].
130. W. H. Philipp, Chemical Reactions of Carbides, Nitrides, and Diborides of Titanium and Zirconium and Chemical Bonding in Their Compounds, Report NASA-TN-D-3533, National Aeronautics and Space Administration, Lewis Research Center, August 1966.
131. J. B. Berkowitz-Mattuck, High-Temperature Oxidation. III, Zirconium and Hafnium Diborides, *J. Electrochem. Soc.*, 113: 908-914 (September 1966).

Section V

Reactor Materials

Special Fabrication Techniques

Melting and Casting

The preparation of intermetallic uranium compounds and their testing in the Materials Testing Reactor (MTR) and in the Engineering Test Reactor (ETR) were recently described by Phillips.[1] Uranium aluminides were prepared by vacuum-induction melting using graphite crucibles coated with magnesium zirconate. In induction melting, both aluminum and uranium were lost during processing. Uranium was absorbed into the crucible; aluminum was distilled off. Uranium aluminides and silicides were also produced by arc melting, which appeared to be much more satisfactory for the preparation of the compounds.

Alloys of aluminum with 18 and 24 wt.% uranium as ingots 70 and 100 mm in diameter were produced by continuous casting in Germany.[2] A specially constructed feeding system was useful in overcoming the gravitational segregation that occurs during casting. After the ingots were heat-treated at 600°C, they were rolled to strip and extruded successfully.

A melting and casting process was developed at Battelle–Northwest[3] for the preparation of Np–Al alloys for use as target elements for irradiation in General Electric's N Reactor. Neptunium oxide was employed as a starting material for reduction and alloying with aluminum to form an Al–12 wt.% Np master alloy. This latter alloy was then diluted with aluminum and cast as tubular shapes. Final alloys were of two compositions: Al–9.2 wt.% Np and Al–6.3 wt.% Np. These alloys were cast into graphite molds around graphite mandrels from a preheated casting ladle. Alloying was performed in an induction-melting crucible. The casting temperature was 720 to 730°C, and the alloys were hand poured into molds preheated to 290°C.

Studies of the preparation of UC crystals by zone melting at Atomics International[4] indicated that special problems in stoichiometry control occur when the melting is done in high vacuum or under an inert gas. Vapor loss of uranium is the problem when melting is done in vacuum; solid–liquid distribution effects occur when zone melting in an inert gas is performed. Crystals prepared by zone melting invariably contained UC_2 platelets. The UC–UC_2 structure, however, could be converted to single-phase UC by heating the crystals at 1800°C in either hydrogen or oxygen at reduced pressures.

The effects of additions of various elements and compounds on the grain refinement of tungsten in electron-beam-melted ingots were studied by NASA–Lewis.[5] Small ingots of tungsten containing selected additives were prepared by electron-beam melting and examined. Measurements on transverse ingot sections from each melt indicated that all the additives decreased the average grain diameter of the columnar grains typical of electron-beam-melted tungsten and that grain-refining effectiveness varied with the concentration of the solutes. Losses of the additives during melting were in excess of 90% in many cases. The most potent grain refiner was boron. A nominal addition of 0.5 wt.% decreased the average grain diameter of the columnar grains from 0.48 to 0.008 cm. The effectiveness of the elemental additives decreased in the following order: B, Y, C, Hf, Zr, Mo, Nb, Re, and Ta. The losses of these elements during melting also decreased in approximately the same order. The elemental additives were generally more effective grain refiners than refractory compounds, and it was noted that elements with the smallest distribution coefficients were the most effective grain refiners

The Russians[6] have been studying the effect of ultrasonic vibration on the ductility of stainless steels containing 2.0 to 3.7 wt.% boron. Generally boron contents above 1.8 wt.% form coarse hypereutectic borides that lower the ductility of the material. It was found, however, that the size and shape of the boron inclusions can be improved by applying ultrasonic vibration to the liquid steel during cooling and solidification. It was also found that the effect of ultrasonic vibration is temperature dependent and varies with the type of steel. The vibration, in general, broke down the boride inclusions into small particles uniformly distributed throughout the metal mass and often improved the ductility, especially in rolling. The structure of high-boron stainless steels was also refined by annealing at 1200 to 1250°C.

Certain modifications in the conventional electron-beam floating-zone technique and its use in the refining of molybdenum have been described by the Franklin Institute.[7] This technique resulted in increased stability of operation, longer filament life,

and excellent uniformity of crystal diameter (0.130 ± 0.001 in.). Molybdenum single crystals grown from vacuum-arc-cast and hot-swaged stock contained inclusions that were not appreciably affected by variations in zoning speed, number of zone passes, and annealing treatments at 1700°C in vacuum or in argon after refining. However, it was found that hydrogen-annealing the as-received materials before zone melting eliminated the inclusions.

An electron-beam floating-zone refining method has been employed at Oak Ridge[8] for the preparation of pure niobium single crystals. Attempts have been made to identify the purification mechanisms that occurred during processing. It was found that little purification was due to movement of impurities by the zone-refining action, but, instead, most metallic impurities were reduced by evaporation. Niobium single crystals are being prepared for mechanical-property studies.

Work is continuing at Argonne[9] on the development of fabrication techniques for a V–20 wt.% alloy. Production of full-scale ingots at Argonne involves compaction of vanadium chips and titanium sponge into drip rods, which are, in turn, electron-beam melted into 5.8-cm-diameter ingots. These ingots are then remelted by consumable-electrode-arc methods. Improvements in yield were noted during electron-beam melting when the melting rate was increased from 31 to 51 g/min. Above 51 g/min splattering of the molten metal became a problem. Charge-weight loss as a function of melting rate is shown in Table V-1.

Table V-1 CHARGE-WEIGHT LOSSES AS A FUNCTION OF MELTING RATE IN ELECTRON-BEAM MELTING V–20 WT.% Ti DRIP RODS[9]

Melt rate, g/min	Charge-weight lost in melting, %
33	5.6
51	2.4
73	2.6
80	3.3
88	3.7
100	3.9

Parameters used in consumable-electrode-arc remelting of the electron-beam ingots were essentially the same as those employed in earlier work, consisting of a melting rate of 1 kg/min with straight polarity (consumable electrode negative) at 84 kw. A stirring coil was used to improve ingot quality, and the ingots were "hot-topped" to reduce secondary pipe. Although arc melting was done under vacuums of 10^{-2} to 10^{-3} torr, no loss of charge material was experienced.

The Canadians[10] have studied the redistribution of oxygen and iron during zone refining of zirconium. Iodide zirconium containing 100 to 200 ppm oxygen and iron and less than 10 ppm tungsten was employed in the experiments. It was found that segregation of oxygen is typical for solutes with a distribution coefficient greater than 1 and that no redistribution of oxygen takes place at high rates of zone travel. It was also noted that the distribution coefficient for oxygen lies between 1.5 and 2.0 and that purification with respect to iron occurs mainly by evaporation.

The melting and casting of precipitation-hardenable stainless steels are discussed in a comprehensive report issued by Battelle–Columbus.[11]

(S. G. Nelson)

Hot and Cold Working of Cast Materials

The fabrication techniques currently being employed in the preparation of nickel- and cobalt-base alloys are reviewed in a Battelle report.[12] Primary operations include rolling, extrusion, and forging and drawing of tube, rod, and wire. Secondary forming described includes brake bending, deep drawing, spinning and shear, drop hammer, trapped rubber, stretch, tube, roll, dimpling, joggling, and sizing.

General Electric–Vallecitos[13] is evaluating a Zr–2.0 at.% Cr–0.16 at.% Fe alloy as a nuclear fuel cladding. A laboratory process was developed which yielded material with excellent corrosion performance. Alloys prepared on a larger scale by an outside vendor, however, did not show properties as good as those of alloys prepared in the laboratory. Laboratory processing parameters included the following:

Melt	2- to 5-cm ingots
Forge	955°C
Solution	955°C, 1 hr
Quench (water)	2.5-cm section
Hot work	605°C, 90%
Cold work	50%, one anneal
Anneal	760°C, 2 hr

The fabrication parameters employed in production were somewhat different.

Techniques for drawing Zircaloy-2 and zirconium tubing down to 0.22-mm wall thickness were discussed by Timmermans.[14] Factors affecting the finished product, such as lubrication, shape of the dies, and thermal treatment after each pass, were studied. The lubrication mechanism during drawing demonstrated the necessity of a well-bonded underlayer to fix the lubricant. Of three underlayers examined—oxide, phosphate, and bonderization—the last was found most satisfactory. Good results were obtained with tungsten carbide dies having an entry angle of 30° and a cylindrical region 3 mm in length. An optimum temperature range for thermal treatment of the tubing was found to be 400 to 500°C.

Two improvements were noted in the fabrication of a V–20 wt.% Ti alloy at Argonne.[9] First, it was found that the alloy in tube form is amenable to heavy reductions by tube reducing. As a result a tube-

reducing machine employing a unique three-roll principle was designed and built. Trials are currently being conducted on this machine. The second improvement was noted in tube drawing when a thin plastic base coat on the tubing was used in conjunction with a chlorinated-wax lubricant. These materials permitted the use of carbide draw dies in place of aluminum–bronze dies and greatly extended die life and the dimensional control of drawn tubes.

Ames[15] has been conducting several programs concerned with the mechanical behavior and development of fabrication techniques for yttrium and chromium. Unusual deformation behavior noted in polycrystalline yttrium has been tentatively attributed to the presence of a very fine dispersion of the second phase. Attempts are currently being made to identify this phase and to determine its effects on deformation parameters. The deformation of single crystals of yttrium is also being studied. Experiments have been performed to determine the high-energy-rate (HER) extrusion characteristics of two grades of yttrium metal. The conditions for satisfactory extrusion are described in Ref. 16. The extrusion of arc-cast and recrystallized yttrium billets into rods and seamless tubing was also studied, and the results are given in another Ames report.[17]

The effect of composition, crystalline condition, and thermal history on the ductility of chromium-base alloys was evaluated.[18] A comparison of the ductility of single crystals and polycrystalline alloys shows that the minima observed in transition-temperature vs. concentration curves for a number of chromium-base alloys cannot be attributed to any systematic variation in grain size. It was also found that previous heat-treatment had a greater influence on the ductility of polycrystalline alloys than on the corresponding single crystals.

Cracking failures occurring in 310 stainless-steel reduction vessels, employed in the preparation of uranium from UF_4, prompted Dow[19] to investigate another material for reduction-vessel construction. Sensitization-resistant 347 stainless steel was selected to replace the former material, and no cracking has been observed thus far.

A status report recently issued by the Defense Metals Information Center[20] summarizes research of interest to the Metalworking Process and Equipment Program (MPEP). Some progress being made in the development of special fabrication techniques applicable to materials for reactor use is reviewed in the following paragraphs.

Battelle–Columbus is studying the possible advantages of using heated rolls for the hot rolling of metals. A heat-transfer analysis of the hot-rolling process was made to permit predicting temperature gradients within the workpiece or strip during rolling. A simplified model was developed for predicting temperatures in the strip-contact zone during rolling, and an analytical solution was applied to the rolling of 0.050-in.-thick beryllium. The effect of increasing the roll temperature from 70 to 1000°F (21 to 538°C) at a roll speed of 100 ft/min on the temperature profiles from surface to center line of the strip is summarized below:

Roll temperature, °F	Calculated strip temperature, °F			
	Entering the roll		Leaving the roll	
	Center	Surface	Center	Surface
1000	1400	1280	1325	1280
70	1400	1000	1100	965

These data show that the temperature gradient from surface to center line is greatly reduced and the overall temperature drop of the strip during rolling is substantially decreased when heated rolls are used. It may be possible by using rolls heated to 1000°F (538°C) to widen the "narrow" range for working beryllium and also to roll the metal at lower temperatures, perhaps in the range 1000 to 1100°F (538 to 599°C). If this were possible, cladding of the beryllium to prevent oxidation might not be necessary. For a roll speed of 1000 ft/min, the ambient roll temperature has almost no effect on the centerline temperature. The effect of heat generation during rolling is more pronounced for tungsten than for beryllium. At 100 ft/min the influence of roll temperature on the centerline-temperature profile is very pronounced for tungsten.

Thompson Ramo Wooldridge is engaged in a program to develop superior lubricants for use in extruding high-temperature refractory metals such as molybdenum, tungsten, niobium, and their alloys. Three laboratory tests have been chosen to evaluate the potential of candidate materials as high-temperature-extrusion lubricants. These are a lubricity test, a reactivity test, and an insulation test. On the basis of the lubricity test, the following materials are being further tested: CaO, SrO, Y_2O_3, La_2O_3, CeO_2, Co_3O_4, WO_3, and MnO_2.

Some materials have been evaluated in the reactivity test by heating in contact with billet and die materials at the following temperatures:

Material	Reaction temperature	
	°F	°C
4340 steel	1900	1040
Mo–0.5 wt.% Ti alloy	3000	1650
Zirconia	3000	1650

Only the Co_3O_4–graphite mixture showed a severe attack with the Mo–0.5 wt.% Ti alloy, and none of the candidates showed an adverse reaction with 4340 steel. Because of the surface attack of the Co_3O_4–graphite mixture with the molybdenum alloy, it was eliminated from further testing during the extrusion trials.

Aeroprojects, Inc., is studying the effect of vibratory energy applied to the die during the drawing of 4340 steel, a Ti–6 wt.% Al–4 wt.% V alloy, and 6061-0 aluminum-alloy rods, in addition to C. P. copper wire. Rods of 6061-0 aluminum, the titanium alloy, and 4340 steel were cold-drawn from a 0.6875-in. diameter for a reduction in area of 15%, both with and without ultrasonic vibration of the tungsten carbide die at 15 kc in the longitudinal mode. Ultrasonic vibration reduced the drawing forces 15 to 20% for aluminum and 4.5 to 6.5% for steel at a drawing rate of 60 ft/min when the input power was 4.5 kw to the ceramic transducers. Measurement of drawing variables showed that force reduction and other parameters, except die temperature, were not constant during drawing but varied periodically because of resonant response of the undrawn lengths of the rod and concomitant changing load on the ultrasonic system. Average force reductions decreased as the drawing rate was increased. Little difference in the surface finishes of rods drawn with or without ultrasonic vibrations was found.

Illinois Institute of Technology Research Institute is investigating the use of both liquid- and gas-pressure media for extruding high-strength and refractory metals. The gas-extrusion technique is expected to combine the advantages of low-temperature hydrostatic extrusion and the use of the high temperatures employed in conventional extrusion. For example, with billet temperatures of 2000 to 2500°F (1043 to 1371°C), pressure-chamber requirements would be reduced to 150,000 to 180,000 psi. Such pressures are within the range of current container technology and might facilitate translating this new technique into a production method. (S. G. Nelson)

Powder Metallurgy

Twenty-one papers were presented in three groups to summarize the proceedings of the International Powder Metallurgy Conference.[21] One group was concerned with nuclear applications; another, with cemented carbides, friction materials, thermoelectric materials, porous materials, and heavy metals; and the third described research programs and future trends in various countries.

A fabricability evaluation[22] of powder-extruded (and sintered) W–25 wt.% Re and W–30 wt.% Re–30 wt.% Mo tubing was conducted by investigators at Argonne. The W–Re–Mo alloy was considerably more ductile than the W–Re alloy, being amenable to sizable reductions by swaging, by ductile-core drawing, and by plug drawing. A 35% reduction in area by drawing at ambient temperatures was possible on the W–Re–Mo tubing. The W–Re alloy was found to tolerate moderate reduction by drawing before cracking. The microstructure of tubing fabricated from the W–Re–Mo alloy indicated that many of the voids were nearly closed but that complete densification had not been accomplished.

In another investigation[23] involving drawing powder-metallurgy billets of a W–30 at.% Re–30 at.% Mo alloy, General Electric evaluated three different tube-drawing procedures. These included drawing on a hardened tool-steel mandrel, drawing on a removable Mo–Hf core, and sinking without material in the bore of the tube. The alloy was drawn to 0.425-cm OD and 0.345-cm ID. Mechanical tolerances of ±0.0005 cm for the inside and outside diameters were consistently maintained. Drawing on a hardened tool-steel mandrel proved to be the most successful technique.

In a similar investigation[24] unalloyed tungsten and W–30 at.% Re–30 at.% Mo powder-metallurgy billets were extruded by the floating-mandrel technique at Oak Ridge to produce tube shells for subsequent processing into large- and small-diameter thin-walled tubing. During the course of the investigation, several significant processing techniques were evolved. The development of a duplex billet was a significant accomplishment that was necessitated by the state of the art of existing drawbench equipment. Thin-walled tungsten tubing could be produced with minimal change in internal diameter by jacketing sections of as-extruded tube shells with molybdenum and extruding the resulting duplex billet over a floating mandrel. The billet design is shown schematically in Fig. V-1. After extrusion the molybdenum jacket is leached from the thin-walled tungsten tube, and the tube can then be finish-drawn to final size. When the inner jacket was omitted, the tungsten tube shell was deformed directly against the mandrel, and thus the tubing surfaces were improved, and a wrought microstructure was produced.

Another development was concerned with the base-metal-oxide lubrication technique. In this technique the volatile tungsten oxide (molybdenum oxide in the case of the duplex billet) formed during transfer of the billet in air from the furnace to the container serves as an adequate lubricant during extrusion.

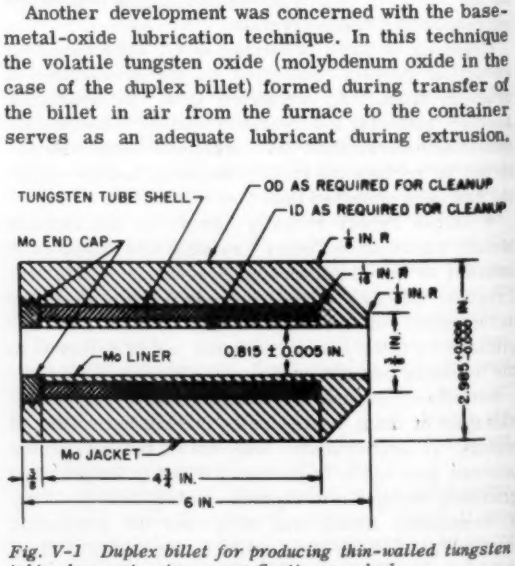

Fig. V-1 Duplex billet for producing thin-walled tungsten tubing by reextrusion over a floating mandrel.

Because the oxide formed on the W–Re–Mo alloy did not provide satisfactory lubrication, a layer of unalloyed tungsten was thermochemically deposited on billet surfaces prior to extrusion. On subsequent operations the oxide-forming tungsten film protected the base metal and provided the desired lubricating film. The application of thermochemically deposited coatings to refractory-metal billets is a significant development in extrusion lubrication since niobium and tantalum billets can be similarly coated.

Submicron unalloyed tungsten powders were consolidated by Livermore[25] using a belt-type high-pressure apparatus. In a survey of the densification capabilities of this apparatus, pressures from 22 to 85 kbars were used. Consolidation temperatures were limited to those up to 1000°C. Measured densities indicated that virtually full densification was obtained within 10 min under 30-kbar pressure at 500 and 1000°C. Mean grain diameter for as-consolidated material was 0.68 μ. Some crack-free compacts with densities greater than 90% of theoretical were obtained.

The characteristics and behavior of porous structures formed from spherical tungsten powders were studied at Thompson Ramo Wooldridge.[26] A near-isostatic powder-compaction technique was developed, and porous compacts exhibiting uniform porosity parameters were prepared. Sintering rates, porosity parameters, permeability, and mechanical-strength data were reported for a series of compacts prepared from six separate size ranges of spherical tungsten particles.

Investigators here and abroad are giving consideration to the development of fabrication techniques and property evaluations for dispersion-strengthened materials. A thorough study of sintered aluminum products (SAP) is being conducted by Oak Ridge[24] to determine the material and processing parameters necessary to produce a desired end product consistently and economically. The evaluation approach is delineated in the flow sheet shown in Fig. V-2. Aluminum flake was compacted to greater than 95% of theoretical density by methods involving hot or cold pressing, and rods measuring 2 in. in diameter were fabricated with existing extrusion facilities. Atomized powders were characterized as chill castings of very fine structure. Controlled oxidation of these atomized particles was difficult because all commercially atomized powder has a very large amount of extremely fine particles (< 1 μ in diameter) that readily convert to oxide. It was demonstrated that SAP materials never exhibit a cold-worked structure in the same manner as the flake input material. Consequently it was concluded that the tensile strength of SAP does not result from the oxide stabilizing a cold-worked structure in aluminum to high temperatures.

Italian investigators[27] have studied the powder metallurgy of SAP materials for nuclear applications.

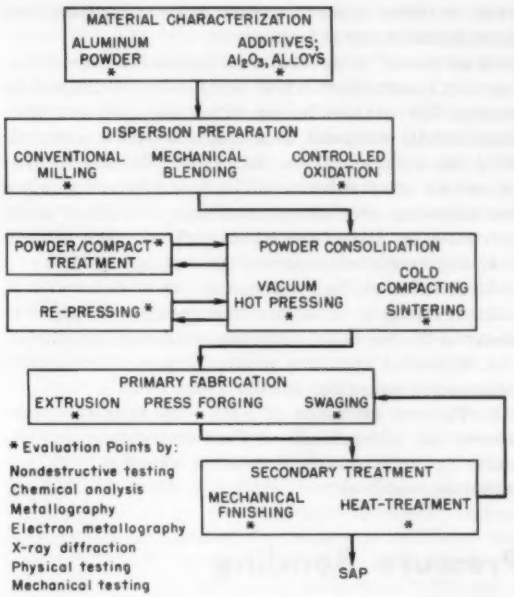

Fig. V-2 Flow sheet for sintered aluminum products.[24]

Results of work on thermally stable structural materials, improvement of the quality of the starting powder, development of methods for fabrication of straight-finned tubes, and elimination of metallic impurities were reported. The structure of SAP was analyzed, and a summary was given of a theory concerning the influence of temperature and strain rate on mechanical properties.

Danish investigators[28] at Risø have evaluated dispersion-strengthened aluminum products. Aluminum and a dispersed phase, namely, Al_2O_3, were considered. Products were manufactured from three different starting materials: aluminum powder covered with the natural layer of Al_2O_3, high-temperature oxidized aluminum, and aluminum blended with Al_2O_3 powder. The following conclusions were drawn:

1. The final structure of the composite was determined by the extrusion technique.
2. Changes in mechanical properties were related to structural changes.
3. The microstructures of extruded $Al-Al_2O_3$ products consisted of an oxide phase finely dispersed in aluminum, containing a substructure of fine grains.
4. In a comparison of the tensile and creep properties of the powder-blended products and commercial SAP, it was found that the powder-blended products have superior creep ductility.

British investigators[29] have prepared oxide-base cermets by infiltration with silver and silver alloys. The aspects covered are infiltration criteria, the dispersion-strengthening and interlocking-network models, refinement of alumina-base cermets, exten-

sion to other oxides, metallographic studies, and selected mechanical tests.

A program[30] to develop a technique for hot-extruding MgO and other oxide bodies was conducted by Boeing. Hot-pressed billets of varying diameter were successfully extruded in a common jacket material. Only the smallest (1-in. diameter) billets were free of cracks after extrusion. The investigators reached the following conclusions concerning the effect of hot extrusion on properties of hot-pressed oxide billets:

1. Hot extrusion improves the strength of MgO.
2. Crack-free MgO extrusions can be obtained.
3. Cracking is due either to excessive cooling or to shear in the ceramic, with data indicating the former.
4. Extruded MgO has residual stress. This can be removed by annealing at 1200°C for 1 hr.
5. The hot extrusion of ZrO_2 (CaO stabilized) improves the homogeneity of CaO distribution and results in little contamination or reaction with the jacketing material.

(C. A. MacMillan)

Pressure Bonding

Oak Ridge[31] has examined fabrication costs of clad-uranium-metal fuel tubes by coextrusion and pressure-bonding techniques. Both zirconium-clad and aluminum-clad elements were considered in this comparison. It was found that processing 5000 or 37,500 zirconium-clad tubes by pressure bonding was more economical than by coextrusion. However, coextrusion was indicated to be less expensive for processing 125,000 tubes. If aluminum cladding is used in place of zirconium (a long-range possibility for further cost reduction), pressure bonding is the preferred fabrication technique. The pressure-bonding process and equipment require only minor modifications to accommodate aluminum-clad elements, whereas coextrusion would require extensive process changes.

Solid-phase bonding of TD nickel by four approaches has been investigated at General Electric.[32] These methods included resistance diffusion bonding, deadweight loading at elevated temperatures, differential-thermal-expansion-die bonding, and vacuum hot pressing. The resistance-diffusion-bonding study utilized the heating and pressure produced by a Taylor Winfield 50-kva weld machine. Parameters were adjusted to avoid interface melting. The deadweight approach provided a pressure of approximately 20 psi at test temperatures of 2000 to 2400°F (1093 to 1316°C). The molybdenum-die-bonding method was used at 2000°F (1093°C) and provided a pressure estimated at 9000 psi. Vacuum-hot-pressing conditions consisted of 0.75 to 1.5 hr at 2000°F (1093°C), with pressures ranging from 9300 to 12,000 psi. With the exception of the deadweight-bonded specimens, good joint efficiency was obtained in room-temperature tensile tests. At elevated temperatures, however, low shear strengths and a tendency of the material to delaminate were observed. Of the diffusion-bonding methods studied, the resistance method was selected for a more detailed investigation. This technique is also being studied as a method for bonding TD-nickel chromium.[33]

(S. W. Porembka)

Plating

Nonelectrolytic Chemical Plating

A summary of the literature relating to the deposition of molybdenum, tungsten, or rhenium from the carbonyls or the halides has been published by Battelle–Frankfurt.[34] Details of deposition conditions and a summary of the results of a number of processes are given.

Workers at Oak Ridge[24] are continuing their study of vapor-deposited tungsten and tungsten-alloy shapes for high-temperature reactor components. Tungsten sheet in thicknesses up to 145 mils has been formed by hydrogen reduction of WF_6. Uniformity of thickness was obtained by the use of a multiple-heating-zone furnace in which deposition conditions were as follows:

Hydrogen-gas flow	300 cm^3/min
WF_6-gas flow	200 cm^3/min
Chamber pressure	5 torrs
Chamber temperatures	
Zone 1 (inlet)	585°C
Zone 2	540°C
Zone 3	530°C
Zone 4	560°C
Zone 5	595°C

An average deposition rate of 3.5 mils/hr was observed at an efficiency of 70%.

Insight concerning the mechanism of the formation of nodular growths often observed in vapor-deposited tungsten was sought in a series of experiments relating grain morphology to deposition parameters. Air contamination and deposition temperatures above 740°C were found to produce nodular growth, whereas mass flow and velocity variation did not. A statistical program was established to study in detail the effects of temperature, pressure, and flow rate on deposition rate and deposit morphology. A total of 81 separate experiments have been performed and are being analyzed.

Tungsten–rhenium alloy vapor deposition is being examined as an alternative fabrication method for refractory-metal cladding. The work reported was directed toward improvement of the compositional uniformity of the deposits. Improvement was obtained at higher temperatures (700 to 1000°C) in an apparatus providing for the WF_6–ReF_6 to be injected directly into the hot zone. Deposition of W–25 wt.% Re on $\frac{5}{8}$-in.-ID tubular steel mandrels with a moving injector gave a smooth textured deposit with an axial

rhenium-content variation of ±1%. This technique was also applied to produce W–Re alloy sheet for mechanical-property evaluation.[35] However, sufficient uniformity of deposit thickness has not been obtained.

Russian workers detected the existence of two morphological transition temperatures in molybdenum and tungsten deposited by pyrolysis of the carbonyls.[36] The structure of the metal deposits was studied by X-ray diffraction and particle-size analysis. The transition temperatures are 250 and 750°C for molybdenum and 350 and 800°C for tungsten. The lower transition temperature is related to the breaking of the bonds in the carbonyl molecule, and the higher, to condensation from supercooled liquid or to formation of crystal nuclei.

The use of electroless-nickel coatings to protect 6061 aluminum against oxidation was further evaluated by workers at Phillips.[37] The purpose was to prevent the buildup of thermally insulating oxide films 1 or 2 mils thick on the aluminum-clad fuel-plate surface. The nickel was deposited in thicknesses of 0.8 ± 0.1 mil from commercial electroless-nickel-plating solutions (Enplate 410-A and 410-B). The effects of various heat-treatments on the nickel-coated aluminum were evaluated by means of metallographic examination and by corrosion tests, as discussed in Sec. IV under the subheading "Corrosion."

Studies at Sandia are reported in which hydrazine is used as the reducing agent in an electroless-nickel-plating process.[38] The objective was to circumvent the embrittlement caused by codeposition of phosphorus from the hypophosphite compounds commonly used as reducing agents. Deposits up to 10 mils thick with 99% purity were obtained. The structure was extremely fine grained. Ductility of the as-deposited nickel was poor but improved markedly on heat-treatment at 760°C. Corrosion resistance was inferior to that of deposits produced by hypophosphite reduction.

The optimum formulation was reported to be

Nickel acetate	60 g/liter
Glycolic acid	60 g/liter
Tetrasodium ethylenediamine-tetraacetic acid	25 g/liter
Hydrazine	100 ml/liter

The optimum bath operating conditions were reported to be a temperature of 90°C and a *p*H of 11.0, although higher values were apparently not studied.

(E. H. Hall)

Electroplating

Precision counting for alpha sources was observed[39] for ^{239}Pu and other actinides electrodeposited rapidly (as oxides or salts) in isopropanol solutions. With a mechanically stirred solution, a rotating cathode, and a cathode current density of 10 ma/cm² (500 volts), over 99% of the plutonium was deposited in only 10 min on nickel-plated stainless-steel cathodes. The isopropanol increased the tolerance of iron and aluminum in the electrolyte to >100 μg. Contamination with organic phosphates did not reduce the yield, nor did common organic diluents. Rubbing the films with moist or dry filter paper caused an almost negligible change in alpha count, indicating that the films had good adherence. The deposition rate in isopropanol solutions was faster than the rate reported previously[40] for electrodeposition of actinides in ethanol solutions.

Researchers in Austria and Russia reported deposition conditions for uranium in aqueous, nonalcoholic electrolytes. Deposition in an ammonium oxalate solution was rapid, but the solution *p*H was critical for preventing loose black deposits.[41] With an ammonium fluoride electrolyte, the rate of deposition was relatively slow and depended on the ammonium fluoride concentration, the solution *p*H, and the rate of rotating the platinum anode.[42]

When 0.004-in.-diameter boron filaments were incorporated in an electroformed aluminum matrix, the tensile strength of the aluminum specimen was increased 250%, from 14,000 to 36,000 psi (Ref. 43). The modulus was increased 100%, from 7,500,000 to 14,000,000 psi. The addition of 15 vol.% tungsten filaments in electroformed nickel improved the strength 30% and increased the cyclic life from 900,000 to 17,000,000 cycles (stress not given). The development appears applicable to improvements for electroforming pressure vessels, cladding fuel elements, and other uses for electrodeposited metals.

(W. H. Safranek)

Explosive Metalworking

The pneumatic-impaction technique was employed at Battelle–Northwest[44] to fabricate tungsten–uranium dioxide cermet fuels into honeycomb configurations. By suitable selection of billet preheat, impaction pressure, and postheat conditions, crack-free structures were obtained with >99% of theoretical density. Ninety-two percent of the honeycomb webs of representative grids were maintained within 0.003 in. of nominal thickness. Part of the dimensional control variation was believed to result from the specified radial gradation of UO_2 content from 30 vol.% at the center of the part to 10 vol.% at the periphery. Since this gradation was achieved by varying the thickness of the vapor-deposited tungsten layer on the initial oxide spheres, the differential in compressibility between the two components impaired dimensional control.

Japanese investigators at Mitsubishi Atomic Power Industry, Inc.,[45a] have been engaged in basic studies of the effects of high-energy-rate impaction on ceramic fuels (UO_2, UC, and UN). Various material combinations that contained UO_2 single crystals, green-pressed pellets of UO_2, and mixtures of Sm_2O_3–

UO_2 and ThO_2-UO_2 suspended in an Al_2O_3 matrix powder were impacted with a Dynapak at 1100°C, applying 290,000 to 435,000 psi for 0.1-sec periods. In each case the resulting samples were evaluated for bonding between samples, evidence of chemical reaction at interfaces, and deformation of the samples. Several of the important conclusions were:

1. Extensive plastic deformation of UO_2 single crystals occurs under these conditions, accompanied by "slight to moderate fracturing." The strain produced is related to pressure gradients within the compact, and not to the crystallographic orientation of the various specimens. Both slip and twin bands were noted after impaction.

2. Pressure is transmitted nonuniformly within the compact.

3. The matrix powder is compacted to a uniform density of greater than 95% of the theoretical, with no apparent density gradients.

4. Bonding is improved by excess oxygen and the presence of an oxide additive compound. Single crystals of UO_2 in contact bonded poorly to each other, whereas a mixture of $UO_{2.08}-20\%$ Sm_2O_3 green-pressed powder bonded well to a UO_2 crystal. Although ThO_2 and Sm_2O_3 improved bond quality, electron-microprobe analysis showed no evidence of their diffusion into the pressed UO_2 powder, UO_2 single crystals, or within the mixed-oxide pellets.

The authors concluded that impaction deforms and densifies individual particles, and thus the intimate surface contact needed for bonding is produced. Bond quality was found to depend on excess oxygen, impurity content, and temperature.

Several studies at Mitsubishi[45b] were directed to the synthesis of uranium compounds by Dynapak impaction. The results of this work are summarized as follows:

Compound formed	Pressure, psi	Temperature, °C
U_2S_2 (approximate), hexagonal a = 3.837 A c = 6.582 A c/a = 1.716	290,000	1000
UP, hexagonal a = 3.800 A c = 6.521 A c/a = 1.716	290,000	1000

Equation-of-state data, useful in the design of contact explosive metalworking processes (i.e., explosive powder compaction, shock hardening, and explosive welding), have been tabulated by Van Thiel at Lawrence Radiation Laboratory.[46] This compendium can be used in conjunction with a previous publication of the U. S. Naval Ordnance Test Station.[47] The two differ in that the former source presents estimates of experimental error in the Hugoniot data, whereas the latter considers shock temperatures in the various materials. (H. S. Gurev)

Joining

Nickel Alloys

In a study[48] to determine the effect of welding on the tensile properties of Alloy 718 (50 to 55 wt.% Ni–17 to 21 wt.% Cr–4.5 to 5.75 wt.% Nb–2.8 to 3.3 wt.% Mo, balance Fe), simulated weld thermal cycles for two heat-treatment conditions were made on 0.75-in. plate. The peak temperatures were 2150 and 2300°F (1177 and 1260°C). The results are shown in Table V-2. It was concluded from these data that alloy 718 is not degraded by short-time exposures to 2150°F, but at 2300°F microcracks and incipient melting greatly reduce strength and ductility.

Recent work on Alloy 718 at NASA[49] indicates that better properties are obtained if welds are solution treated at 1800°F (982°C) rather than at the usually recommended 1950°F (1066°C). Apparently a direct relation can be shown between temperature and microfissuring in the weldment.

The repair-welding characteristics of Alloy 718 were examined by North American researchers.[50] Conclusions based on tungsten–inert-gas (TIG) welds on 0.25-in. plate using Alloy 718 filler were:

1. Repairs can be made in either the solution-annealed or the aged condition.

2. Repairs should not be left in the as-welded condition.

3. Direct aging after repairing seriously reduces ductility.

4. Alloy 718 filler is preferred for repair welding.

The properties of the repaired welds are compared with base-metal properties in Fig. V-3.

Table V-2 AVERAGE ROOM-TEMPERATURE TENSILE PROPERTIES OF ALLOY 718 PLATE EXPOSED TO SIMULATED WELD THERMAL CYCLES[48]

Peak temperature exposure, °F	Heat-treatment	Yield strength (0.2% offset), 1000 psi	Ultimate tensile strength, 1000 psi	Elongation, %	
				In 1 in.	In 0.5 in.
2300	Anneal and age*	168.8	177.9	7.5	8.5
2150	Anneal and age*	172.4	198.1	15.5	23.0
2300	Direct age†	153.5	175.2	7.0	9.0
2150	Direct age†	171.8	196.7	13.0	16.5

*1950°F for 1 hr; AC + 1400°F for 10 hr, FC to 1200°F, and hold for total age cycle of 20 hr.
†1400°F for 10 hr; FC to 1200°F and hold for total age cycle of 20 hr.

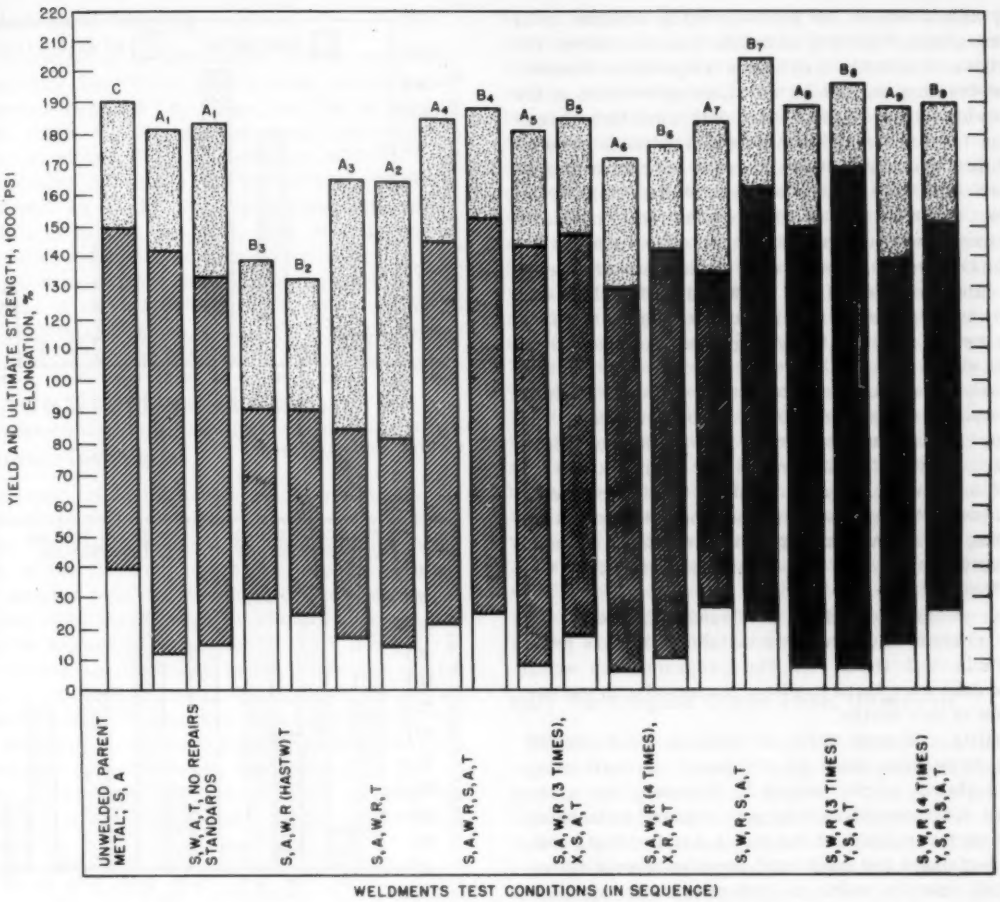

Fig. V-3 Mechanical properties of Alloy 718 weldments and repaired weldments.[50] A, *50% of weld repair;* B, *100% of weld replaced by repair;* C, *unwelded parent metal.* ▭, *elongation (%);* ▨, *tensile yield strength (1000 psi);* ▩, *ultimate tensile strength (1000 psi).*

KEY TO TEST CONDITIONS

S = solution anneal	X = solution anneal and age between repairs
A = age	Y = no thermal treatment between repairs
W = weld	T = test
R = repair weld	

At Battelle–Northwest the effect of aging on dissimilar-alloy welded joints in Hastelloy X, X-280, Haynes 25, and 316 stainless steel was studied.[51] Exposures for 500 and 1000 hr at 1000, 1200, 1400, and 1600°F (540, 650, 760, and 870°C) indicate that Hastelloy W-filler welded joints lose significantly less ductility than joints made with Hastelloy X filler.

Niobium

For convenience, refractory-metal alloys discussed in this subsection are referred to by their commercial designations. Representative compositions (wt.%) are as follows:

B-66: Nb–5 V–5 Mo–1 Zr
D-43: Nb–10 W–1 Zr–0.1 C
C-129Y: Nb–10 Ta–10 Hf–0.1 Y
D-36: Nb–10 Ti–5 Zr
FS-85: Nb–28 Ta–10 W–1 Zr
Cb-752: Nb–10 W–2.5 Zr
FS-82: Nb–34 Ta–0.75 Zr
F-48: Nb–15 W–5 Mo–1 Zr–0.1 C
D-31: Nb–10 Mo–10 Ti
T-111: Na–8 W–2 Hf

General Electric has completed a program on the stability of welds in niobium alloys.[52] The effects of oxygen and nitrogen on postweld aging and bend-transition behavior were determined for alloys B-66, D-43, and C-129Y. Both TIG and electron-beam welds were used. In general, increased quantities of the interstitial elements nitrogen and oxygen substantially reduced as-welded ductility but produced

only minor effects on postweld aging kinetics in all three alloys. Nitrogen additions caused greater reductions in ductility than oxygen in equivalent amounts. Heat-treating studies on uncontaminated welds of the three alloys were conducted to determine those overaging treatments which would yield optimum thermal stability. As a result, welds were successfully produced that were ductile at room temperature, even after exposure to reaging cycles that normally produced maximum embrittlement without prior overaging treatments. The possible occurrence of delayed cracking in welds of the B-66 and D-43 alloys was also investigated. It was noted that delayed cracking may be encountered in hydrogen-contaminated D-43 alloy welds.

Gerken has also reported on an extensive study of the welding characteristics of niobium alloys.[53] The major effort was devoted to TIG welding of alloys D-36, FS-85, Cb-752, and B-66 in the 0.020- to 0.060-in. thickness range. Many of the data collected are presented graphically and show the effect of welding parameters and aging treatments on the bend ductility. Other data are summarized in Figs. V-4 and V-5.

The welding conditions developed at Oak Ridge for four niobium alloys and one tantalum alloy are given in Table V-3 (Ref. 54). The program from which these data were taken has been discussed in an earlier review in this series.

Quality roll-spot welds in 0.012-in.-thick Cb-752 alloy have been made at McDonnell Aircraft using silver-plated copper wheels.[55] However, the electrodes deteriorated rapidly and required redressing after each revolution of the wheel. Limited tests with silver-rimmed and infiltrated-tungsten wheels did not produce quality welds as determined by metallographic examination. Niobium alloys FS-85 and Cb-752 of 0.001-in.-foil thickness were spot welded using copper, tungsten-tipped, and molybdenum-tipped electrodes.[56] The highest quality welds were made with the molybdenum-tipped electrodes. Welds having an average nugget diameter of 0.007 in. in FS-85 alloy had an average lap–shear strength of 4.8 lb; 0.005-in.-diameter nuggets in Cb-752 alloy had a lap–shear strength of 4.0 lb. Problems concerning electrode pickup and foil thicknesses were encountered.

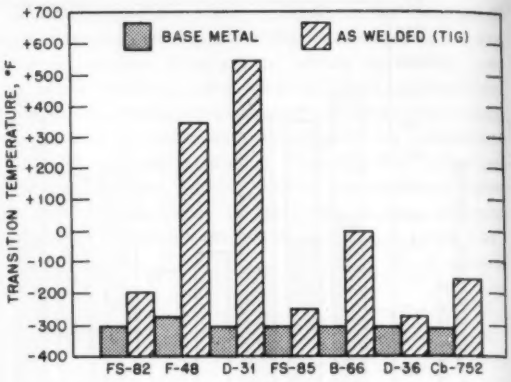

Fig. V-4 Ductile-to-brittle transition temperatures of several niobium alloys.[53]

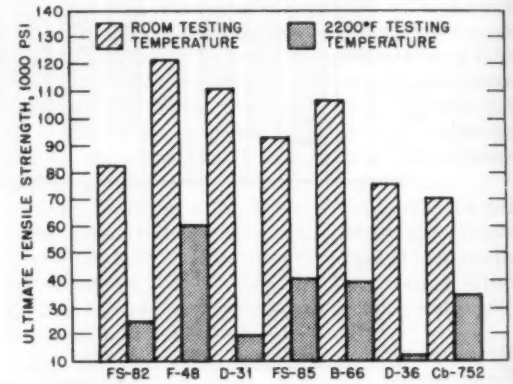

Fig. V-5 Ultimate tensile strengths of several welded niobium alloys.[53]

Table V-3 WELDING CONDITIONS FOR REFRACTORY-ALLOY SHEET SPECIMENS[54]

Alloy	Thickness, in.	Automatic gas–tungsten arc (argon gas)			Manual gas–tungsten arc (argon gas)		Electron beam		
		Welding speed, in./min	Welding current, amp	Arc voltage, volts	Welding speed, in./min	Welding current, amp	Welding speed, in./min	Welding current, ma	Voltage, kv
D-43	0.060	15	210–240	9					
	0.060	10	200–240	9	~3	140–150	30	6.5	130
	0.040	10	145–150	9	~6	~100	30	4.5	130
	0.475				4–6	310–400			
B-66	0.060	10	190–240	9	~3	140–150	30	4.5	130
	0.545				4–6	310–380			
FS-85	0.050	10	165–175	9	~4	155–180	30	5.0	130
	0.490				4–6				
C-129Y	0.030	10	70–100	7	~6	~80	30	3.5	130
T-111	0.060	10	245–260	9	~3	190–220	30	6.8	120
	0.515				4–6	310–400			

Stainless-Steel Brazing

An investigation of alternatives for the expensive Cu–Au alloy filler metal used in large rocket-engine components revealed two alloys that can be used to reduce costs significantly on large structures.[57] Aerojet-developed alloys AGC-200 and AGC-201 have a gold content 57% lower than that of the commercial Cu–35 wt.% Au–3 wt.% Ni alloy, and they offer a 50% reduction in filler-metal cost. Both AGC alloys are of the solid-solution type, and no secondary phases or phase changes were encountered. Both alloys have a liquidus at about 1930°F (1055°C) and are used at about 1970°F (1075°C). (R. M. Evans)

Nondestructive Testing

Ultrasonic Techniques

The length of an ultrasonic pulse is controlled by the electrical signal supplied by the electronic driver and by the characteristics of the transducer. The length of the electrical signal can usually be made much shorter than that to which the transducer can respond; thus the transducer usually controls how short the ultrasonic pulse may be. Very short ultrasonic pulses are desirable in nondestructive testing for good resolution. This is accomplished by backing the piezoelectric element with damping material. The best condition is obtained when the backing material is matched acoustically to the element so that no energy is reflected from the interface and when the absorption of the energy within the backing material is complete.

Argonne[23,58,59] researchers have investigated various backing materials for piezoelectric elements. Two materials that appear to provide good acoustical matching with the elements are Fiberglas-loaded epoxy and 65.5% sintered nickel. A 30° cone added to the opposite end of the sintered nickel increases the attenuation by increasing the path length of the unabsorbed energy by scattering. The cone is not necessary with a 1.27-cm-long Fiberglas-loaded epoxy transducer operating at 5 Mc and higher.

Dutch investigators[60] have conducted noteworthy studies relative to inspecting welds in heavy steel plates having thicknesses of 100, 200, and 300 mm. Factors influencing flaw detectability are (1) surface condition, (2) the condition of the parent metal, and (3) the size, position, and orientation of defects. Surface roughness was found to affect the acoustic coupling and thus cause beam distortion. Laminar flaws in the thick plate which occurred in the vicinity of the weld obscured the image of the internal weld condition. The position, orientation, size, and width (i.e., the distance that the defect is "open" in the direction of wave propagation) of defects have a combined effect on detectability. In one case very small defects (5 mm) were found in welds up to 300 mm thick, whereas in other cases the detection of gross defects in thinner sections called for special techniques. The Dutch investigators recommend scanning with a low-frequency (2 Mc) fairly wide ultrasonic beam to locate the defect, followed by a narrow beam of high frequency to identify the defect.

Unexpected deviations in wave refraction may be caused by surface irregularities, and these deviations can lead to errors in defect location. Weld ripples may cause mode conversion and irrelevant indications. A planar defect such as lack of fusion can be readily detected, provided the pulse can strike it nearly at right angles. The width of a defect also influences its detectability. Deviations of more than 7° from the normal are generally sufficient to lose trace of the flaw echo signal, but this angle depends also on the smoothness of the reflecting surface and its size. Under these conditions detectability decreases with the size of such a defect because the beam spread of the reflected signal is reduced. Its influence becomes more pronounced with increasing material thickness, and here, because of the usual angle of weld preparation, lack of side fusion is most unfavorably oriented. A solution to this problem is the use of a special scanning technique whereby two probes are used in tandem. (D. Ensminger)

NDT Techniques Other Than Ultrasonic

Further improvement of sensitivity has been achieved in the neutron image-intensification system being developed at Argonne.[22] An objective is to realize neutron radiography with nonreactor neutron sources. The successful development of such a nonreactor system appears to offer many new industrial-inspection applications (in the fields of liquids, plastics, etc.) for many nonmetal materials that might not otherwise be observable by methods such as X ray because of intervening metals. Applications are also visualized in the field of neutron-diffraction measurements.

For direct visual observation of the neutron image at the output phosphor of the intensifier tube, the minimum observable signal-to-noise ratio is 3 for the required signal accumulation time of about 0.2 sec. The number of neutrons contributing to the image is 15% of those incident on the intensifier tube, allowing 50% absorption in the intensifier-tube window and 30% absorption in the neutron scintillator. Considerable improvement of sensitivity could be realized if the various points of absorption could be eliminated or improved.

Measurements conducted to determine the low-threshold neutron intensities observable on a television presentation indicated a 100× improvement in low-level detection by means of an image-orthicon system. Neutron intensities as low as 2×10^4 neutrons/(cm^2)(sec) were observed with a vidicon system and an improved neutron image-intensifier tube.

Image-orthicon tests with a 5-cm, f/0.95 lens illustrated that television brightening could be observed for neutron intensities as low as 200 neutrons/(cm^2)(sec). The television image of a cadmium test object approximately 2 by 4 cm was detectable for neutron intensities as low as 1000 neutrons/(cm^2)(sec). It was concluded that the neutron image intensifier is providing a brightness gain of 2×10^4, which is reasonably in line with brightness gains available from X-ray image-intensifier tubes.

The pulsed eddy-current inspection system that has been in use for some time at Argonne continues to serve well for inspection of tubing integrity and thickness of metal cladding.[61] A mask-aperture assembly serves to restrict the extent of the magnetic field created by the driving coil, so that a defect will tend to have a greater effect on pickup-signal amplitude than otherwise. It appears that the differential-pickup-coil approach is used for tubing; thus gradual effects that are normal will affect both pickup coils equally and tend to cancel. The investigators noted that with the mask-aperture system the signal voltage induced in each of the two pickups is so strongly influenced by the counterinduced current flowing in the test specimen that it is not necessary to use any bridge or bucking voltage.

On the basis of a knowledge of the speed of inspection, the electronic measuring equipment can be arranged to discriminate against random signals. Further discrimination and separation of inside- and outside-diameter defects in tubing is obtained by arranging time gating to take advantage of the finite time required for induced-current diffusion into the test object. More detail on the theory and operation of the mask-aperture assemblies and sampling will be given in Report ANL-7172. (A. F. Leatherman)

References

1. G. W. Gibson and M. Zukor, Development and Fabrication of Fuel Materials, USAEC Report IDO-17154, Phillips Petroleum Company, February 1966.
2. W. Duerrschnable, On the Continuous Casting of Aluminum-Uranium Alloys, *Z. Metallk.*, 57: 451-454 (June 1966).
3. C. H. Bloomster, Preparation of Neptunium-Aluminum Alloy Target Elements, USAEC Report BNWL-311, Battelle–Northwest, October 1966.
4. G. Ervin, Jr., A. K. Smally, and H. Nadler, Control of Stoichiometry in the Growth of Crystals of Uranium Monocarbide, *Mater. Res. Bull.*, 1: 151-159 (November 1966).
5. W. R. Witzke, Effect of Alloying on Grain Refinement of Electron-Beam-Melted Tungsten, Report NASA-TN-D-3531, National Aeronautics and Space Administration, Lewis Research Center, July 1966.
6. L. E. Al'Shevskii and Yu. S. Kuz'michev, Effect of Ultrasound on the Ductility of High-Boron Stainless Steels, *At. Energ. (USSR)*, 20: 440-442 (May 1966).
7. H. L. Prekel and A. Lawley, Innovations in Electron-Beam Zone Refining of Molybdenum, Report AED-CONF-66-119-4, 1966.
8. R. E. Reed, Electron Beam Floating Zone Refining of Niobium, USAEC Report ORNL-P-2108, Oak Ridge National Laboratory, April 1966.
9. W. R. Burt, Jr., W. C. Kramer, F. J. Karasek, and R. M. Mayfield, Improvements in Consolidation and Fabrication of Vanadium-20 Wt.% Titanium, USAEC Report ANL-7127, Argonne National Laboratory, May 1966.
10. D. Mills and G. B. Graig, Redistribution of Oxygen and Iron During Zone Refining of Zirconium, *Trans. Met. Soc. AIME*, 236: 1228-1229 (August 1966).
11. J. G. Kura, V. D. Barth, and H. O. McIntire, The Casting and Powder-Metallurgy Forming of Precipitation-Hardenable Stainless Steels, Report NASA-TM-X-53444, Battelle Memorial Institute, Apr. 20, 1966.
12. D. E. Strohecker, T. G. Byrer, A. F. Gerds, J. H. Gehrke, and F. W. Boulger, Deformation Processing of Nickel-Base and Cobalt-Base Alloys, Report NASA-TM-X-53439(N66-23857), Battelle Memorial Institute, Apr. 18, 1966.
13. H. H. Klepfer and R. E. Blood, Specific Zirconium Alloy Design Program, USAEC Report GEAP-5134, Vallecitos Atomic Laboratory, April 1966.
14. W. Timmermans, Hot Drawing of Thin-Walled Zircaloy-2 Tubes, *Metallurgie (Mons. Belg.)*, 2: 43-48 (1964).
15. Ames Laboratory, Annual Summary Research Report of Chemistry, Engineering, Metallurgy, Physics, and Reactor Divisions, July 1, 1965–June 30, 1966, USAEC Report IS-1500, July 1966.
16. C. V. Owen, T. E. Scott, and O. N. Carlson, Pneumatic-Mechanical High-Energy-Rate Extrusion of Yttrium, USAEC Report IS-1227, Ames Laboratory, August 1965.
17. C. V. Owen, T. E. Scott, and O. N. Carlson, Extrusion of Clad and Unclad Yttrium for Rod and Tubing, USAEC Report IS-1031, Ames Laboratory, August 1965.
18. O. N. Carlson, L. L. Sherwood, and F. A. Schmidt, The Effect of Composition, Crystalline Condition, and Thermal History on the Bend Transition Temperatures of Chromium Alloys, *Amer. Soc. Metals, Trans. Quart.*, 58: 403 (1965).
19. L. L. Nelson, Improved Service Life of 15-Kg Reduction Reactor Vessels, USAEC Report RFP-741, Dow Chemical Co., Rocky Flats Division, June 6, 1966.
20. F. C. Holden and F. W. Boulger, Fifth Status Report of the U. S. Government Metalworking Processes and Equipment Program, DMIC-Report-225, Battelle Memorial Institute, Defense Metals Information Center, June 10, 1966.
21. H. H. Hausner (Ed.), Modern Developments in Powder Metallurgy, Vol. 3, Development and Future Prospects, Report CONF-650631, 1965.
22. W. D. Wilkinson (Ed.), Fuels and Materials Development Program Quarterly Progress Report for Period Ending September 30, 1966, Argonne National Laboratory.
23. General Electric Company, Nuclear Materials and Propulsion Operation, High-Temperature Materials Program Progress Report No. 61, USAEC Report GEMP-61, Sept. 30, 1966.
24. S. Peterson (Comp. and Ed.), Metals and Ceramics Division Annual Progress Report for Period Ending June 30, 1966, USAEC Report ORNL-3970, Oak Ridge National Laboratory, October 1966.
25. G. E. Zima and J. F. Lakner, High-Pressure Consolidation of Submicron Tungsten, USAEC Report UCRL-14502(Rev. 1), University of California, Lawrence Radiation Laboratory, Nov. 9, 1965.
26. M. E. Kirkpatrick and R. A. Mendelson, Investigation of Porous Tungsten Formed from Spherical Tungsten Powders, *Int. J. Powder Met.*, 2(3): 35-44 (July 1966).
27. P. Jehenson, Powder Metallurgy of Al-Al_2O_3 Composites (SAP) for Nuclear Applications, Report CONF-650631-4, 1965.
28. N. Hansen, Dispersion-Strengthened Aluminum Products, Danish Report RISO-113 (CONF-660915-1), May 1966.

29. L. S. Williams, Infiltrated Oxide Cermets, in *Special Ceramics 1964*, P. Popper (Ed.), pp. 147-165, Academic Press, London, 1965.
30. Boeing Co., Identifying Optimum Parameters of Hot Extrusion, Progress Report No. 7, October 12, 1965–January 14, 1966, Report NASA-CR-71016(N66-20141).
31. R. J. Beaver, Estimated Large-Scale Production Costs for Cladding Uranium Metal Fuel Tubes, USAEC Report ORNL-TM-596, Oak Ridge National Laboratory, November 1966.
32. R. E. Yount, R. E. Kutchera, and D. L. Keller, Development of Joining Techniques for TD Nickel, Report AFML-TR-66-137, General Electric Company, May 1966.
33. R. E. Yount, Development of Joining Techniques for TD Nickel Chromium, Interim Progress Report 2-8-211A, April–July 1966, General Electric Company.
34. M. Kadner, Literature Search on the Deposition of Layers of Molybdenum, Tungsten, and Rhenium by Thermal Decomposition of Their Carbonyls or Reduction of Their Gaseous Halides, Report BMWF-FBK-66-09, Battelle–Frankfurt, April 1966.
35. P. Patriarca (Comp.), Oak Ridge National Laboratory, unpublished, December 1966.
36. N. Matyushenko, A. Rozen, and V. Sagalovich, Morphology and Texture of Molybdenum and Tungsten Carbonyl Deposits, *Fiz. Metal. Metalloved.*, 21: 403-408 (March 1966).
37. Phillips Petroleum Company, Nuclear Technology Branches Quarterly Report, January 1–March 31, 1966, USAEC Report IDO-17192, August 1966.
38. J. Dini and P. R. Coronado, Thick Nickel Deposits of High Purity by Electroless Methods, USAEC Report SCL-DC-66-22, Sandia Corp., June 1966.
39. M. Y. Donnan and E. K. Dukes, Quantitative Electrodeposition of Actinides from Isopropyl Alcohol, USAEC Report DP-1048, Savannah River Laboratory, August 1966.
40. S. M. Kim, J. E. Noakes, L. K. Akers, and W. W. Miller, Electrodeposition of Actinides and Lanthanides, USAEC Report ORINS-48, Oak Ridge Institute of Nuclear Studies, Inc., Dec. 15, 1965.
41. V. S. Roslyakov and M. P. Ezhova, Electrodeposition of Small Amounts of Uranium from Solutions, *Radiokhimiya*, 7(5): 625-627 (1965).
42. V. Pfeifer and H. Bildstein, Electrodeposition of Uranium on Metals, *Ichnoanal Acta*, 5–6: 822-829 (1965).
43. J. F. Judge, EOS Probes Electrodeposited Composite Structures Market, *Technol. Week*, 19(20): 26, 31 (Nov. 14, 1966).
44. D. Drumheller and K. R. Sump (Comps.), Fabrication of Tungsten-Uranium Dioxide Honeycomb Fuel Element Structures, Final Report May 1963–July 1965, USAEC Report BNWL-253, Battelle–Northwest, September 1965. (Classified)
45. Japan–U. S. Research Newsletter No. 5, Oxide and Carbide Fuels, October 1966,
    a. J. L. Daniel, Jr., B. Ishi, and S. Takahashi, Basic Studies on Deformation and Bonding Mechanisms of Ceramic Nuclear Fuels During High Energy Rate Impaction, pp. 107-114.
    b. Y. Akimoto, M. Kojima, H. Itoh, and S. Takashashi, The Formation of New Phase in U-S and U-P Systems, p. 125.
46. M. Van Thiel (Ed.), Compendium of Shock Wave Data, USAEC Report UCRL-50108(Vol. 1), University of California, Lawrence Radiation Laboratory, June 1966.
47. J. S. Rinehart (Ed.), Compilation of Dynamic Equation-of-State Data for Solids and Liquids, Report NOTS-TP-3798, U. S. Naval Ordnance Test Station, May 1965.
48. R. D. Betts and R. E. Fish, Room-Temperature Tensile Properties of Inconel 718 Plate Exposed to Simulated Weld Thermal Cycle Conditions, Report MPR 5-175-261, North American Aviation, Inc., June 9, 1966.
49. R. E. Monroe, Battelle Memorial Institute, personal communication, Aug. 12, 1966.
50. R. E. Fish and R. W. Poseley, The Influence of Multiple Weld Repairs on Mechanical Properties of Inconel 718, Report MPR 4-175-462, North American Aviation, Inc., Dec. 11, 1964.
51. D. R. Ireland, The Effects of Aging on Dissimilar-Metal Welded Joints with Multipass Welding of Hastelloy X and Hastelloy W Filler Metal, USAEC Report BNWL-290(Pt. 1), Battelle–Northwest, July 1966.
52. S. R. Tompson, W. R. Young, and W. H. Kearns, Investigation of the Structural Stability of Welds in Columbium Alloys, Report ML-TDR-64210(Pt. 2), General Electric Company, December 1965.
53. J. M. Gerken, Welding Characteristics of Advanced Columbium Alloy, *Welding J. (N. Y.)*, 45(5): 210-s to 226-s (May 1966).
54. R. G. Connelly and G. M. Slaughter, Weldability Evaluation of Advanced Refractory Metals, *Welding J. (N. Y.)*, 45(6): 250-s to 257-s (June 1966).
55. W. J. Nowak, Roll Spot Welding of Columbium-Base Alloys, Final Report 513-367.16, McDonnell Aircraft Corp., Oct. 26, 1965.
56. R. R. Wilar, Resistance Welding of Columbium Alloy Foil, Final Report 513-367.04, McConnell Aircraft Corp., Sept. 23, 1965.
57. K. L. Gustafson, Development and Evaluation of Braze Alloys for Vacuum Furnace Brazing, Report NASA-CR-514, Aerojet-General Corporation, July 1966.
58. Argonne National Laboratory, Reactor Development Program Progress Report, August 1966, USAEC Report ANL-7249, Sept. 23, 1966.
59. Argonne National Laboratory, Reactor Development Program Progress Report, September 1966, USAEC Report ANL-7255, Oct. 26, 1966.
60. A. de Sterke, Ultrasonic Examination of Welded Joints in Steel Plate of Thicknesses Up to 300 MM, USAEC–Euratom Report EURAEC-1695, Roentgen Technische Dienst N. V., Aug. 9, 1966.
61. C. J. Renken, N. P. Lapinski, C. W. Cox, and R. H. Selner, Nondestructive Testing in the Argonne Nuclear Rocket Program, USAEC Report ANL-7169, Argonne National Laboratory, July 1966. (Classified)

LEGAL NOTICE

This journal was prepared under the sponsorship of the U. S. Atomic Energy Commission. Neither the United States, nor the Commission, nor any person acting on behalf of the Commission:

A. Makes any warranty or representation, expressed or implied, with respect to the accuracy, completeness, or usefulness of the information contained in this journal, or that the use of any information, apparatus, method, or process disclosed in this journal may not infringe privately owned rights; or

B. Assumes any liabilities with respect to the use of, or for damages resulting from the use of any information, apparatus, method, or process disclosed in this journal.

As used in the above, "person acting on behalf of the Commission" includes any employee or contractor of the Commission, or employee of such contractor, to the extent that such employee or contractor of the Commission, or employee of such contractor prepares, disseminates, or provides access to, any information pursuant to his employment or contract with the Commission, or his employment with such contractor.